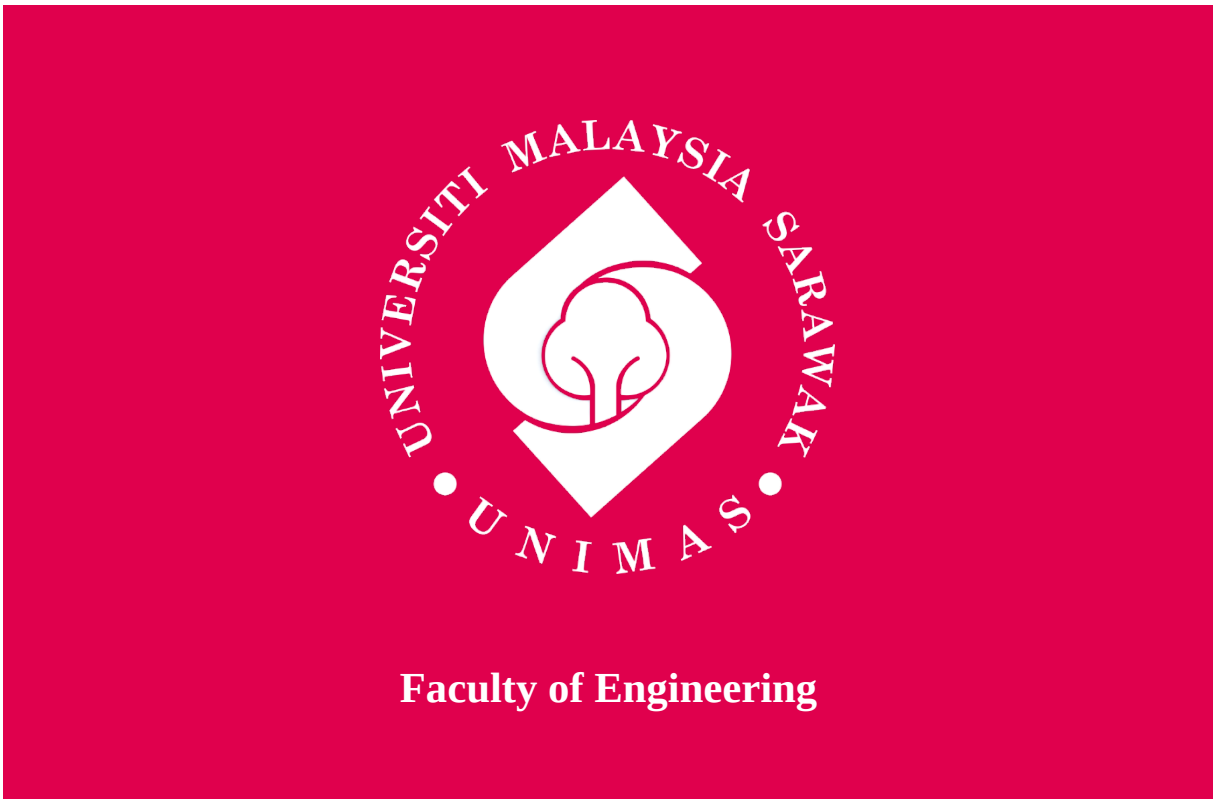

Smartphone-based GPS-integrated Location Prediction Model for OBD-II-Equipped Land Vehicle Localization

Chai Nee Ping

Doctor of Philosophy
2018

Smartphone-based GPS-integrated Location Prediction Model for OBD-II-Equipped Land Vehicle Localization

Chai Nee Ping

A thesis submitted

In fulfillment of the requirements for the degree of Doctor of Philosophy

(Electrical and Electronics Engineering)

Faculty of Engineering
UNIVERSITI MALAYSIA SARAWAK
2018

DECLARATION

I, Chai Nee Ping (11011557) from Faculty of Engineering UNIMAS hereby declare that the work entitled, Smartphone-based GPS-integrated Location Prediction Model for OBD-II-Equipped Land Vehicle Localization is my original work. I have not copied from any other students' work or from any other sources except where due reference or acknowledgement is made explicitly in the text, nor has any part been written for me by another person. The thesis has not been previously accepted for any degree and is not concurrently submitted in candidature for any other degree.

_____

Chai Nee Ping (11011557)

Date:

ACKNOWLEDGEMENT

First of all, I would like to dedicate thousands of thank to my supervisor, Assoc. Prof. Dr. Wan Azlan Bin Wan Zainal Abidin for his supervision, guidance, advices and encouragement throughout the progress of this research work. Dr. Wan has always been patient in giving motivation during the hard time of research and he is patient in discussing about the problems and the solutions for the research work. His efforts and contributions are highly appreciated.

Furthermore, I would like to thank all the lecturers of the Faculty of Engineering, UNIMAS and all my colleagues in postgraduate room for their patient knowledge sharing, advices and guidance throughout the time of research work being carried on. They are always helpful and their help contributed towards the actualization of this thesis.

Last but not least, a grateful appreciation is dedicated to my beloved family and dearest friends for their help and support. Their endless love, patience, understanding and encouragement never fail to motivate me to work harder in completing this research. Their mental support and financial support are significant along the completion of this thesis.

ABSTRACT

Vehicle localization is important to track the movement of a particular land vehicle especially company vehicle. Global Positioning System (GPS) is commonly utilized in current vehicle localization applications. However, GPS has the issues of Non-Line-of-Sight (NLOS). Tremendous of research works had been carried out to remedy the shortcoming. Most of the research works deployed off-the-shelf Inertial Measurement Unit (IMU) to support GPS positioning when GPS signal lost. However, the IMU that can provide high accuracy positioning is usually expensive and the size is bulky. These make it not user-friendly and not applicable for civilian users. Thus, the objective of the study is to develop affordable smartphone-based GPS-integrated location prediction model for OBD-II-equipped vehicle localization to track the real-time location of vehicle. The focus of this study is the development of location prediction model which can perform integration of GPS data, OBD-II data and the vehicle's heading direction to present the location of vehicle with high continuity and reasonable accuracy. To validate the findings, experimental works were carried out for 5 different scenarios, involving straight road, right-angle-turning, non-right-angle-turning, roundabout and U-turn. The results are presented in the graphical form to show its continuity and in the form of Root Mean Square Error (RMSE) to show its accuracy. The accuracy shows that the GPS-integrated location prediction model is within an accuracy range of 5.2 to 15.8 meters while the cost is affordable and the size is small.

Keywords: Smartphone-based, GPS; OBD-II, Vehicle's Heading Direction, Location Prediction Model

Penentuan Lokasi Kenderaan Darat yang Mempunyai OBD-II dan Berasaskan Telefon Pintar dengan Integrasi GPS dan Ramalan Algoritma

ABSTRAK

Penentuan lokasi kenderaan adalah penting untuk mengesan pergerakan kenderaan darat terutamanya kenderaan syarikat. Sistem Kedudukan Global (GPS) biasanya digunakan dalam aplikasi penentuan lokasi kenderaan semasa. Walau bagaimanapun, GPS mempunyai isu Bukan Dalam Garis Penglihatan (NLOS). Banyak kerja-kerja penyelidikan telah dilakukan untuk membetulkan kelemahan tersebut. Kebanyakan kerja-kerja penyelidikan menggunakan Unit Pengukuran Inersia (IMU) untuk menyokong penentuan kedudukan GPS apabila isyarat GPS hilang. Walau bagaimanapun, IMU yang boleh memberikan kedudukan dengan ketepatan yang tinggi biasanya mahal dan bersaiz besar. Ini menjadikannya tidak sesuai diguna oleh pengguna awam. Oleh itu, objektif kajian adalah untuk membangunkan model ramalan lokasi bersepadu dengan GPS berasaskan telefon pintar yang mampu dimiliki oleh pengguna awam untuk memantau lokasi kenderaan yang mempunyai OBD-II. Tumpuan kajian ini adalah pembentukan model ramalan lokasi yang boleh melakukan integrasi data GPS, data OBD-II dan arah pergerakan kenderaan untuk membentangkan lokasi kenderaan dengan kesinambungan yang tinggi dan ketepatan yang munasabah. Demi mengesahkan penemuan kerja ini, eksperimen dijalankan bagi 5 senario yang berbeza, melibatkan jalan lurus, putaran bersudut tegak, putaran bukan bersudut tegak, bulatan dan pusingan U. Hasilnya dibentangkan dalam bentuk graf untuk menunjukkan kesinambungannya dan dalam bentuk Kesilapan Punca Kuasa Min (RMSE) untuk menunjukkan ketepatannya. Ketepatan

menunjukkan bahawa model ramalan lokasi bersepadu dengan GPS adalah berada dalam lingkungan 5.2 hingga 15.8 meter manakala kosnya berpatutan dan saiz adalah kecil.

Kata kunci: *Berasaskan telefon pintar, GPS, OBD-II, Arah Pergerakan Kenderaan, Model Ramalan Lokasi*

TABLE OF CONTENTS

LIST OF TABLES

LIST OF FIGURES

LIST OF ABBREVIATIONS

4G	Fourth Generation of GSM
5G	Fifth Generation of GSM
ABAS	Aircraft-based Augmentation System
AI	Artificial Intelligence
ANFIS	Adaptive Neuro-Fuzzy Inference System
AOA	Angle of Arrival
AP	Access Point
AR	Auto Regression
AR	Axial Ratio
ASFP	AI-based Segmented Forward Predictor
ASFP	AI-based Segmented Forward Predictor
BDS	BeiDou Navigation Satellite System
BKF	Backward Kalman Filtering
BS	Base Station
CDKF	Central Difference Kalman Filter
CEP	Circular Error Probability
CGI	Cell Global Identity
CI	Cell Identity
CKF	Cubature Kalman Filter
CN	Cellular Network
CR	Circular Polarization
dB	Decibel

dBic	Decibel (measurement unit for circular polarization)
DF-CSA	Dipole-Fed Cross Spiral Antenna
DoD	Department of Defense
DOP	Dilution of Precision
DR	Dead Reckoning
DTC	Diagnostic Trouble Code
ECU	Engine Control Unit
EKF	Extended Kalman Filter
EOBD	European On-Board Diagnostic systems
ETCS	Electronic Toll Collection System
EU	European Union
FKF	Forward Kalman Filtering
FOG	Fiber Optical Gyro
FOS	Fast Orthogonal Search
GBAS	Ground-based Augmentation System
GEO	Geostationary Orbit
GHz	Giga Hertz
GIS	Geographic Information System
GLONASS	Global Navigation Satellite System
GM	Gauss Markov
GNSS	Global Navigation Satellite System
GPRS	General Packet Radio Service
GPS	Global Positioning System
GSM	Global System for Mobile Communication

GSO	Geosynchronous Orbit
HDCKF	High Degree Cubature Kalman Filter
HPE	Horizontal Positioning Error
IDNN	Input-Delayed Neural Network
IMM-EKF	Interactive Multi Model Extended Kalman Filter
IMU	Inertial Measurement Unit
INS	Inertial Navigation System
IRNSS	Indian Regional Navigation Satellite System
ISO	International Standardization Organization
ITS	Intelligent Transportation System
IVC	Inter-Vehicle Communication
kbps	Kilobyte per second
KF	Kalman Filter
km	Kilometre
km/h	Kilometre per hour
LAC	Local Area Code
LMA	Levenberg-Marquardt Algorithm
LMU	Location Measurement Unit
LOS	Line-of-Sight
LP	Linear Polarization
m	Meter
Mbps	Megabyte per second
MCC	Mobile Country Code
MEMS	Micro-Mechanical System

MHz	Mega Hertz
MNC	Mobile Network Code
MS	Mobile Station
NLOS	Non-Line-of-Sight
NN	Neural Network
OBD-II	On-board Diagnostics-II
PDF	Probability Density Function
PDR	Pedestrian Dead Reckoning
PF	Particle Filter
PID	Parameter Identification Number
PIFA	Planar Inverted-F Antenna
PPS	Precise Positioning Service
QZSS	Quasi Zenith Satellite System
RBFNN	Radial Basis Function Neural Network
RFID	Radio Frequency Identification
RHCP	Right-hand Circular Polarization
RMSE	Root Mean Square Error
RNS	Regional Navigation System
RSS	Received Signal Strength
RTSS	Rauch–Tung–Striebel Smoother
RTW	Real Time Workshop
s	Second
SA	Selective Availability
SAE	Society of Automotive Engineers

SAR	Specific Absorption Rate
SBAS	Satellite-based Augmentation System
SINS	Strapdown Inertial Navigation System
SM-EKF	Single Model Extended Kalman Filter
SPS	Standard Positioning Service
STCKF	Strong Tracking Cubature Kalman Filter
TA	Timing Advance
TDOA	Time Difference of Arrival
TFS	Two-Filter Smoother
TOA	Time of Arrival
UKF	Unscented Kalman Filter
US	United States
UTM	Universal Transverse Mercator
V	Speed/Velocity
V2V	Vehicle-to-Vehicle
VaNet	Vehicular Ad Hoc
VUT	Vehicle Under Test
WAVE	Wireless Access Vehicular Environment
WBNN	Wavelet-based Neural Network
WLAN	Wireless Local Area Network
ZUPT	Zero Velocity Update

CHAPTER 1

INTRODUCTION

1.1 Background of the Study

Country development and population growth have increased mobility demand globally. Apart from smartphone, land vehicle is another significant representative of mobility which is highly demanded by civilians. The number of vehicles in the world is rising drastically from year to year. The average annual percentage change of the world car registration from 1960 to 2013 is 2.6% and the average annual increment is calculated as approximately 13 million [1]. The highest increment is hitting up to 25 million per annum. The significantly increasing number of land vehicles creates many challenges, such as safety, mobility and environmental issues.

Land vehicles include bicycle, motorcycle, car, van, bus, truck, lorry, and so on. In terms of safety issue, the company vehicle need to be kept track and monitored to ensure the driver is on the correct route/path and on time. In the existing vehicle monitoring system, Global Positioning System (GPS) is commonly used for the localization purpose. GPS is the well-known positioning approach with high accuracy global availability [2]. GPS technology is getting common and is extensively utilized due to its improvement in term of accuracy, price and size [3].

The successfulness of GPS by the United States (US) motivated Russian Federation to develop Global Navigation Satellite System (GLONASS), Europe countries to develop Galileo and China to develop BeiDou Navigation Satellite System (BDS), which formerly was known as COMPASS. Regional Navigation System (RNS) is then introduced to improve the performance of existing Global Navigation Satellite System (GNSS) over

limited geographical area [4]. In addition, there are Satellite-based Augmentation System (SBAS), Ground-based Augmentation System (GBAS) and Aircraft-based Augmentation System (ABAS) that are developed to improve the performance of GNSS as well [5].

While the above-mentioned GNSS offers significant benefits, the technology has its errors which are contributed by different sources. The error sources include Selective Availability (SA), atmospheric effects, orbital errors, clock errors, multipath effects and noise issues as well as Dilution of Precision (DOP) [6]. The major drawback of GNSS is the Non-Line-of-Sight (NLOS) problem in buildings, tunnels, jungles or urban canyons. NLOS occurs when the satellite signal transmissions are totally blocked by obstacles [7-8]. GPS receiver cannot perform positioning under NLOS condition as no satellite signals can be received.

Since GNSS has NLOS issue, investigation on other positioning technologies is necessitated to remedy the shortcomings to meet the goal of continuous positioning. The positioning technologies can be categorized into two major kinds, which are network-based positioning and location prediction [9].

The network-based positioning performs with the signals of cellular network or Wireless Local Area Network (WLAN) by employing the techniques of Received Signal Strength (RSS), Angle of Arrival (AOA), Time of Arrival (TOA), and Time Difference of Arrival (TDOA) to compute the location of receiver [10]. The accuracy of these techniques ranges from 50 meter to 500 meter [2]. The relatively low accuracy results in lower application rate of this type of positioning.

Another to be mentioned network-based positioning is Vehicular Ad Hoc Network (VaNet), which is also known as Inter-Vehicle Communications (IVC) or

Vehicle-to-Vehicle (V2V) [11]. There is a range of communication technologies that can be incorporated in VANet, such as WiFi, WiMax, WAVE, cellular, Bluetooth and RFID. These communication technologies have different performance in terms of range and data rate. This technology is not commonly implemented due to the widespread adoption is needed while the privacy and security issue is a concern to public.

The integration of GPS and Inertial Navigation System (INS) is not a new phenomenon. GPS/INS has been used in the last decade in wide span of applications [12-22]. The integration is typically carried out through Kalman Filter (KF) [23-31], which has been proven to be the benchmark and the best solution of integration. KF has been highly applied in GPS/INS schemes either loosely-coupled mode or tightly couple mode. However, the sensor errors and random errors might occur thus degrade the accuracy of this complementary system.

1.2 Research Problem Statement

The main topic discussed in this dissertation is about the integration of GPS and location prediction technique. Researchers have investigated this topic especially integration of GPS and INS [28-35], considering high-end and low-end inertial sensors. The high-end inertial sensors include navigation grade and tactical grade, which allow sub-metric position accuracy during GPS signal blockage. The high-end inertial sensors are more applicable to technical high accuracy application owing to their price and size. The price can be up to hundred thousand or 1 million dollars while the size is about 6-inch x 6-inch x 6-inch. The smaller size low-end inertial sensors include industrial grade and automotive grade, which provide relatively low positioning accuracy and affordable to

civilians. The low-cost sensors might range from $7 and above, up to few hundred dollars [36].

The automotive grade is typically known as the lowest grade of inertial sensor. Previously, they are often sold as individual accelerometers or gyroscopes. Currently, they are mostly combined to form a self-contained Inertial Measurement Unit (IMU) unit. This grade of inertial sensor is considered as insufficient to provide accurate positioning information even integrated with other navigation systems such as GPS. A reasonable calibration after installation can upgrade it to industrial grade but its accuracy still far apart from tactical and navigation grade.

The accelerometer bias error and gyro angle random walk cause the horizontal position error from millimeter up to several thousand kilometers. Based on Table 1.1 and Table 1.2, it can be observed that accelerometer is much more sensitive and create significant change in horizontal position error as the time is extended. The horizontal position error causes by industrial and automotive grade sensors within one hour is very high if compared to navigation and tactical sensors.

Table 1.1: Horizontal Position Error of Different Grade of Accelerometer [36]

	Accelerometer Bias Error	Horizontal Position Error [m]			
Grade	[mg]	1 s	10 s	60 s	1 hr
Navigation	0.025	0.13 mm	12 mm	0.44 m	1.6 km
Tactical	0.3	1.5 mm	150 mm	5.3 m	19 km
Industrial	3	15 mm	1.5 m	53 m	190 km
Automotive	125	620 mm	60 m	2.2 km	7900 km

Table 1.2: Horizontal Position Error of Different Grade of Gyrometer [36]

	Gyro Angle Random Walk (ARW)	Horizontal Position Error [m]			
Grade	[deg/hr]	1 s	10 s	60 s	1 hr
Navigation	0.002	0.01 mm	0.1 mm	1.3 mm	620 m
Tactical	0.07	0.1 mm	3.2 mm	46 m	22 km
Industrial	3	10 mm	0.23 m	3.3 m	1500 km
Automotive	5	20 mm	0.45 m	6.6 m	3100 km

In the past few years, tremendous research works about integration of GNSS with low cost inertial sensor are carried out, especially the focus on GPS/INS integration with the aid of Kalman Filter (KF) [30-34]. Apart from Extended Kalman Filter (EKF) and Unscented Kalman Filter (UKF), the techniques involved in research include artificial intelligence, both the fuzzy and neural network (NN) [37-41]. However, most of the research works are limited to simulations (C/C++, Matlab, Simulink) and do not implement to the real-life applications [38-41]. Moreover, they are not practical to be used in real-life due to the size of the inertial sensors in the investigated work are normally bulky [32, 42]. Some works do not present the exact accuracy improvement in the conclusion [33, 43-44].

Another matter that is worth to be mentioned is the research in the smartphone-based dead reckoning which the researchers focus on the application on pedestrians [45-46] instead of vehicles. Both smartphone and vehicle are items with high mobility function and they are essential to be located in real-time. Therefore, the smartphone-based GPS-integrated location prediction model for OBD-II-equipped land vehicle localization should be investigated and developed to improve the convenience of civilian users.

1.3 Aim and Objectives of the Study

To address the problems under investigation, the current research work aims to study about the GPS-integrated location prediction technique. This can be achieved through the following objectives:

i. To compile, categorize and evaluate current positioning techniques

ii. To analyze and identify key parameters of location prediction algorithm

iii. To formulate and validate location prediction algorithm

iv. To propose and develop smartphone-based GPS-integrated location prediction model

v. To define portability, applicability, continuity, accuracy and price of smartphone-based GPS-integrated location prediction model

1.4 Research Novelty and Expected Outcomes

The primary motivation of current research work is to develop a new GPS-integrated location prediction model. At the end of the research, the following outcomes are expected:

i. Current positioning techniques are compiled, categorized and evaluated

ii. Key parameters of location prediction algorithm are analyzed and identified

iii. Location prediction algorithm is formulated and validated

iv. Smartphone-based GPS-integrated location prediction model is proposed and developed

v. Portability, applicability, continuity, accuracy and price of smartphone-based GPS-integrated location prediction model is defined

1.5 Outline of Thesis

The thesis consists of five chapters and the structure is organized as following:

Chapter 1: This chapter describes the background of the study and focuses on the research problem statement. Furthermore, it presents the aim and objectives of the study as well as research novelty and expected outcomes.

Chapter 2: This chapter introduces the fundamentals of positioning technologies and provides a basic understanding of the research background. The satellite-based positioning, network-based positioning and location prediction techniques are also presented. The previous works about non-real-time and real-time vehicle positioning are discussed. The previous works about On Board Diagnostic-II (OBD-II) and antenna are also being studied. Moreover, the performance assessment methods for the positioning technologies are described.

Chapter 3: This chapter presents the system architecture of integrating two different types of measurements, which are GPS and location prediction. The conceptual framework is illustrated, showing the data retrieval and manipulation, prediction algorithm and the GPS-integrated location prediction model. Apart from that, the system evaluation and validation methods are clarified by showing the way of data collection and data analysis.

Chapter 4: This chapter addresses the validation of functionality of prediction algorithm and prediction model. The results of the new GPS-integrated location prediction model in five scenarios are presented and evaluated based on the discussed performance assessment method. Moreover, the comparison of this original work with other works is carried out and shown in this chapter. The analysis and discussion is also presented.

Chapter 5: This chapter provides conclusions of the research work and recommendations for future works. The significant finding and main contributions are highlighted. In addition, some suggestions for the future research are also given.

CHAPTER 2

LITERATURE REVIEW

2.1 Overview

This chapter introduces the fundamentals of positioning technologies and provides a basic understanding of the research background. The satellite-based positioning, network-based positioning and location prediction techniques are also presented. The previous works about non-real-time and real-time vehicle positioning are studied and discussed. The previous works about On Board Diagnostic-II (OBD-II) and antenna are also being studied. Moreover, the performance assessment methods for the positioning technologies are described.

2.2 Satellite-based Positioning

Satellite-based positioning is a technology that can provide the location and position of a device with the computation of information provided by the satellites which are readily installed in the space. The main and major satellite-based system is Global Navigation Satellite System (GNSS).

The later emerging systems include Regional Navigation System (RNS) and Satellite-based Augmentation System (SBAS). These two systems are present to provide aid to GNSS at certain region or country, which is not globally.

2.2.1 Global Navigation Satellite System (GNSS)

GNSS is a navigation satellite system which can provide location information with global coverage. Satellite receiver can identify its location through mathematical calculations involving the orbit and time information from a number of satellites of GNSS.

Table 2.1: GNSS [47-52]

Country	**GNSS**	**Satellites**
United States	GPS	32
Russia	GLONASS	25
Europe	Galileo	22
China	BDS	28

The first GNSS in the world is GPS, which is developed by the United State (US) in early 1970 [50]. GPS was initially conceived by Department of Defense (DoD) to provide accurate navigation in military [51]. In the beginning of 1980s, US committed to make GPS available for civilian users and become the pioneer of civilian navigation [51].

GPS provides Standard Positioning Service (SPS) to civilian users and Precise Positioning Service (PPS) to authorized users in the field of military [5]. Although civilian users can navigate with SPS, the implementation of Selective Availability (SA) degraded the GPS accuracy intentionally [52]. SA was ceased on May 1, 2000 and the SA removal has greatly improved the accuracy from 100 m to 10-20 m [47-49].

Widespread adoption of GPS in civilian navigation has attracted attention of other countries and has raised their intention to develop own GNSS. Russia was triggered and becomes the second country that has own GNSS, namely GLONASS. GLONASS launched its first satellite in October 1982 and peaking at 24 satellites in 1995 [5].

However, GLONASS satellites constellation started to decay due to short design life. In 2008, there are only 13 operational satellites available [5]. Fortunately, reinvigoration of GLONASS constellation since 2001 [5] had recovered the capability of GLONASS navigation and its full-constellation operational was restarted in 2011 [49].

Other than Russia, Europe countries and China realize the significance to have their own GNSS. Thus, European Galileo and China BDS are approaching to contribute to worldwide navigation.

GPS has 31 operational satellites and 1 in maintenance while GLONASS has 24 operational satellites and 1 in flight test phase. Galileo has 14 operational satellites, 2 under testing, 2 unavailable and 4 under commissioning whereas BDS has 15 in operation and 13 not in operational orbital constellation.

Apart from fulfilling large demand of civilian users on navigation and its potential commercial market, GLONASS, Galileo and BDS are developed to improve the accuracy of positioning system and reduce the dependency on GPS. Moreover, the integration of at least 2 GNSSs can improve the performance of navigation. For example, the combination of GPS and GLONASS is a solution to the issue of limited visible satellites.

Interoperation of the GNSS systems makes more satellites available and visible to satellite receiver with additional signals selection function to increase accuracy, stability, reliability, and operation speed. A dual-channel reconfigurable GNSS receiver is required to be reconfigurable to support all possible GNSS signals and incorporate two independent channels to receive incoming signals simultaneously [53].

With clear sky view, the accuracy of GNSS is promising. The only challenges of GNSS are NLOS of satellite signals and multipath effect. These challenges promote the

innovation of implementing the Regional Navigation System (RNS) and Satellite-based Augmentation System (SBAS).

2.2.2 Regional Navigation System (RNS)

Regional Navigation System is an additional satellite constellation to improve the performance of existing GNSS over limited geographical area. It helps to increase the visibility of satellites in the view of receiver by the installation of Geosynchronous Orbit (GSO) satellites or combination of Geostationary Orbit (GEO) and GSO satellites.

Table 2.2: RNS [54]

Country	RNS	No. of satellites
Japan	QZSS	3
India	IRNSS	7

There are two major RNSs, which are Japan's Quasi Zenith Satellite System (QZSS) and India's Indian Regional Navigation Satellite System (IRNSS) [54]. As shown in Table 2.2, QZSS will have 3 satellites while IRNSS will have 7 satellites.

The 3 QZSS satellites are installed on 3 GEOs which are 45 degree inclined to the equatorial plane with altitude of 35786 km from the surface of the Earth [5]. QZSS GSOs are highly elliptical (Figure 2.1) and they are orbiting around the Earth with the same speed as the Earth orbits. The orbiting of 3 satellites on GSOs forms a special figure-eight-pattern ground track on the earth, as illustrated in Figure 2.2.

The asymmetric figure-eight-pattern ground track covered Japan with much smaller northern loop meanwhile Australia and New Guinea are widely covered by the larger southern loop. The ground track has a central line at 135º E in longitude [5].

The QZSS is unique as at least 1 out of the 3 GSO satellites will be near the zenith over Japan all the time [55]. High elliptical characteristic of QZSS GSOs with high altitude makes the satellites to be further away from the Earth if compared to any other GNSS satellite constellations. These can raise the elevation angle of QZSS above 70º in Japan [56]. Larger elevation angle reduces the probability of NLOS occurrence and thus improves the availability of positioning system.

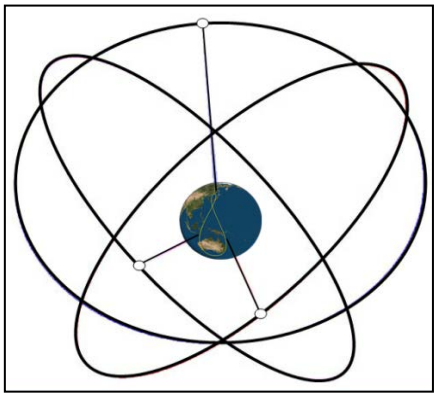

Figure 2.1: QZSS Constellation [56]

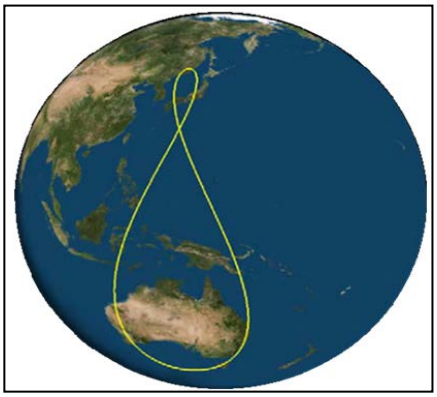

Figure 2.2: QZSS Ground Track [56]

In contrast, IRNSS planned to combine the use of GEO and GSOs by installing 3 satellites on GEO and 4 satellites on GSOs. GEO is a kind of GSO which orbits around the equator. Satellite on GEO supposes to be at the same point over the sky in the point of view of people on the Earth as they both orbits the identical center point with the equal speed and direction.

The GEO satellites are anticipated to be placed on 34ºE, 83ºE and 132ºE while the other four satellites are planned to be sited on GSOs which are inclined 29º to the equatorial plane [57]. The location of GEO satellites and ground tracks (figure-eight pattern) of GSO satellites are presented in Figure 2.3.

The intended coverage area is bounded by red dot line in Figure 2.3 with the center point at 90º E on equator. IRNSS is expected to provide absolute position accuracy better than 20 m throughout India [58].

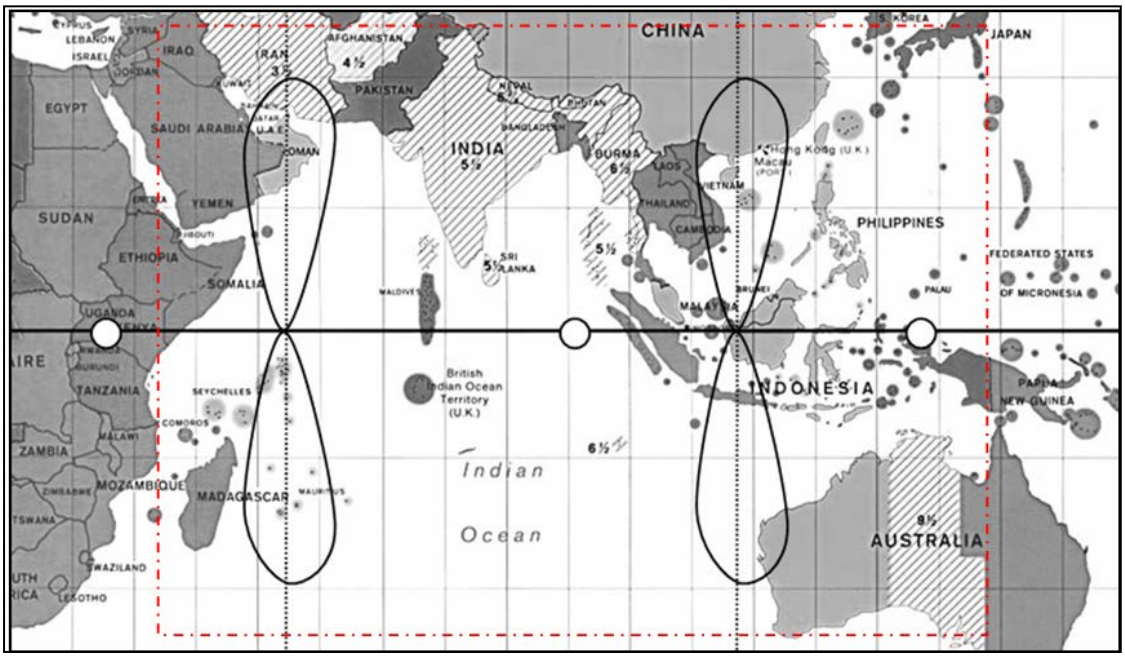

Figure 2.3: IRNSS Satellite Constellation [57]

With the IRNSS satellite constellation, seven satellites are assured to be visible throughout India. Positioning performance can be significantly improved by combining IRNSS with existing fully operational GNSS (GPS and GLONASS) as the number of visible satellites is raised up to at least 26 [57]. The higher visibility improves the availability, accuracy and reliability of positioning.

2.2.3 Satellite-based Augmentation System (SBAS)

The capabilities of GNSS are well known as it provides worldwide navigation service with adequate accuracy for the use of civilians. However, some shortfalls such as lack of civil international control and inadequate accuracy for aviation purpose prompted the need for GNSS performance enhancement [59].

In spite of RNS, SBAS is a suitable approach to improve the performance of GNSS. The major difference between RNS and SBAS is that SBAS has satellite constellation on GEO only. SBAS installs GEO satellites on equator to provide differential corrections, integrity parameters and ionosphere data over a region spanned by a network of ground reference stations [59].

Reference stations are strategically positioned to monitor and measure satellite signals to be backhauled to master stations for error and correction calculations [60]. The generated correction message is sent to GEO satellites by uplink stations. Lastly, GEO satellites broadcast the SBAS correction message on GPS frequency to improve the accuracy of GNSS positioning.

The seven countries listed in Table 2.3 have put their initiative on developing SBASs to supplement to existing GNSS. It also shows that current established SBASs and planned SBASs. American WAAS, Japanese MSAS and European EGNOS are operational SBASs while Indian GAGAN, Russian SDCM, African ASAS and Chinese SNAS are still in development [61].

These SBASs at least has 2 satellites or at most 5 satellites on GEO. The total number of satellites that will be installed on GEO is estimated to be 20. The locations of GEO satellites are clearly revealed in Table 2.3.

Table 2.3: SBAS [59-61]

Country	SBAS	GEO	Longitude on Equator
US	WAAS	2	133 ºW, 107ºW
Japan	MSAS	2	140 ºE, 145 ºE
Europe	EGNOS	3	15.5ºW, 21.5ºE, 64.5ºE
India	GAGAN	2	55ºE, 83ºE
Russia	SDCM	3	16ºW, 95ºE, 167ºE
Africa	ASAS	3	15.5ºW, 15ºE, 65.6ºE
China	SNAS	5	58.75ºE, 80ºE, 110.5ºE, 140ºE, 160ºE

The estimated coverage area of each SBAS is presented in Figure 2.4. It is seen that MSAS and GAGAN with the least number of GEO satellites have the smallest coverage area. Although WAAS has the same number of satellites, the installation of more reference stations extends the coverage area. Other SBAS has wider service area with 3 or 5 GEO satellites and more reference stations.

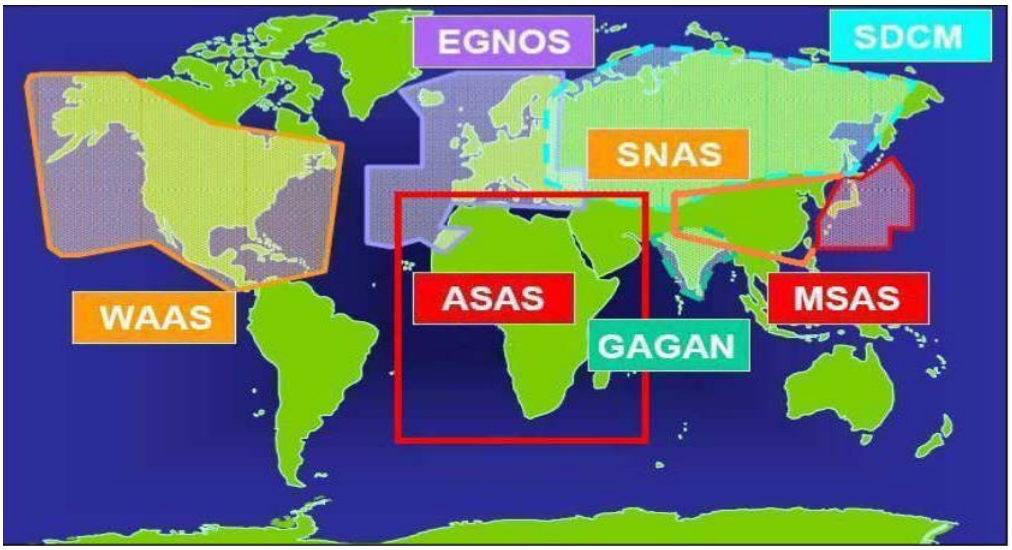

Figure 2.4: SBAS Coverage Area [61]

2.3 Network-based Positioning

Network-based positioning is different from satellite-based positioning because it does not involve any satellite. It involves other signals that form a network on ground such

as cellular Network (CN), Wireless Local Area Network (WLAN) and Vehicular Ad Hoc Network (VaNet). Network-based positioning is able to provide location information within the network coverage area but not globally.

2.3.1 Cellular Network (CN)

Cellular Network (CN) has been extensively extended because of its reliability and commercial potential in the field of communication. This leads to the tremendous research interest in mobile positioning.

Mobile positioning using cellular network is a newsworthy technology as the location unknown mobile station (MS) can be calculated with the existence of known position base stations (BSs) [62]. In addition, its availability and reliability provides this technology with added value.

With the well-founded cellular network and existing Global System for Mobile Communication (GSM) infrastructures, the investigation in CN-based positioning is simpler than the installation of any satellite-based positioning system. However, this kind of positioning method is location estimation with less accuracy if compared to GNSS, RNS and SBAS.

The location estimation is done through computation on the parameters of signal transmission between BS and MS. The signal transmission parameters that can help in location computation are Cell-ID, Received Signal Strength (RSS), Angle of Arrival (AOA), Time of Arrival (TOA), and Time Difference of Arrival (TDOA) [63].

The performance of each CN-based approach is presented in Table 2.4. The Cell-ID and RSS approaches have advantages of high reliability, high applicability, low cost, and low latency but the greatest shortcoming is low accuracy. The other 3 methods have medium reliability, low applicability and higher latency. AOA requires higher cost with moderate accuracy while TOA and TDOA need medium cost for higher accuracy.

The reliability and applicability of Cell-ID and RSS are high due to the reason that no further modification is needed for their implementation. Cell-ID approach is supported by all current smartphone while signal strength is always available because it is forwarded regularly for the handoff purpose [2]. Therefore, no extra installation cost is required.

On the other hand, AOA, TOA and TDOA techniques required the installation of additional hardware named Location Measurement Unit (LMU) at BS. For TOA and TDOA, LMUs must have a shared common clock reference with MS to achieve strict time synchronization between LMUs and MS.

As network modification is required, the reliability is medium since the modification must be implemented at all BSs. However, this will increase the overall cost. The inability to implement modification at all BSs will contribute to low applicability. Moreover, the latency is higher because of the synchronization process. The major benefit of these 3 approaches is the improved accuracy if compared to Cell-ID and RSS.

Table 2.4: CN-based Positioning Approaches [64]

Techniques	**Reliability**	**Applicability**	**Cost**	**Latency**	**Accuracy**
Cell-ID	High	High	Low	<5s	100-1500m
RSS	High	High	Low	<5s	200-500m
AOA	Medium	Low	High	<10s	100-200m
TOA	Medium	Low	Medium	<10s	50-200m
TDOA	Medium	Low	Medium	<10s	50-150m

Figure 2.5 shows the structure of CN-based positioning approaches. Cell-ID is the simplest technique as only 1 BS is required to estimate the location. The location estimation is according to the Cell Global Identity (CGI) of MS such as Mobile Country Code (MCC), Mobile Network Code (MNC), Location Area Code (LAC), and Cell Identity (CI) [2].

Despite its simplicity, Cell-ID approach has the worst accuracy where the accuracy can be up to 1.5 km. To enhance its accuracy, Timing Advance (TA) that measures the distance between MS and BS can reduce the positioning error. TA is a number range from 0 to 63 and each increment represents 554 m from BS [2]. Thus, TA helps narrow down the estimation range to a ring with radius of 554 m.

Both RSS and TOA require 3 BSs for triangulation computation (Figure 2.5), whereas the MS location can be estimated by finding the intersection point of 3 signals from nearby BSs. The only difference is the computational parameters.

RSS calculates the location with signal strength while TOA uses the time of arrival from BSs to MS. RSS is less accurate as compared to TOA owing to the fact that signal strength is highly affected by the obstacles along the signal transmissions. The signal strength attenuation occurs as the results of path loss, multipath fading, and shadowing [65].

TOA requires the time of arrival to calculate the distance between the MS and 3 BSs respectively. The timing error strongly affects the distance calculation, which in turns will affect the precision of location estimation. The timing error may be caused by the clock synchronization error or propagation delay.

AOA approach can estimate the location with the signal elevation angle to 2 BSs. Though the number of BSs required is reduced, this method involves the use of specialized

antenna arrays [66]. The requirement of this specialized hardware causes the AOA to be costly and not attractive to be widely implemented. Furthermore, a minor error in angle measurement would result in severe error in positioning. The condition is even worse if the NLOS problem occurs and angle measurement is unavailable.

TDOA has similar performance to TOA but with slight improved accuracy. The higher accuracy credited to the removal of timing error in TOA. The difference in the time of arrival of the signal at multiple LMUs is calculated respectively to determine the hyperbolic curves. The best intersection of hyperbolic curves is the estimated MS location.

Obviously, there are pros and cons of each CN-based positioning technology. Consequently, the integration of different techniques is investigated by researchers to complement the limitations for better positioning performance. There are various hybrid CN-based positioning systems such as RSS/TOA, RSS/AOA, AOA/TOA, AOA/TDOA, and TOA/TDOA [67-71].

Since it is difficult to measure Line-of-Sight (LOS) signals from 3 BSs simultaneously, AOA algorithm that utilizes signals from 2 BS antenna arrays can be used to solve the problem of TOA and TDOA. When 3 or more BSs can be detected, TOA algorithm will be dynamically adjusted to perform positioning [72]. The implementation of AOA to augment RSS, TOA or TDOA is proved to perform better.

According to the simulation by Laaraiedh *et al.*, the performance of standalone is worse than the RSS/TDOA, RSS/TOA, TOA/TDOA and RSS/TOA/TDOA cooperative models [73]. Chen and Abedi also stated that the hybrid localization RSS/AOA/TOA/TDOA scheme in cellular network shows a high improvement if

compared to standalone technique [74]. The accuracy of the hybrid localization can be improved up to 73.6%.

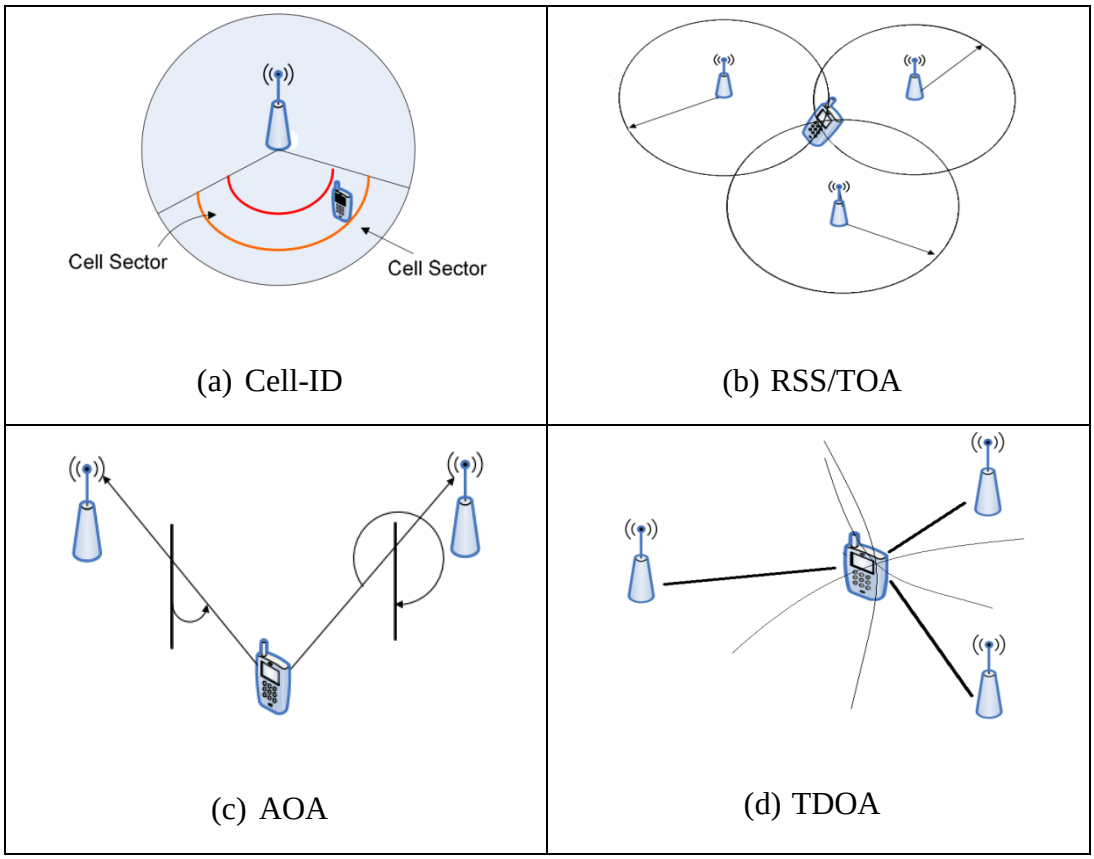

Figure 2.5: CN-based Positioning Approaches [2]

2.3.2 Wireless Local Area Network (WLAN)

In recent year, Wireless Local Area Network (WLAN) has become popular in the field of communication apart from cellular network [75]. The rapid development of WLAN has drawn researchers' attention towards positioning based on WLAN infrastructure as it has existing infrastructure that needs no further installation and investment. This would make the system cheaper and easier to be implemented.

WLAN-based positioning uses the similar approaches as CN-based positioning. It performs position estimation by calculating the signal strength, time of arrival, angle of

arrival, time difference of arrival of WLAN transmission to/from WLAN Access Points (APs) [76]. The difference between WLAN and CN is the signal transmission characteristics.

WLAN-based positioning is more common in indoor positioning applications, where satellite-based positioning has limitation of NLOS. The success of WLAN indoor positioning has attracted attention of researchers to implement this technology to outdoor positioning in order to overcome the limitations of other existing positioning technology.

Both of the indoor and outdoor positioning techniques require a large number installation of WLAN APs with well-planned allocation of each AP in order to optimize the estimation results. The more APs can cover wider area of positioning and the exact location of APs helps in the positioning estimation.

Among the WLAN-based positioning techniques, RSS is the simplest as no modification is needed yet it is difficult to have an ideal signal propagation medium. NLOS or multipath signal propagation causes error in RSS positioning, resulting in poor accuracy.

Hence, location fingerprinting is designed to enhance the RSS approach. The key idea of this approach is approximating the location by comparing the RSS measured to a set of premeasured RSS values that is being store in the fingerprint database. The location fingerprinting is outperforming the standalone RSS because it can address some of the RSS problems.

The main difficulties of this system are the development and maintenance of the fingerprint database. The process of collecting the RSS data at calibration points and updating the database from time to time is a challenging task. The survey procedure of this method is time consuming as well [77].

Instead of traditional fingerprint database, there is a new design with added value of directional RSS information which can improve the average positioning error from 35.8 m to 23.5 m [78]. The test results presented by Li *et al.* [78] also shows that the fingerprinting can perform well in outdoor environment with positioning error of the tens of meter.

Despite the fact that WLAN has stronger signal in outdoor environment, the ever-changing environment with buildings, vehicles and people makes the signal transmission complex and affects the RSS. The slightly outdated traditional or directional fingerprint database can estimate the location with larger error.

The other techniques such as AOA, TOA, and TDOA are not preferred in WLAN-based positioning as a lot of efforts are needed in the modification on software and hardware of WLAN infrastructure. They are considered to have better accuracy in indoor environment.

An indoor AOA-based WLAN positioning can have accuracy better than 2 m but its accuracy degrade as the distance between mobile receiver and WLAN infrastructure increases [79]. This shows its suitability to be indoor positioning scheme but not for complicated outdoor environment.

In addition, TOA and TDOA technique is good for indoor positioning because it gets rid of the multipath issue. Thereby, a WLAN positioning based on joint RSS and TOA system is proposed [76]. This system is claimed that the accuracy is improved with no extra cost of firmware or hardware. Nevertheless, it performs better in indoor instead of outdoor.

2.3.3 Vehicular Ad Hoc Network (VaNet)

Vehicular Ad Hoc Network (VaNet) is also called Inter-Vehicle Communications (IVC) or Vehicle-to-Vehicle (V2V), with the objective of enhancing the road safety [11]. VANet becomes a key for future Intelligent Transportation System (ITS) services. The advancement of communication technologies in VANet promotes the investigation of positioning using VANet.

There is a range of communication technologies that can be incorporated in VANet, such as WiFi, WiMax, WAVE, cellular, Bluetooth and RFID. These communication technologies have different performance in terms of range, and data rate as shown in Table 2.5. Subsequently, different technology is deployed in different VANet applications.

Table 2.5: VaNet Communication Technologies [80-82]

Technologies	Protocol	Frequency Band (GHz)	Range (m)	Data Rate (Mbps)
Cellular	GSM/GPRS/3G	0.85/0.9/1.7/1.8/1.9/2.1	15000	2.0
WiFi	IEEE 802.11	2.4/5	100	54.0
Bluetooth	IEEE 802.15.1	2.45	100	1.0
RFID	IEEE 802.15.4	2.45	10	0.1
WiMax	IEEE 802.16	2.5/3.5/5.8	50	72.0
WAVE	IEEE 1609	5.9	1	27.0

Since VANet applications are for vehicles with high mobility, the data transmission rate is crucial factor in consideration of communication channel implementation. Delivery latency also highly affects the reliability of the VANet positioning system.

Though cellular, WiFi, and WiMax have the location computation ability, the process of computation and communication between vehicles is time consuming and power consuming. Therefore, these technologies are not suitable for positioning in VANet but can

be used as communication between vehicle and road infrastructure to obtain the location information.

Among the VANet communication technologies, cellular network has the lowest frequency bands (850/900/1700/1800/1900/2100 MHz). However, it has good BS coverage range up to 15 km with reasonable data rate up to 2 Mbps. It is not suitable as the communication medium in VANet is due to the burdening data charge rate of real-time transmission.

WiFi and WiMax have outstanding data rate than other communication technologies but Wireless Access Vehicular Environment (WAVE) is the most mature wireless technology that potentially meets the extremely short latency and high data rate requirement of VANet positioning [83]. Nevertheless, these technologies require continuous service fees for constant positioning.

Bluetooth and Radio Frequency Identification (RFID) are developed under IEEE 802.15 protocol with the same bandwidth of 2.45 GHz. These two communication technologies offer the smallest coverage range and lowest data rate. As the Bluetooth data transmission needs signal synchronization between two terminals, it is not qualified in the high mobility vehicular environment.

On the other hand, RFID has the potential to be the primary tool in vehicular communication service as it is implemented successfully and effectively in similar transportation application. The examples are RFID implementation in intelligent traffic management expert system [84], bus monitoring system [85], Electronic Toll Collection System (ETCS) [86] and public transit smart card [87].

RFID tags can be installed at the roadside with the exact coordinates respectively and the vehicle that is embedded with RFID reader can update its current location whenever it passes the tag. The small coverage range is sufficient to disseminate the location data from roadside infrastructure to approaching vehicles. Moreover, 100 kbps data rate is adequate to transmit the instant location data to the reader.

Besides, RFID is exploited to a RF-GPS localization system to calibrate the GPS error and improve the accuracy [88]. This system also allows the location data broadcasting to nearby vehicles that do not have GPS receiver, enabling non-GPS vehicles to estimate the location through single peer localization scheme.

The advantages of RFID technology is its free service after device installation meanwhile the installation is cheaper than others especially the RFID passive tags that are to be installed at the roadside. Furthermore, no synchronization or encryption process is needed. This makes the system so simple to be executed. The added value is its extendibility whereas the system can be implemented with the adoption of RFID reader in vehicle.

2.4 Location Prediction

Location prediction is a technique to provide an estimation of a location by using the appropriate parameters or data. There are several ways of location prediction such as Dead Reckoning (DR), Inertial Navigation System (INS), Kalman Filter (KF), and Artificial Intelligence (AI). Some of the techniques suitable to be implemented in outdoor while some suitable for indoor. Besides the applicability, they also differ at the point of accuracy. Thus, each technique is discussed below as well as the key parameters involved.

2.4.1 Dead Reckoning (DR)

Dead Reckoning (DR) is claimed as the simplest method to determine the location but also been declared as a low accuracy method [89]. Dead Reckoning for pedestrian tracking is widely investigated by researchers [73-79]. Among the DR applications for pedestrian, indoor localization [73, 76, 77, 79, 80] and outdoor navigation [74, 75, 78] studies were carried out. The applications of DR are normally carried out with the aid of smartphone.

A smart Pedestrian Dead Reckoning (PDR) was developed and tested in an office environment with a total distance of 168.55 m, duration of 2 minutes and walk step of 215 steps [90]. The authors compared the performance between magnetometer-based PDR, gyroscope-based PDR and proposed SmartPDR. The comparison of performance is shown in Figure 2.6. The magnetometer-based PDR shows the localization error of 10 m while the gyroscope-based PDR shows the error of 13 m. The proposed smartPDR is outperforming by giving 1.62 m of error.

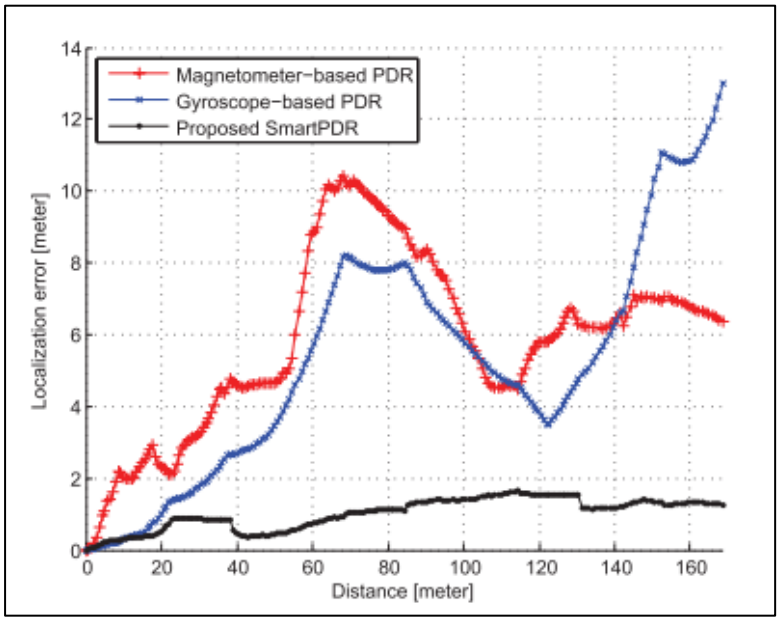

Figure 2.6: Comparison of Performance by Kang & Han [90]

A proposed smartphone-based dead reckoning and 3D map-aided GNSS is proved to be able to provide positioning error in a range of 1.5 m to 5.5 m in middle class or deep urban canyon [45]. The authors used step detection, stride length estimation, and direction estimation before fusing the information with a total state closed loop Kalman Filter to estimate the position of pedestrian.

Ojeda and Borenstein [94] implemented a technique namely “Zero Velocity Update” (ZUPT) in the Personal Dead Reckoning System to reduce the significant errors caused by the Inertial Measurement Unit (IMU) [94]. Along the 104 m rectangle-shaped path, the test was carried out with 5 rounds clockwise and 5 rounds anti-clockwise. The absolute return position errors are 3.85 m and 1.83 m respectively.

2.4.2 Inertial Navigation System (INS)

The earliest location prediction system is Inertial Navigation System (INS) which deploys accelerometers, gyroscopes, and odometers to obtain acceleration, angular rate, and heading angle measurements for next location prediction [97]. The acceleration, angular rate, and heading angle are the key parameters for INS.

Although INS is a self-contained system with a set of mathematical algorithms to forecast position information, it is not an ideal standalone system [21]. It is always incorporating with GPS to support the continuity of navigation especially during the GPS signal outages.

INS provides high short term accuracy, high positioning update rate and immunity to external interference yet it has the limitation of accuracy degradation in long term due to deterministic and random error [40].

The deterministic errors occur due to uncompensated sensors' error, scale factor instability and misalignment. These errors can be minimized with calibration procedure but the random errors that happen naturally cannot be avoided or removed.

The errors mentioned above make the standalone INS being claimed as inaccurate. The RMS error in horizontal position grows up to 2000 m in 20 minutes and 3500 m in 30 minutes [98]. Therefore, GPS/INS always needs to be aided by other filtering method to rectify the errors, giving positioning with better accuracy. The most common filter in the area of positioning is Kalman Filter (KF), which will be discussed in following section.

2.4.3 Kalman Filter (KF)

Kalman Filter (KF) is a mature data fusion model that uses a series of measurements to estimate an unknown variable with certain precision and accuracy. Kalman Filter is over 50 years but is still one of the most important and common data fusion algorithms in use today [99]. KF can be considered as a benchmark for GPS/INS integration [15]. It is a set of mathematical equations that provides recursive solution to the discrete data linear problem by minimizes the mean of the squared error. It has been highly applied in GPS/INS schemes either loosely-coupled mode or tightly couple mode [38].

The general KF equation is presented as

$$\widehat{X}_k = K_k \cdot Z_k + (1 - K_k) \cdot \widehat{X}_{k-1} \quad (2.1)$$

where $\widehat{X}_k$ is the current estimation, K_k is the kalman gain, $Z_k$is the measured value while $\widehat{X}_{k-1}$ is the previous estimation.

A linear system can be described by the following two equations:

State equation:

$$x_k = Ax_{k-1} + Bu_k + w_{k-1} \quad (2.2)$$

Output equation:

$$z_k = Hx_k + v_k \quad (2.3)$$

where entities A, B and H are in general form matrices, k is the time index, x_k is the state of the system, u_k is the known input to the system, z_k is the measured output, w_{k-1} is the process noise and v_k is the measurement noise.

The process noise and measurement noise are both considered as Gaussians and they are statistically independent. Even though the Gaussian noise parameters might not be perfectly estimated, Kalman Filter minimizes the errors and converges the estimations to the nearest values. The noises, w_{k-1} and v_k are with normal probability distributions as below:

$$p(w) \sim N(0, Q) \quad (2.4)$$

$$p(v) \sim N(0, R) \quad (2.5)$$

where Q is the process noise covariance while R is the measurement noise covariance.

The process noise covariance can be found through equation:

$$Q = E(w_k w_k^T) \tag{2.6}$$

where w_k^T is transpose of w random noise vectors and E(·) means the expected value.

The measurement noise covariance can be found through equation:

$$R = E(z_k z_k^T) \tag{2.7}$$

where z_k^T is transpose of z random noise vectors and E(·) means the expected value.

There are two distinct sets of equations, which are Time Update and Measurement Update. Time Update functions as prediction while Measurement Update functions as correction. The equations are shown in Table 2.6 and the iteration process of Kalman Filter is shown in Figure 2.7.

In Time Update equations, $\hat{x}_k^-$ is the prior estimate and P_k^- is the prior error covariance. In Measurement Update equations, $\hat{x}_k$ is the estimate of x at time k while P_k is necessary for next prediction step. The values from Time Update equations are prior values while the values from Measurement Update equations are posterior values. Through the iteration process of KF, the variance of estimation error can be minimized [101].

Table 2.6: Time Update and Measurement Update Equations

Time Update (Prediction)	Measurement Update (Correction)
$\hat{x}_k^- = a\hat{x}_{k-1} + Bu_k$	$K_k = P_k^- H^T (HP_k^- H^T + R)^{-1}$
$P_k^- = AP_{k-1}A^T + Q$	$\hat{x}_k = \hat{x}_k^- + K_k(z_k - H\hat{x}_k^-)$
	$P_k = (1 - K_k H)P_k^-$

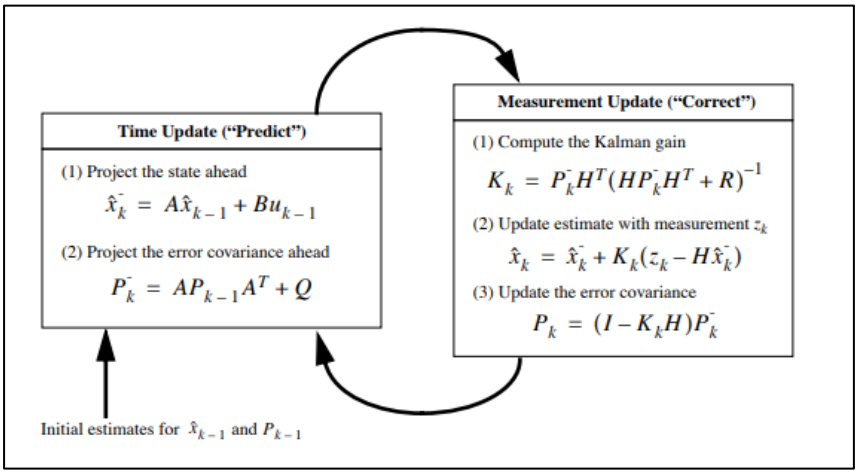

Figure 2.7: The Iteration Process of Kalman Filter [100]

The authors in [98] evaluated the performance of two types of KFs, which are loosely coupled KF and tightly coupled KF. Loosely coupled KF is with small size of error state model and with less computation complexity while tightly coupled KF is large in error state model and with more complex processing [98]. From Figure 2.8, it can be observed that tightly coupled KF and loosely coupled KF reduce the RMSE significantly. Besides, tightly coupled KF performs better than loosely coupled KF. Tightly coupled KF is claimed as an optimal solution and more accurate with faster ambiguity estimation if compared with loosely coupled KF [98].

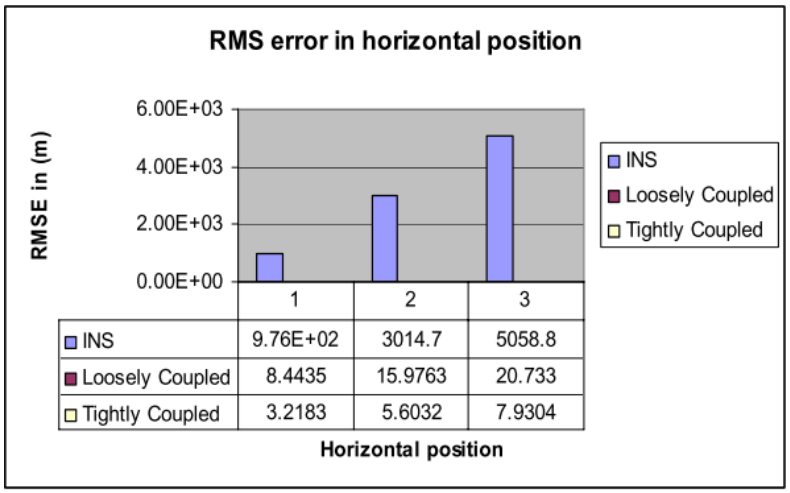

Figure 2.8: RMSE in Horizontal Position for INS, LC and TC [98]

Apart from aforementioned KF, there are extensions named Extended Kalman Filter (EKF) and Unscented Kalman Filter (UKF) which can work on non-linear system. EKF has the largest ratio of precision and computational cost. In comparison, UKF which avoids the use of the Jacobian Matrix of uncertainty and realized the modeling uncertainty by manipulation of sigma points slightly increases the computational cost [102]. There is another kind of modification of KF, named Particle Filter (PF) [103].

Toledo-Moreo *et al.* [104] proposed Interactive Multi Model-Extended Kalman Filter (IMM-EKF) for the integrity of low cost GPS/SBAS/INS. IMM-EKF was suggested to mitigate the provoked unrealistic noise during the high dynamic state of vehicles [104]. Tests were carried out to verify that IMM-EKF has better performance than Single Model-Extended Kalman Filter (SM-EKF) [105]. The position error is reduced and the level of confidence on the solutions is increased.

A 15-state EKF for INS/GPS navigation system was designed by Van *et al.* [23]. The simulation model was developed using Simulink in Matlab environment. According to the accuracy evaluation, the deviation between the GPS and the proposed system is fluctuating from 0 to 18 m. When it was further tested with fast turning point with a 50 s GPS outage, the error could rise to about 700 m [23].

Skog [106] presented loosely coupled position aided closed loop implementation of a GPS aided INS system, as shown in Figure 2.9. The KF denotes EKF and H the map between navigation output and GPS data. The result of test trajectory is presented in Figure 2.10. The RMSE of standalone GPS is 13.7987 m and this error can be reduced to 2.0948 m with the aid of INS and EKF.

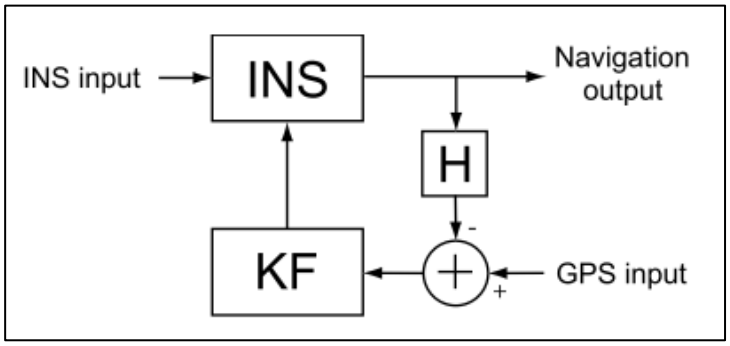

Figure 2.9: Loosely Coupled Position Aided Closed Loop Implementation of a GPS Aided INS System [106]

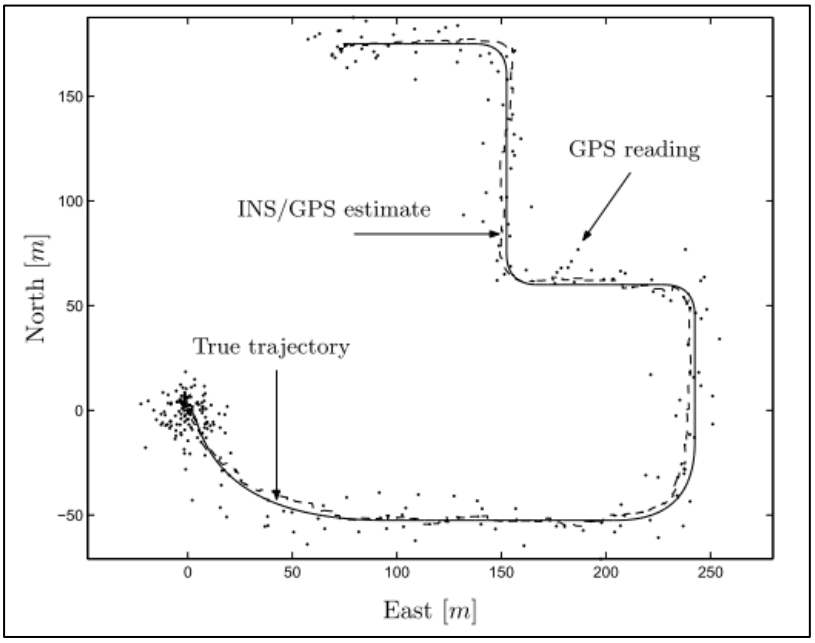

Figure 2.10: Estimated and True Trajectory of a Typical Driving Sequence [106]

UKF algorithm is utilized in GPS/INS navigation and the simulation results indicate that UKF can maintain better filter stability than KF [107]. From Figure 2.11, it can be observed that the error of estimated data can be improved from 500 m to 100 m. The position error is able to be maintained in a range of 100 m.

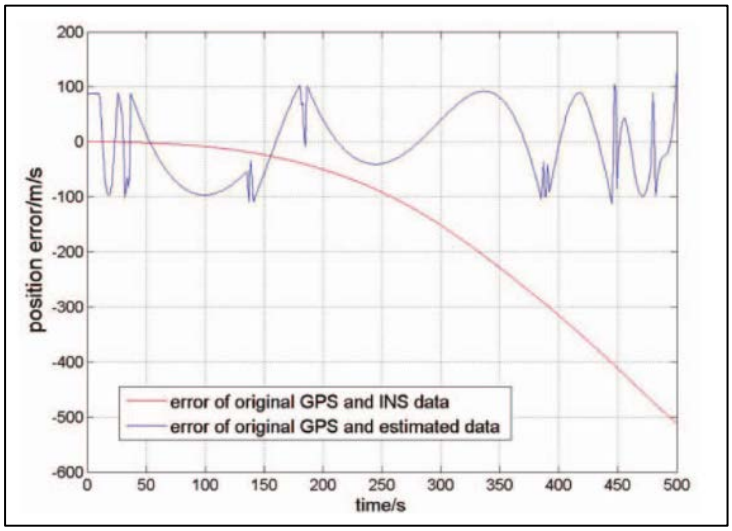

Figure 2.11: Contrast Diagram of Error of the Original GPS Data and INS Data, Error of GPS Data and Optimal Estimated Data [107]

There is another kind of Kalman Filter (KF), namely Cubature Kalman Filter (CKF). To be more advanced, there are Strong Tracking Cubature Kalman Filter (STCKF) [28], Central Difference Kalman Filter (CDKF) and High Degree Cubature Kalman Filter (HDCKF) [108]. STCFK is presented for simulation and the results show that it is outperforming if compared to EKF. The author also claimed that STCKF has the advantages of high reliability, low sensitivity, strong robustness and strong stability and convergence [28]. The simulation results in [108] show that HDCKF gives superior performance for all navigation states if compared to non-linear filters such as EKF, UKF, CKF and CDKF.

KF has some restrictions such as requisite of predefined accurate stochastic model as well as prior information of measurement covariance matrices for each new sensor [37]. During the system linearization process or system mismodeling, divergence of approximation results is possible. Consequently, the systems based on Artificial Intelligence (AI) have been suggested as solution.

2.4.4 Artificial Intelligence (AI)

Currently, comprehensive research has been done in the field of Artificial Intelligence due to its potential to be implemented in every single application in life. Among AI, fuzzy and neural network are commonly used and investigated.

The Adaptive Neuro-Fuzzy Inference System (ANFIS) is an AI-based system that is proposed to improve the performance of KF-based GPS/INS with fuzzy correction algorithm in the absence of GPS signals [109]. The ANFIS has a set of trained data about the evolution of INS errors in several scenarios to provide adaptive positioning.

The ANFIS fuzzy correction system calculates the variation between INS data with the trained data to compute a location with minimized error probability. This system can execute a result with 7 times better accuracy through the implementation of fuzzy correction [38]. The accuracy for position, velocity and angle are greatly enhanced.

In past few years, inertial sensor based on Micro-Electro-Mechanical System (MEMS) has been considered to be implemented in INS/GPS navigation applications as it is commercially available at lower cost [15]. The performance enhancement with first order Gauss Markov (GM), second order Auto Regression (AR) and ANFIS is performed and compared. KF-ANFIS shows its outperforming over KF-GM and KF-AR with better accuracy and consistency over the trajectory [15].

Besides ANFIS, more systems based on Artificial Intelligence (AI) have been suggested as solution to KF-based GPS/INS scheme. The AI-based systems to assist KF include Radial Basis Function Neural Network (RBFNN) [110], Input-Delayed Neural Network (IDNN) [111] and so forth.

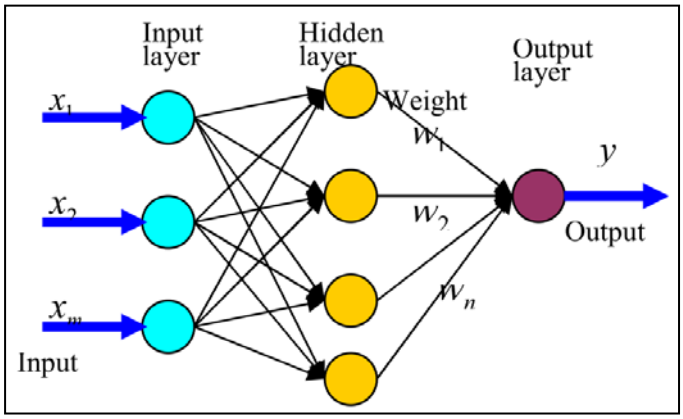

Figure 2.12: Architecture of RBFNN [112]

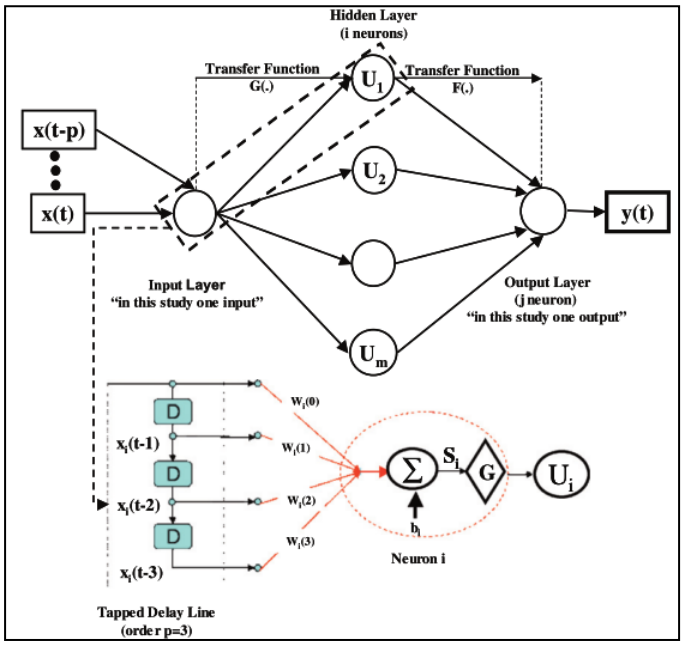

Figure 2.13: Architecture of IDNN [37]

GPS/INS scheme that uses RBFNN as improvement solution is because of its simple architecture, universal approximation and fast training [113]. RBFNN is a feed forward three layers network, which comprises input layer, hidden layer and output layer [114]. The architecture of RBFNN is as shown in Figure 2.12. Mapping is nonlinear from input to output while the output is linear to adjustable parameters. Even if RBFNN has

been claimed as has fixed topology and lack of dynamicity, it does show accuracy improvement [111].

In contrast, IDNN has high complexity with higher accuracy. The IDNN method holds the input data at the input layer through the input delay elements, allowing the output INS position to be modeled based on present and past samples [37]. From the architecture of IDNN shown in Figure 2.13, the complexity can be seen if compared to RBFNN. According to Noureldin *et al*., IDNN has superior performance during short term and long term GPS signal outages if compared to other conventional and recent AI-based systems [15].

Another recent AI-based approach in KF-based GPS/INS is Wavelet-based Neural Network (WBNN). The wavelet de-noising is able to remove the noise and disturbance of the signal before it is sent to neural network. This method is claimed to have better performance than standalone KF as the de-noised information allows neural network to provide better approximation [32].

2.5 Previous Works

Researchers are putting efforts in studies on positioning due to the high demand of civilians especially when vehicles' mobility is getting significant in the developed areas. There are two major categories of vehicle positioning, which are non-real-time vehicle positioning and real-time vehicle positioning.

Non-real-time vehicle positioning indicates the location of vehicle is logged and stored in database for reference purpose while real-time vehicle positioning means the

location of vehicle can be observed in real-time by driver and even by the control center in a distance away. The real-time vehicle positioning system can record the location of vehicle as well.

In addition, there are researchers who investigated into OBD-II and antenna to improve positioning technologies. Thus, the previous work of these researchers will be mentioned in sub-topics in the following section.

2.5.1 Non-Real-Time Vehicle Positioning

Generally, researchers carry out experiments or road tests of non-real-time vehicle positioning due to observation purpose and the recorded data can be further analysis better. Franca and Morgado [42] proposed a real-time implementation of integrated INS/GPS algorithm by using Real Time Workshop (RTW) and xPC Target toolboxes. According to the paper, the INS/GPS system (Figure 2.14) was mounted on a vehicle which traveled a georeferenced path with the results recorded and evaluated later. The results are not displayed in real-time or sent to monitoring center in real-time so it is categorized as non-real-time vehicle positioning.

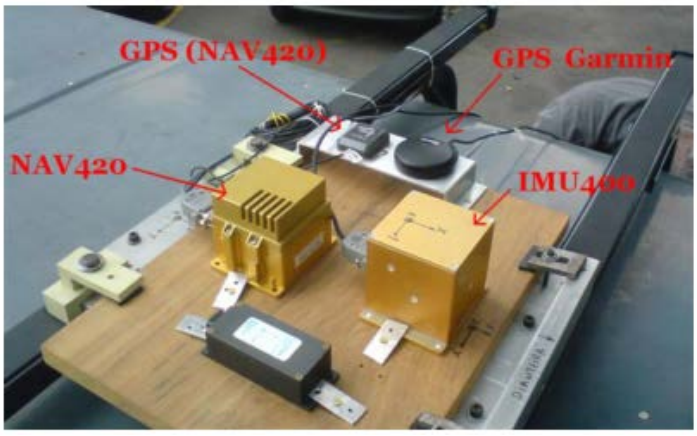

Figure 2.14: INS/GPS System [42]

The test results show that the signal appears to be available and unavailable along the trajectory in between 300th second to 1000th second, as shown in Figure 2.15. The time of signal outages is random and the duration of signal outages is considered as short. The results show that the latitude error maintains in the range of 25 m while the longitude error stays in the range of 20 m. The size of the Inertial Measurement Unit (IMU) deployed in this experiment is bulky (as seen in Figure 2.14) and is not practical for civilian users' real-time positioning. Moreover, the accuracy of the system should be further improved.

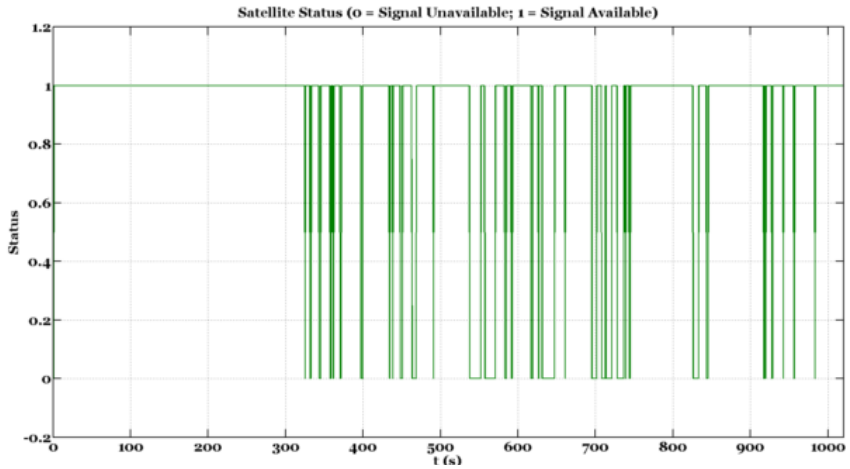

Figure 2.15: GPS Outages [42]

For IMM-EKF based Vehicle Navigation with low cost GPS/INS mentioned in [105], observation models were implemented for data fusion of raw measurements from sensors. The Single Model EKF(SM-EKF) provides a RMSE of 1.703 m and the Interactive Multi Model EKF (IMM-EKF) provides a RMSE of 1.219 m in a 45 second test drive on trajectory of 390 m [105]. The RMSE which is lower than 2 m is considered as great accuracy but the test drive time and test trajectory is too short.

A GPS/INS integration utilizing Dynamic Neural Network for vehicular navigation was introduced in [37]. The performance of IDNN module was examined during the artificial 100 s GPS outages which were intentionally introduced in order to test its ability

to perform prediction. The 100 s GPS outages were selected at different time slots and different locations. From the results in Figure 2.16 and Table 2.7, IDNN outperforms AI-based Segmented Forward Predictor (ASFP) and KF. For the 100 s GPS outage at different location, IDNN shows the maximum longitude error 33.50 m while maximum latitude error 30.93 m.

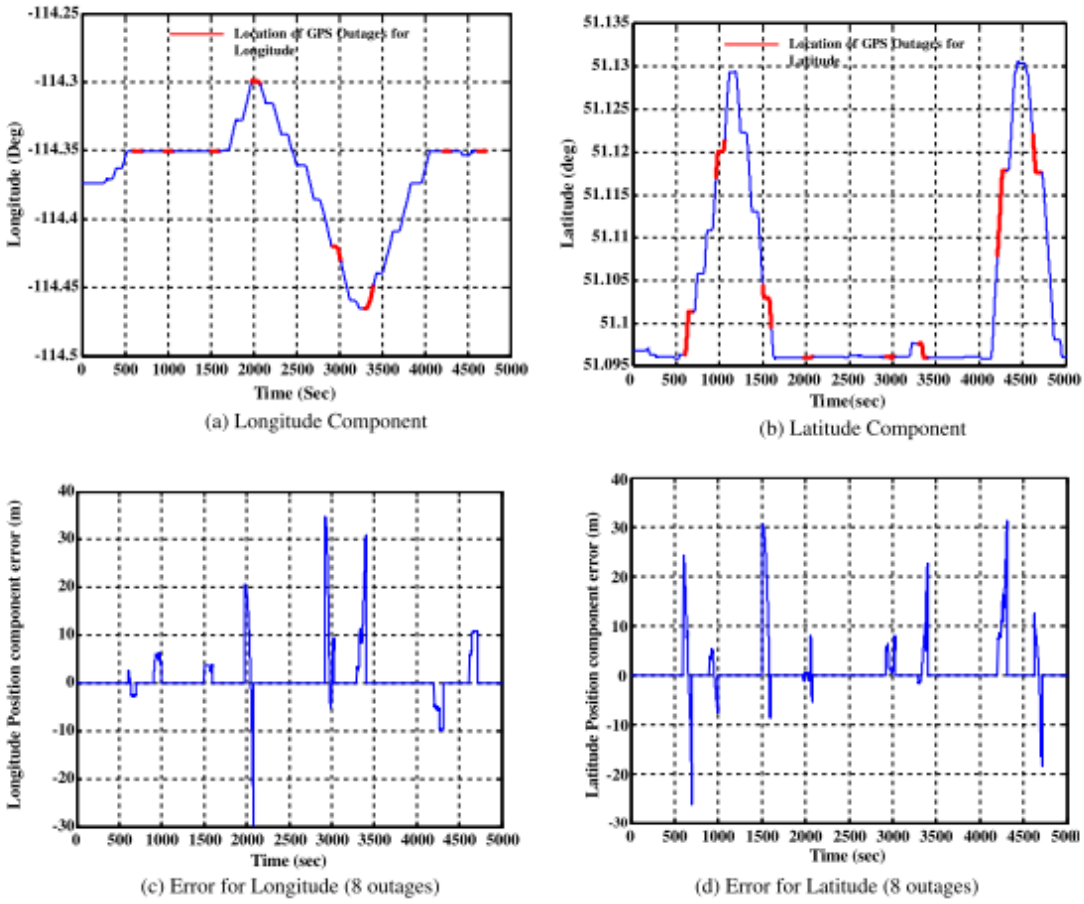

Figure 2.16: Position Error Distribution along GPS Outages [37]

Table 2.7: Summary of Position Errors for 100 s GPS Outages [37]

Position Component	Method	1st Outage	2nd Outage	3rd Outage	4th Outage	5th Outage	6th Outage	7th Outage	8th Outage
Longitude	IDNN	2.86	5.92	2.53	30.05	33.50	30.91	9.82	10.13
	ASFP	3.71	5.49	14.11	43.33	44.51	34.49	10.63	11.32
	KF	7.09	10.25	21.21	63.26	70.19	41.15	13.85	16.08
Latitude	IDNN	26.25	8.45	30.32	8.20	8.25	22.12	30.93	18.95
	ASFP	26.09	17.86	31.82	7.87	21.71	31.16	28.21	25.32
	KF	29.43	24.14	40.32	11.51	35.16	45.92	40.32	69.27

On the other hand, a low cost 2D navigation using augmented KF/Fast Orthogonal Search (FOS) module for integration of reduced inertial sensor system and GPS was suggested by author in [115]. The MEMS-grade gyroscope, OBD-II device Carchip, and off-the-shelf NovAtel G2 Pro-Pack SPAN unit were installed in a land vehicle for road test experiment purpose.

The data were logged and then evaluated after experiment. In each trajectory, several artificial 60 s and 120 s GPS outages were intentionally introduced. KF/FOS module shows improvement if compared with KF-only method. The RMS position error of KF/FOS module improves KF-only method from 30.98 m to 9.87 m (as shown in Table 2.8).

Table 2.8: Positioning Errors of KF/FOS and KF-only Methods during 120s Outages [115]

GPS Outage	Avg Speed (km/h)	App. Dist. (km)	KF/FOS max pos. err. (m)	KF-only max pos. err. (m)	KF/FOS RMS pos. err. (m)	KF-only RMS pos. err. (m)
1	63.7	2.1237	7.71	47.08	5.40	26.29
2	67.1	2.2371	27.00	94.37	10.94	43.87
3	73.3	2.4439	11.22	42.32	5.33	23.53
4	100.8	3.3597	25.87	91.19	13.19	43.18
5	108.0	3.5999	14.92	40.44	10.78	23.59
6	78.6	2.6188	17.83	46.74	10.64	20.83
7	60.4	2.0141	16.63	37.64	9.78	14.56
8	49.4	1.6469	20.97	101.77	9.88	39.76
9	64.1	2.1357	14.00	37.71	8.63	22.78
10	39.2	1.3064	25.53	90.99	14.16	51.41
Average	70.5	2.3486	18.17	64.03	9.87	30.98

A method using neural network (NN) and wavelet-based de-noising technology was introduced into the Strapdown Inertial Navigation System (SINS)/GPS/magnetometer integrated navigation system to improve the system accuracy. The current application of the wavelet-based de-noising technique is based on Matlab implementation. Thus, the author suggested that adaptive technique to be applied in real scenario with performance enhancement.

Among the learning algorithms, Levenberg-Marquardt Algorithm (LMA) was chosen. The NN with five or more hidden neurons can be successfully trained. Meanwhile, the training process shows that NN with nine neurons has the least number of learning steps and thus the number of hidden neurons is set to be nine.

Several road tests on NN were conducted on a land vehicle as shown in Figure 2.17 with the setup of navigation grade INS PHINS, a fiber optical gyro (FOG)-INS, a magnetometer and a TRIUMPH-1 GPS receiver. The GPS signals were artificially blocked in between 1000 s and 1500 s to observe the effect of GPS signal outages on system errors.

Figure 2.17: Test Vehicle and Setup of the IMU Systems [32]

When the GPS signal is normal, the position error remains below 4 m. During the 500 s GPS signal outages, the position error grows up to 30 m. With the NN-aided KF system, the position error improves significantly from 30 m to 10 m.

The experiment was further carried out with 10 artificial signal outages in order to evaluate the Wavelet-based NN (WBNN). Each outage was maintained to be below 100 s. The result of third outage segment is shown in Figure 2.18. The application of WBNN is showing an obvious improvement of the prediction if compared to the prediction with KF. The improvement can be seen in Figure 2.19 bar chart as well. KF gives mean of position error below 25 m while WBNN gives mean of position error below 10 m.

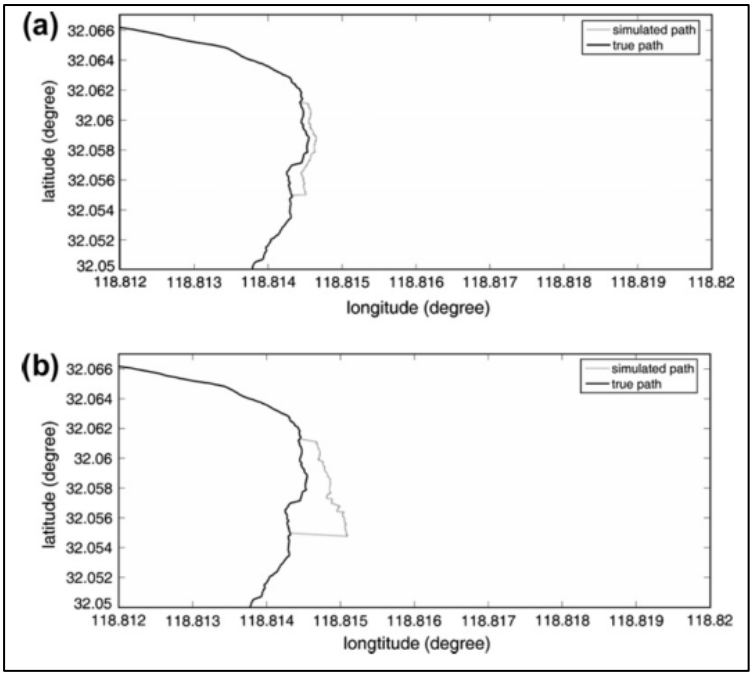

Figure 2.18: Result Trajectory (a) Result of WBNN (b) Result of KF [32]

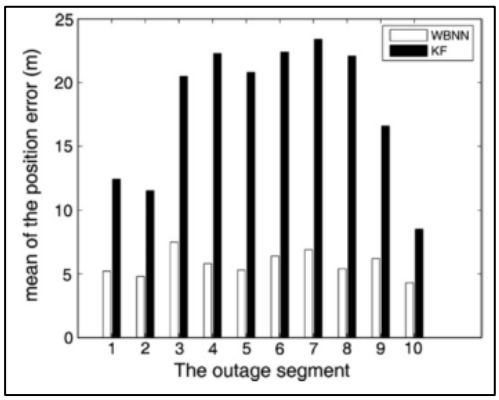

Figure 2.19: Mean Positioning Errors in 10 Outage Segments [32]

Liu *et al.* [116] introduced a two-filter smoothing for accurate INS/GPS land vehicle navigation in urban centers. In this paper, two types of algorithms are mentioned. Firstly, Two-Filter Smoother (TFS) which is performing by combining the results of Forward Kalman Filtering (FKF) and Backward Kalman Filtering (BKF) to minimize the error covariance. Secondly, Rauch-Tung-Striebel Smoother (RTSS) is an algorithm with optimal smoothing for linear system based on the maximum likelihood criterion. It can be considered as an add-on correcting factor to KF.

Like aforementioned systems, the GPS outages were intentionally applied on the collected data with the outage period 10 s, 30 s and 60 s. The post-processing data goes through the FKF, RTSS and TFS to evaluate the performance of each smoother. The mean position error for FKF in 60 s outage can grow up to 186.06 m while the RTSS and TFS can both improve the position error to 7.91 m [116].

Several authors [30, 33, 41, 43] carried out simulation works instead of apply the positioning/navigation technologies in real-time or practically. Moreover, some of these works do not make accuracy analysis neither in term of RMSE nor CEP [33, 43]. Without the accuracy evaluation, it is tough to define or compare the performance of the model or system developed.

2.5.2 Real-Time Vehicle Positioning/Monitoring

For real-time vehicle positioning/monitoring, the system can display the location of vehicle in real-time either in the vehicle or monitoring center. There is a design and development of farm vehicle monitoring and intelligent dispatching system where the

vehicle terminal has a GPS device, a GSM device and a display screen while the monitoring center has a GSM device and a computer [117].

At the vehicle terminal, the GPS device will update the location of vehicle in real time and display on screen. The GPS data is then packed with the vehicle's identity and sent to monitoring center through GSM device. The monitoring center will receive the data through GSM device and save the data in database. For high speed vehicle on road, data is transferred every 1 s. For low speed vehicle in field, data is transmitted every 10 s. This system is functioning without location prediction, which indicates the system will fail to provide location once the GPS signal lost.

Maurya *et al.* [118] proposed a real-time vehicle tracking system using GPS and GSM technology. A microcontroller AT89C51 is the core of the system on vehicle, interfacing the GPS receiver and GSM modem. The block diagram to illustrate the concept of the system is presented in Figure 2.20.

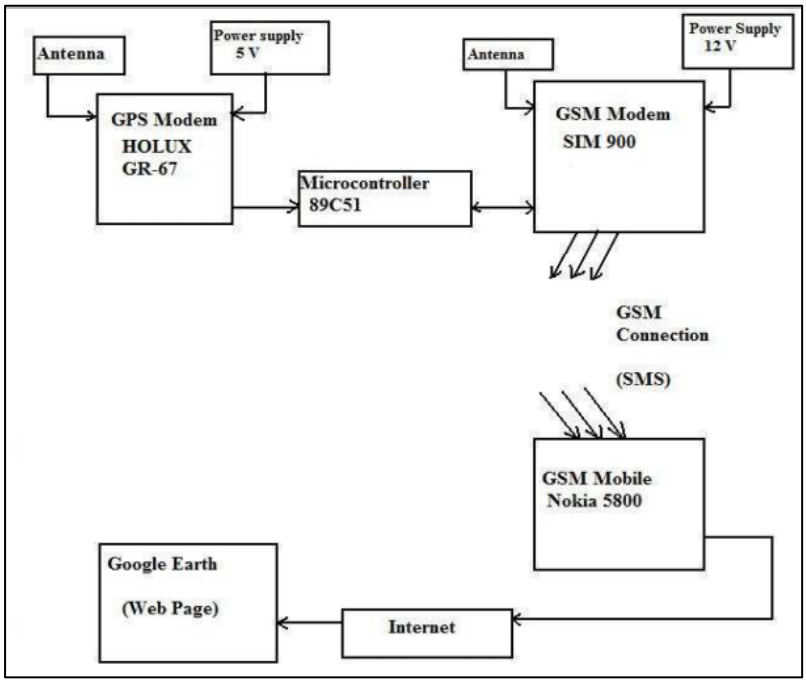

Figure 2.20: Block Diagram Illustrating the Concept of System [118]

The system will monitor a moving vehicle and report the position of the vehicle to the GSM mobile unit in the other end in real-time once request is sent by the user. The user can view the location of vehicle on Google Earth or Google Map with the existence of internet. However, the paper only presents the design of tracking system without showing the results. The concept is illustrated but the applicability and accuracy of positioning is doubtful.

Apart from the system above, several types of vehicle monitoring system based on GPS/GSM/GIS were introduced [119-122]. The design of these vehicle monitoring systems were presented in international conference papers and international symposium papers. In these papers, the authors emphasized on explaining the frameworks of system where as the real-time positioning is provided by GPS device, data transmission is done by GSM device or General Packet Radio Service (GPRS) device and mapping function is developed with Geographic Information System (GIS). Only the author in [120] performed the experiment and showed the successfulness of the real-time monitoring system with mapping function. However, there is no accuracy analysis and the experiment was carried out without consideration on the loss of GPS signal.

There is an intelligent vehicle monitoring system developed using global positioning system and cloud computing [123]. Data such as location, fuel level, altitude, tire pressure, driver conditions (drunken or not) and speed of the vehicle are sent to cloud server using GSM-enabled device [123]. However, this device will fail to pinpoint the location when GPS outage because it does not consider about the location in case of NLOS happens. Moreover, the researcher does not define the accuracy of the positioning in this system.

Real-time remote onboard diagnostics using embedded GPRS surveillance technology [124] is a completely developed vehicle monitoring system which is capable to read Diagnostic Trouble Code (DTC) through OBD-II in real time and transmit all the data including vehicle's ID, GPS data, vehicle's status and DTC to the server system through GPRS mobile communication. The OBD-II device is worth to be studied and utilized because it can provide a long list of vehicle's parameters that are useful to monitor the condition of vehicle.

This system is excellent to be taken as reference. Its server system interface display is illustrated in Figure 2.21. The system displays the location of vehicle, name of vehicle's owner, vehicle model, owner's contact number, vehicle's plate number, vehicle's issue, and suggested immediate solution. The main concern of this system is the DTC extraction and the communication method. The recommendation for this system is the addition of prediction model to overcome the NLOS issue that will cause the loss of the GPS data at certain area.

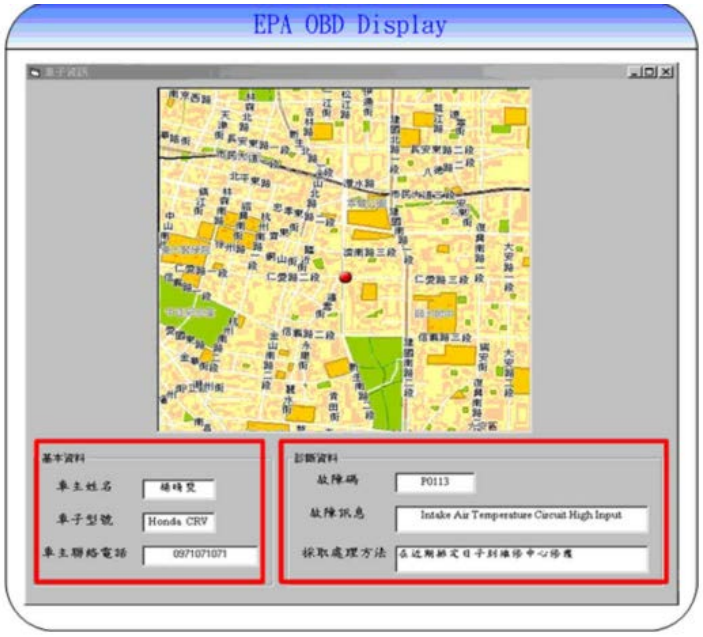

Figure 2.21: Server System Interface Display [124]

2.5.3 On-Board Diagnostics (OBD)-II

Every vehicle has dashboard with gauges that display details such as the distance, vehicle speed, engine speed and fuel level [125]. These details are in analog form and are retrieved from Electronic Control Unit (ECU). The On-Board Diagnostic-II (OBD-II) is a standard which was developed by Society of Automotive Engineers (SAE) in US [126] and it specification was made mandatory for all US vehicles staring in 1996 [127]. In 1996, every light duty car sold in the US has an OBD-II port. This is then followed by the integration of OBD-II port in medium duty car (2005) and heavy duty car (2010).

Subsequently, European Union (EU) made European On-Board Diagnostic systems (EOBD) an obligatory of petrol cars since 2001 and diesel cars since 2003 onwards [128]. In addition, Australia started emission control for light vehicles in 2005 based on OBD-II. From year 2008 onwards, gasoline vehicles in Taiwan are also compulsory to be outfitted with OBD-II system [129].

OBD-II is a very useful invention which is specially designed to diagnose the condition of a vehicle through raw data that is collected from ECU. OBD-II as a diagnostic tool checks the issue of a vehicle by sending the Parameter Identity (PID) to the vehicle through specific protocol and the signaling protocol will response to the particular request, displaying the issue on board.

The PIDs can be in hexadecimal or decimal form, each PID representing a code to request specific information. The PIDs include fuel system status, calculated engine load, engine coolant temperature, short term fuel trim, long term fuel trim, fuel pressure, engine RPM, vehicle speed, intake air temperature, throttle position, and so forth. Table 2.9 shows the example of OBD-II PIDs and its corresponding information.

Table 2.9: Example of OBD-II Command and its Description [130]

Mode/Service	PID	Description
01	01	Number of DTCs
01	04	Engine load
01	05	Engine coolant temperature
01	0B	Intake manifold absolute pressure
01	0C	Engine RPM
01	0D	Vehicle speed sensor
01	0F	Intake air temperature
01	10	Air flow rate from mass air flow sensor
01	11	Absolute throttle position

The OBD II had been standardized by SAE and upheld by International Standardization Organization (ISO) [128]. There are five communication protocols of OBD-II, as shown in Table 2.10. Different vehicle manufacturers deploy different kind of OBD-II protocol with different speed and signaling type. Though most of the vehicle manufacturers implemented OBD-II in the vehicles, Malaysia's local manufactured vehicles have not installed any.

Table 2.10: Communication Protocols and Signaling Protocols of OBD II [128, 131]

No	Protocol	Speed (kbps)	Signal Type	Manufacturer (s)
1	SAE J1850 (VPW)	10.4	Variable Pulse Width	GM Vehicles
2	SAE J1850 (PWM)	41.6	Pulse Width Modulation	Ford Vehicles
3	ISO 9141-2	10.4	Asynchronous Serial Communication	European, Asia and Chrysler Vehicles
4	ISO 15765-4 (CAN)	500	Single/Dual Wire Serial Lines	Most Vehicle Manufacturers
5	ISO 14230-4 (KWP 2000)	10.4	Asynchronous Serial Communication	European, Asia and Chrysler Vehicles

The interface of OBD-II port is as shown as in Figure 2.22. OBD-II has 16 pins and each of them in charge of different function. The function description of each pin is listed

in Table 2.11. The OBD-II scanning tool or OBD-II reader is designed to interface with the vehicle via the OBD-II 16-pins port. The price is varies from RM10 to RM1000, depending on the specifications and functions of the scanning tool or reader. The example of Bluetooth OBD-II scanner is shown in Figure 2.23.

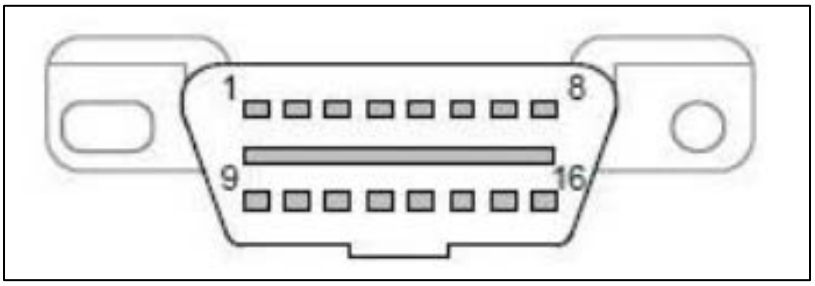

Figure 2.22: The Interface of OBD-II Port [126]

Table 2.11: Vehicle Connector Contact Allocation of OBD-II [129]

Pin No	Allocation
1	Discretionary
2	Bus positive line of SAE J1850
3	Discretionary
4	Chasis ground
5	Signal ground
6	CAN_H line of 15765-4
7	K line of ISO 9141-2 and ISO 14230-4
8	Discretionary
9	Discretionary
10	Bus negative line of SAE J1850
11	Discretionary
12	Discretionary
13	Discretionary
14	CAN_L line of 15765-4
15	L line of ISO 9141-2 and ISO 14230-4
16	Permanent positive voltage

Figure 2.23: Bluetooth OBD-II Scanner [132]

The data flow of data acquisition of OBD-II is as shown in Figure 2.24. Firstly, a smartphone is connected to OBD-II scanner (ELM327) through bluetooth connection and the OBD command is sent through queue. The scanner will read the command and send the instruction to ECU while ECU will retrieve data acquired from vehicle sensors through the specific protocol. The data which is obtained from sensors will be sent to buffer before outputted to smartphone through the scanner.

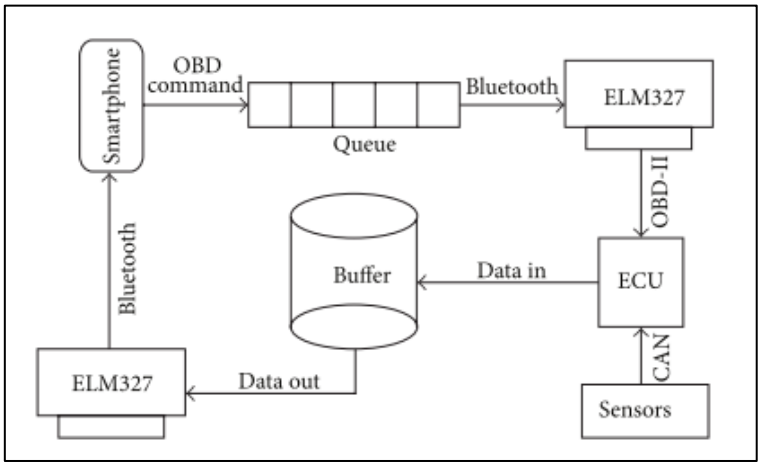

Figure 2.24: Data Flow of Data Acquisition [130]

Besides the deployment of OBD-II in [124] as surveillance system, it is used by the researchers in development of driver information system [125, 128] as well as vehicle

management and safety [133]. The information extracted from the OBD-II is majorly used to diagnose the vehicle's issue. There is no research that utilizes the OBD-II data for positioning purpose.

2.5.4 Antenna

Since this dissertation is studying about smartphone-based GPS-integrated location prediction model for vehicle location, the antenna of smartphone which in charge of signal retrieval is necessary to be studied as well.

The fourth generation of GSM (4G) has been widely used and it is considered as mature technology. However, it is noted that antenna of 4G mobile phone is mainly focus on land communication and is not specially designed for satellite communication. The fifth generation of GSM (5G) mobile phone may include the function of satellite communication. Mobile satellite communication service is claimed as a complement to current technology as it includes safety communications, broadcasting and accurate global positioning [134]. The design of antenna in the mobile phone is very important as it needs to be designed to specific radiation pattern that is able to cover complete azimuth range and wide range of elevation angles.

According to the author in [49], Right-hand circular polarization (RHCP) is universally required for GNSS. The axial ratio (AR) less than 3 dB and cross polarization less than -10 dB is desired for medium quality GNSS antenna. A compact circular polarized patch antenna with wide beamwidth for handheld devide for future 5G application has been presented and it is proven to cover wide elevation angles and

complete azimuth range of 360 degree [134]. The result is promising where the medium gain is 5 dBic and the measured 3 dB axial ratio bandwidth is 3.05%.

Research on a compact GPS/WLAN antenna design for mobile device with full metal housing was carried out [135]. A contact tri-band antenna (GPS band, WLAN b/g band and WLAN a band) was proposed and fabricated for mobile phone application. The average measured gains at the three bands are about 0.5, 3 and 3.5 dBi respectively.

The authors in [136] realized that variety of GPS antennas are designed according to Right-Handed Circular Polarized (RHCP) theory. Since linear polarized antenna has better coverage, more convenient to be designed and more cost-saving, some linear polarized GPS antennas have been done. A dual-band Planar Inverted-F Antenna (PIFA) for GPS and WiMAX applications was designed to provide linear polarization which is anticipated to alleviate the multipath fading of circularly polarized GPS antenna [136]. This design exhibits good impedance matching performance, relatively high gain and wide reception angle from satellite constellation. It is thus suitable to be implemented as the antenna of the new generation of mobile phone to provide good satellite signal reception.

To further study on PIFA, it is compact and is able be designed in the housing of the mobile phone instead of the use of whip, rod or helix antennas. Besides, PIFA can depreciate the electromagnetic wave power absorption or so called Specific Absorption Rate (SAR), reduce the backward radiation toward user's head and improve antenna performance. Moreover, it presents moderate to high gain in both states of vertical and horizontal polarization which is useful in certain wireless communication under multipath scenarios [137].

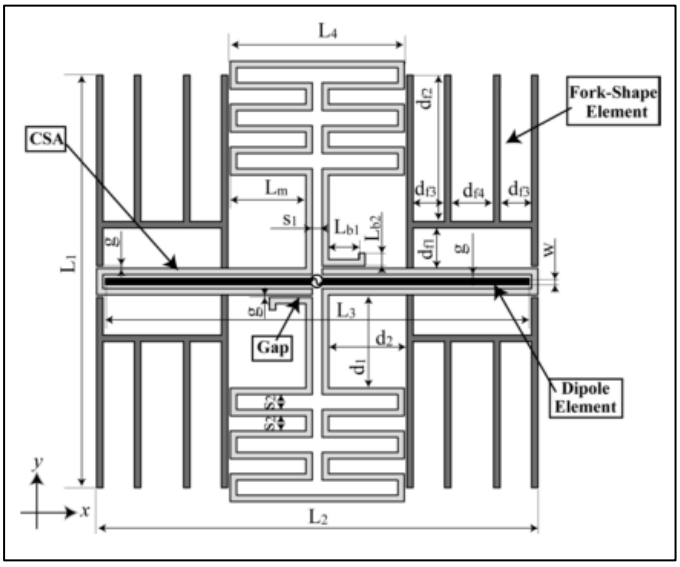

Figure 2.25: Design of Electrically Small Three-Band Multi-polarization Cross Spiral Antenna [138]

An electrically small three-band multi-polarization cross spiral antenna has been designed [138] and the design is as shown in Figure 2.25. It is a planar structure design which is printed on single side of circuit board. The three bands are GPS band, RFID band and mobile phone band while the multi-polarization is realized by circular polarization (CP) and linear polarization (LP). Its multi-polarization is achieved by using a dipole-fed cross spiral antenna (DF-CSA) [138]. This design can radiate good CP and LP with 0 dBi or more gain and 62% or more efficiency within 28 MHz bandwidth.

A small size planar dual wideband antenna for ultra-slim smartphones was proposed. The proposed antenna design involves a directly fed inverted L-shaped feeding strip, branch strip coupled to feeding strip with inductor, an inductively loaded shorted strip, and a matching circuit like shown in Figure 2.26. This design is proven to support multiple communication protocols including the GPS/GLONASS, DCS, PCS, UMTS2100, Bluetooth LTE2300/2500/3400 and 2.4-GHz WLAN and WiMAX 2.3/2.5/3.5GHz bands [139].

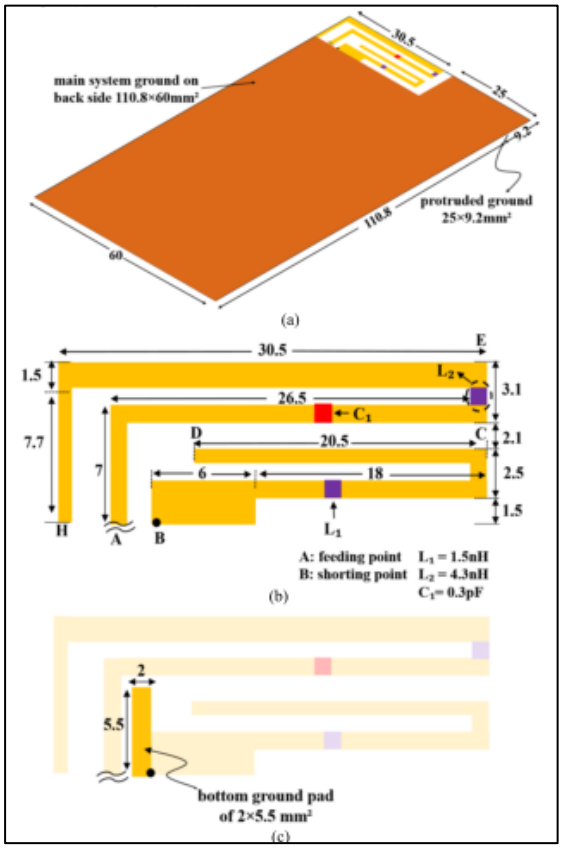

Figure 2.26: Proposed Antenna Structure (a) Overall View (b) Front View (c) Bottom View [139]

For the antenna design in Figure 2.27, T-shaped feeding strip and an encircled T-shaped parasitic shorted strip formed a coupled-fed antenna to achieve a low-wideband and high-wideband. The low-wideband and high-wideband are covering GSM850/900 bands and GSM1800/1900/UMTS2100/LTE2300/2500 bands. On the other hand, a loop antenna working at 1/2 wavelengths is formed to cover the bands of GPS, GlONASS, Galileo and COMPASS [140]. The switching between two kinds of antenna is controlled by a PIN diode. The proposed antenna is able to achieve effective impedance matching in the desired bands [140].

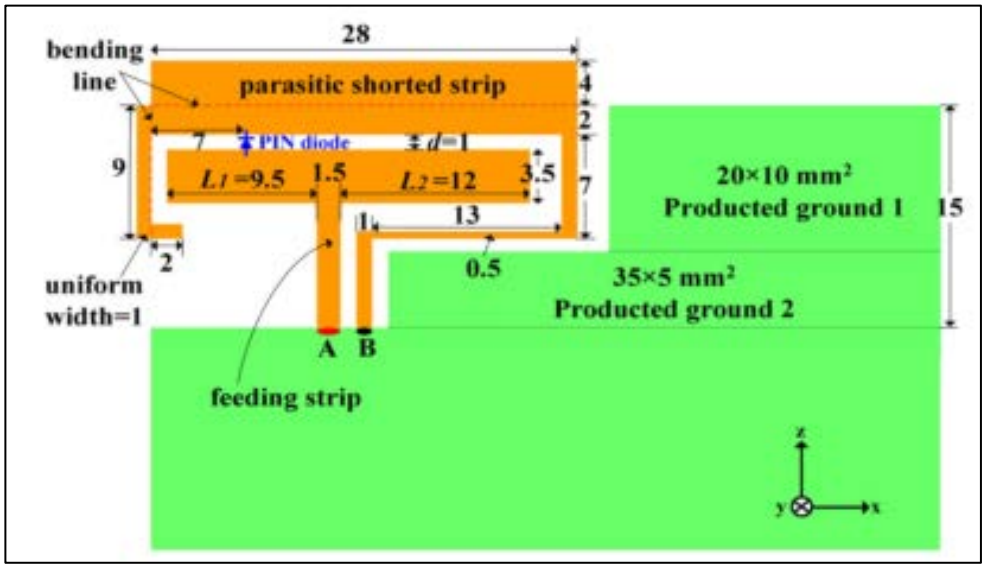

Figure 2.27: Dimensions of Metal Pattern in Antenna Area [140]

The antennas that were specially designed by researchers in [127-133] are suitable to be implemented in current smartphone to improve the GNSS signals receive. This can enhance the use of smartphone as a positioning device for vehicle localization purpose.

2.6 Performance Assessment

The positioning requirement parameters are accuracy, coverage, integrity, availability, continuity, update rate, applicability, reliability and latency. This research work assesses the performance in term of continuity and accuracy. The continuity can be verified by testing at area with LOS and NLOS conditions. The accuracy will be evaluated through the calculations that are described later.

Accuracy of positioning technology is a measurement that defines how close the measured location is to the actual location. The closer measured location to the actual location indicates higher accuracy and better performance. There are three types of

accuracy measurements, which are Root Mean Square Error (RMSE), Circular Error Probability (CEP) and Horizontal Positioning Error (HPE). The categorization of performance assessment is presented in Figure 2.28.

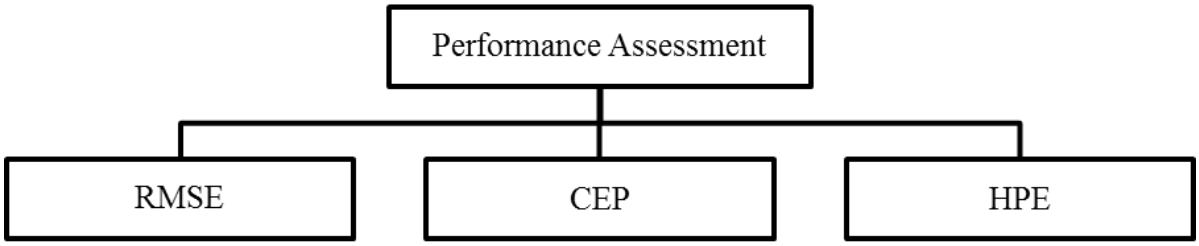

Figure 2.28: Performance Assessment

2.6.1 Root Mean Square Error (RMSE)

Root Mean Square Error (RMSE) is widely used in accuracy evaluation of positioning and the equation is as below:

$$\mathrm{RMSE} = \sqrt{\frac{\sum_{i=0}^{n}(\hat{x}_i - x)^2 + (\hat{y}_i - y)^2}{n}} \tag{2.8}$$

where (x, y) is the actual location while $(\hat{x}_i, \hat{y}_i)$ is the measured location with the subscript i denotes the i th of n realizations. This equation can be further simplified as following:

$$\mathrm{RMSE} = \sqrt{{\sigma_x}^2 + {\sigma_y}^2} \tag{2.9}$$

where σ_x is the standard deviation of horizontal positioning error while σ_y is the standard deviation of vertical positioning error.

To perform the calculation of this RMSE, the coordinates collected have to be converted into Universal Transverse Mercator (UTM). UTM is a 2-dimensional Cartesian coordinate system which provides horizontal position representation in terms of Easting and Northing on the planar surface of Earth. The system divides the Earth into sixty zones with the intersection of the equator and the zone's central meridian as the point of origin of each zone.

The WGS 84 Spatial Reference System describes the Earth as a oblate spheroid with equatorial radius, $a = 6378.137$ km and inverse flattening, $\frac{1}{f} = 298.257223563$. Assuming the point with latitude, φ and longitude, λ with a reference meridian of longitude, λ_0, the Easting and Northing value can be computed with formulas as shown from Equation 2.10 to Equation 2.20. By convention, in Northern Hemisphere, $N_0 = 0$ km and in Southern Hemisphere, $N_0 = 10000$ km. Also, by convention, initial point scale factor, $k_0 = 0.9996$ and $E_0 = 500$ km.

$$n = \frac{f}{2 - f} \tag{2.10}$$

$$A = \frac{a}{1 + n}\left(1 + \frac{n^2}{4} + \frac{n^4}{64} + \cdots\right) \tag{2.11}$$

$$\alpha_1 = \frac{1}{2}n - \frac{2}{3}n^2 + \frac{5}{16}n^3 \tag{2.12}$$

$$\alpha_2 = \frac{13}{48}n^2 - \frac{3}{5}n^3 \tag{2.13}$$

$$\alpha_3 = \frac{61}{640}n^3 \tag{2.14}$$

$$\lambda_0 = \text{Zone} \times 6° - 183° \tag{2.15}$$

$$t = \sinh\left(\tanh^{-1}\sin\varphi - \frac{2\sqrt{n}}{1+n}\tanh^{-1}\left(\frac{2\sqrt{n}}{1+n}\sin\varphi\right)\right) \tag{2.16}$$

$$\xi' = \tan^{-1}\left(\frac{t}{\cos(\lambda - \lambda_0)}\right) \tag{2.17}$$

$$\eta' = \tanh^{-1}\left(\frac{\sin(\lambda - \lambda_0)}{\sqrt{1+t^2}}\right) \tag{2.18}$$

$$E = E_0 + k_0 A(\eta' + \sum_{j=1}^{3} \alpha_j \cos(2j\xi')\sinh(2j\eta')) \tag{2.19}$$

$$N = N_0 + k_0 A(\xi' + \sum_{j=1}^{3} \alpha_j \sin(2j\xi')\cosh(2j\eta')) \tag{2.20}$$

Equation 2.10 to Equation 2.18 is equation to compute preliminary values and intermediate values. The Easting, E and Northing, N values can be obtained from the simplified equations, Equation 2.19 and Equation 2.20. The Easting and Northing values are the positions in term of kilometers. After conversion, the RMSE can be calculated by substitution of Easting and Northing values into Equation 2.8 and Equation 2.9.

Apart from the technique above, Spherical Law of Cosine can calculate the distance between 2 points with much easier and simpler formula. The distance calculated is same as the Root Mean Square Error (RMSE), where the equation of distance is

$$d = \cos^{-1}[\sin\varphi_1 \sin\varphi_2 + \cos\varphi_1 \cos\varphi_2 \cos\Delta\lambda] \times R \tag{2.21}$$

where φ is the latitude, λ is the longitude, $\Delta\lambda$ is the difference between 2 longitudes and $R = 6371000\text{m}$.

2.6.2 Circular Error Probability (CEP)

Another common way to evaluate accuracy of location measurement is Circular Error Probability (CEP). CEP is defined as the radius of a circle with center (x, y) and 50% of the measured locations are targeted to be within this circle. The basic equation of a circle with CEP as radius and (x, y) as center is

$$(\hat{x}_i - x)^2 + (\hat{y}_i - y)^2 = CEP^2 \tag{2.22}$$

where $\hat{x}_i$ is the moving x coordinate while $\hat{y}_i$ is the moving y coordinate. By assuming $u = (\hat{x}_i - x)$ and $v = (\hat{y}_i - y)$, the equation of a circle can be rewritten as below:

$$u^2 + v^2 = CEP^2 \tag{2.23}$$

Gaussian function is a probability density function of distributed variable that is widely used in statistic to describe the normal distribution. (u, v) is assumed as Gaussian variables with mean $(0,0)$ and variance $({\sigma_u}^2, {\sigma_v}^2)$.

$$P(u) = \frac{1}{2\pi\sigma_u} e^{-\frac{1}{2}\left(\frac{u}{\sigma_u}\right)^2} \tag{2.24}$$

$$P(v) = \frac{1}{2\pi\sigma_v} e^{-\frac{1}{2}\left(\frac{v}{\sigma_v}\right)^2} \tag{2.25}$$

The joint distribution of $P(u)$ and $P(v)$ is given by

$$P(u, v) = P(u) \times P(v) \tag{2.26}$$

$$P(u, v) = \frac{1}{2\pi\sigma_u} e^{-\frac{1}{2}\left(\frac{u}{\sigma_u}\right)^2} \times \frac{1}{2\pi\sigma_v} e^{-\frac{1}{2}\left(\frac{v}{\sigma_v}\right)^2} \tag{2.27}$$

$$P(u,v) = \frac{1}{2\pi\sigma_u\sigma_v} e^{-\frac{1}{2}\left[\left(\frac{u}{\sigma_u}\right)^2+\left(\frac{v}{\sigma_v}\right)^2\right]} \tag{2.28}$$

The double integral of the joint Probability Density Function (PDF) is equals to 50% as the requirement is that the CEP has a 50% probability of containing the target. This equation has to be solved in order to obtain the correct CEP value.

$$\iint P(u,v)dudv = 0.5 \tag{2.29}$$

$$\iint \frac{1}{2\pi\sigma_u\sigma_v} e^{-\frac{1}{2}\left[\left(\frac{u}{\sigma_u}\right)^2+\left(\frac{v}{\sigma_v}\right)^2\right]} dudv = 0.5 \tag{2.30}$$

Evaluation of equation above involves numerical approximation since the integral has no known anti-derivative except for some specific values of σ_u and σ_v. However, there is a formula which approximates the solution for the equation above which high degree of accuracy. The average error of this approximation is less than 1% and the maximum deviation is 1.5%.

When the error variables are uncorrelated and the Gaussian distribution is of mean $(0,0)$ and variance $({\sigma_u}^2, {\sigma_v}^2)$, the approximating formula for CEP may be used:

$$CEP = \begin{cases} \sigma_L(0.67 + 0.8w^2) & \text{if } 0 < w < 0.5 \\ 0.59\sigma_L(1+w) & \text{if } 0.5 \leq w \leq 1 \end{cases} \tag{2.31}$$

where

$$\sigma_L = \text{Maximum}\left(\sigma_{dx}, \sigma_{dy}\right) \tag{2.32}$$

$$\sigma_s = \text{Minimum}\left(\sigma_{dx}, \sigma_{dy}\right) \tag{2.33}$$

$$w = \frac{\sigma_s}{\sigma_L} \tag{2.34}$$

In [141], the formula of CEP is defined as

$$\text{CEP} = 0.62\sigma_y + 0.56\sigma_x \tag{2.35}$$

and the paper stated that it is accurate when $\frac{\sigma_y}{\sigma_x} > 0.3$.

In [142], the formula of CEP is defined as

$$\text{CEP} \approx 0.75\sqrt{{\sigma_x}^2 + {\sigma_y}^2} \tag{2.36}$$

where $\sqrt{{\sigma_x}^2 + {\sigma_y}^2}$ is the RMSE.

2.6.3 Horizontal Positioning Error (HPE)

Apart from the aforementioned popular ways to evaluate the performance of location prediction, Horizontal Positioning Error (HPE) is used to evaluate the accuracy of positioning. There is a formula namely Haversine Formula which can compute the distance between 2 coordinates. It is found that the obtained distance is the HPE of the measurement between the predicted coordinate and the GPS coordinate.

$$a = \sin^2\frac{\Delta\varphi}{2} + \cos\varphi_1 \cos\varphi_2 \sin^2\frac{\Delta\lambda}{2} \tag{2.37}$$

$$c = 2\text{atan2}(\sqrt{a}, \sqrt{1-a}) \tag{2.38}$$

$$d = RC \tag{2.39}$$

where φ is the latitude, λ is the longitude, $\Delta\varphi$ is the difference between 2 latitudes, $\Delta\lambda$ is the difference between 2 longitudes and $R = 6371000\text{m}$.

2.7 Chapter Summary

This chapter presents the satellite-based positioning, network-based positioning and location prediction techniques. The satellite-based positioning (GNSS, RNS and SBAS) techniques are recognized as mature technologies in the field of positioning, providing location with high accuracy. However, satellite-based positioning has the shortcoming of continuity. It cannot avoid NLOS issue. The positioning will fail to perform when the satellite signals are blocked or out of polarization. This is the point where the research on network-based positioning enters.

Cellular network can provide estimated location according to Cell-ID, RSS, AOA, TOA and TDOA. The Cell-ID and RSS with high reliability, high applicability and low cost have the worst accuracy which is 200 m to 1500 m. The AOA, TOA and TDOA are techniques with medium reliability and low applicability and medium/high cost give better accuracy, ranges from 50 m to 200 m. Thus, cellular network positioning is not considered.

WLAN positioning requires large amount of installation of WLAN access points and development of large fingerprint database. The data collection for the database is time consuming and the maintenance of the database requires a lot of efforts from manpower from time to time. Thus, it has low applicability especially if it is outdoor positioning. The NLOS and multipath signal propagation issue degrades the accuracy.

VaNet can be implemented if the vehicles are installed with devices that having compatible communication protocol, frequency band, range and data rate. WAVE is mature technology but it requires continuous service fees for constant positioning. VaNet is not commonly implemented due to the privacy and security issue.

A lot of researchers investigate on GPS/INS with aid of KF in the field of location prediction. Most of the experiments are carried out with low cost IMU and some of them are with bulky size. This is not practical and applicable in real life. IMU with high accuracy and small size is normally expensive. Therefore, it is suggested to use smartphone which is a daily essential device for civilian users and it is readily integrated with IMU.

AI gives improvement in location prediction but its application is limited because the research works are emphasizing on simulation works instead of real life application. DR is the simplest method of location prediction which requires the least parameters. However, the studied research papers show that the researchers are focusing on smartphone-based Dead Reckoning for pedestrian instead of vehicle.

According to the studied previous work, the non-real-time vehicle positioning systems are presented with simulation approach while those real-time vehicle positioning systems are mostly presented the design without further verification on the frameworks and without showing results or analysis. With a few of successfully developed systems, the authors do not focus on the positioning accuracy and do not consider the possibility of GPS signal lost.

OBD-II is appeared to be suitable to retrieve necessary data from vehicle while antenna of smartphone is found that can be modified to obtain great GNSS signals. Thus,

smartphone is considered as a major component of this research work with the aid of OBD-II device to retrieve data from vehicle.

Therefore, there is a need to have smartphone-based vehicle localization with integration of GPS and prediction algorithm. There are very less papers explaining about how to compute accuracy of positioning. Thus, the performance assessments of positioning are highlighted in this dissertation, making a clear vision on how to evaluate accuracy of positioning. In short, RMSE will be chosen for performance assessment in this thesis.

CHAPTER 3

METHODOLOGY

3.1 Overview

This chapter presents methodology that is set out to achieve the stated objectives. The primary objective of this research is to come out with a GPS-integrated location prediction model that can provide Vehicle Under Test (VUT) coordinates with reasonable accuracy under LOS and NLOS condition. The overall system architecture of integrating two different types of measurements, GPS and location prediction algorithm is explained. The chapter focuses on system architecture and conceptual framework. Apart from that, the system evaluation and validation are clarified by showing the methods of data collection and data analysis.

3.2 System Architecture

Figure 3.1 presents the methodology flow chart of system development. Firstly, the key parameters for location prediction are identified. A list of parameters in the field of positioning is listed out in Table 3.1 according to the studies in Chapter 2. The most appropriate parameters will be chosen from this list as the key parameters. For example, if dead reckoning method is chosen, position updates, distance travelled and heading direction will be selected as key parameters.

This is following by application programming to obtain the key parameters. If the application fails to obtain the key parameters, the process will be loop back to design and

program again. If the application successes, the process proceeds to the formulation of location prediction algorithm and testing.

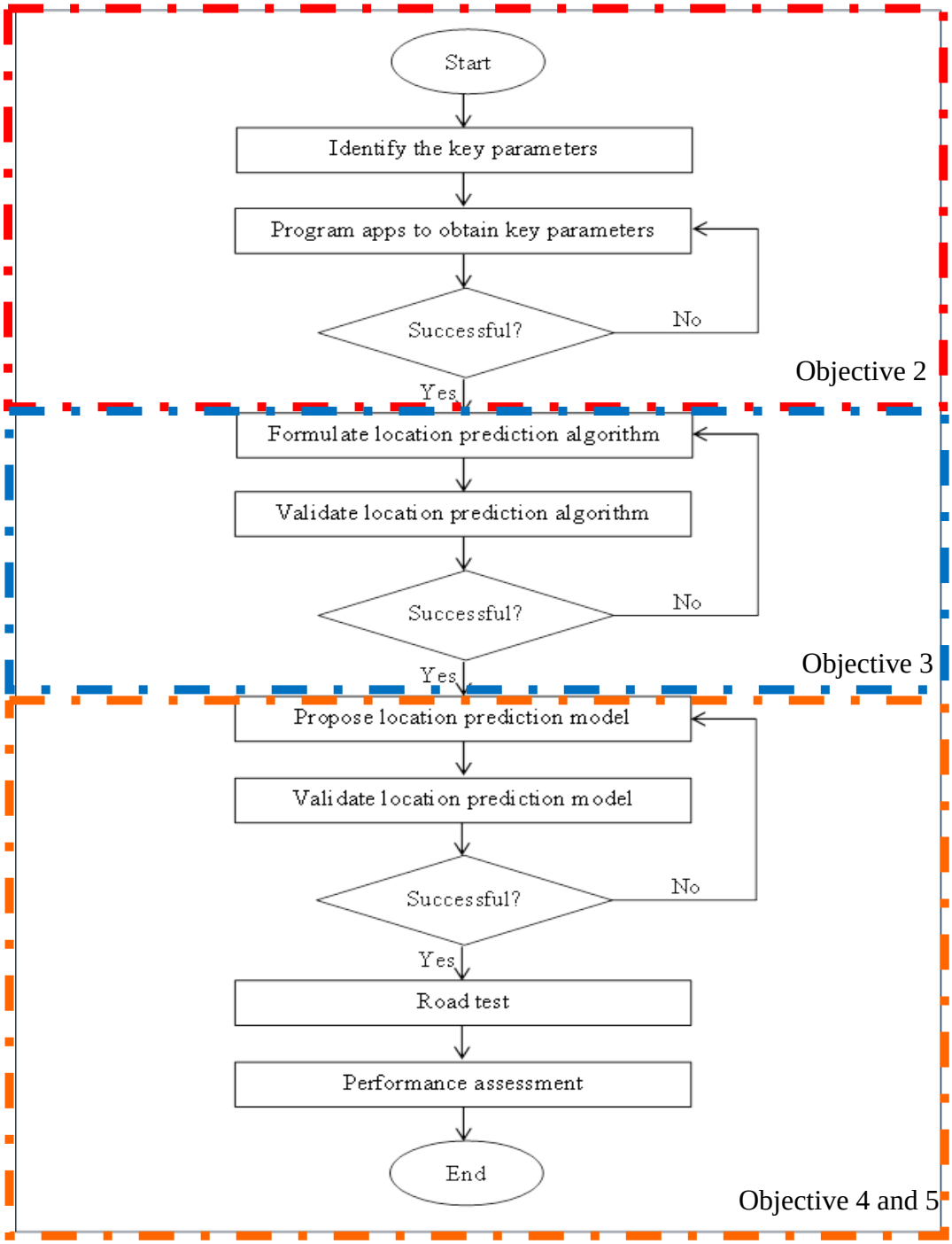

Figure 3.1: Methodology Flow Chart

Table 3.1: Location Prediction and Parameters

Location Prediction	Parameters	Devices
DR	Position/velocity updates	GPS
	Distance travelled	Odometer
	Heading direction	Accelerometer Gyroscope Magnetometer
INS	Body's specific force Angular rate Magnetic field	Accelerometer Gyroscope Magnetometer
	Altitude	Altimeter
	Velocity	Air speed/wind estimation
	Heading direction	Compass
	Pixel video updates	Video sensor
	Position/velocity updates	GPS
	TOA	COMM
KF	Position/velocity	GPS
	Heading direction	Accelerometer Gyroscope Magnetometer
	Steering angle	Steering angle sensor
	Throttle setting	Throttle
	Braking force	Brake

If the location prediction algorithm validation process fails, the formulation and validation will be continued until it success. Next, the loosely-coupled integration of GPS with location prediction model will be performed. Then, the location prediction model and its validation will be carried out. This process will be going on until success. Consequently, road tests will be performed and the performance assessment will be done.

This research attempts to propose a simple smartphone-based GPS-integrated location prediction model that can provide the vehicle's coordinates with reasonable accuracy under LOS and NLOS condition. The proposed system architecture is as shown in Figure 3.2.

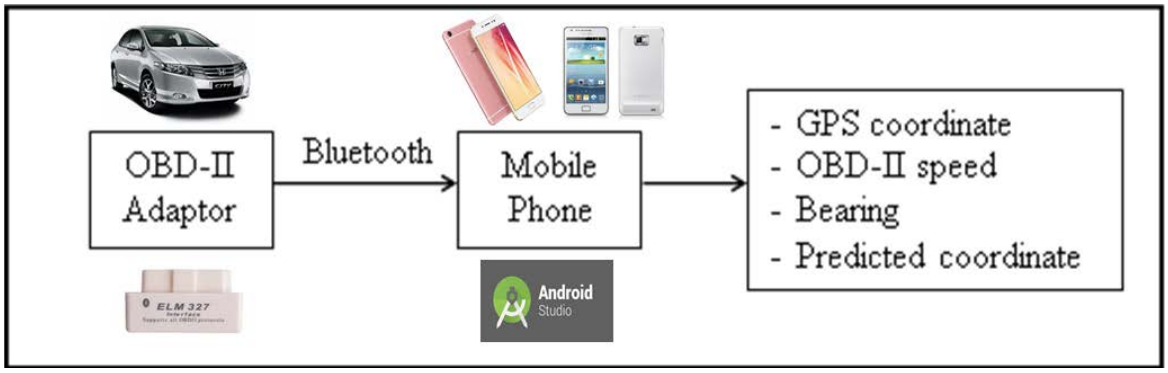

Figure 3.2: Proposed System Architecture

OBD-II is an automotive device that is able to diagnose and capable to report the vehicle's problem through ECU. With the implementation of OBD-II scanner or reader on vehicle, vehicle owner or mechanic can access the various parameters by PIDs and identify the malfunction parts within seconds. The standardized digital communication port can provide real-time data, showing the status of the various vehicle subsystems. Thus, the various valuable information obtains from OBD-II should be utilized.

Malaysia's local manufacture vehicles do not have the ECU and OBD-II but most of the Asian vehicles such as Toyato and Honda have. Thus, any vehicle that equipped with ECU and OBD-II can utilize this smartphone-based GPS-integrated location prediction model for localization.

With the smartphone application, the information obtains from OBD-II can be accessed in real-time. The information includes GPS latitude, GPS longitude, GPS speed and GPS heading direction/bearing as well as vehicle's speed. This data is helpful in positioning under LOS condition. While under NLOS condition, the last known coordinate, vehicle's speed and vehicle's heading direction/bearing are needed to predict the next location. Thus, an android application coding was written to log the vehicle's heading

direction/bearing as there is no ready-made application available with this function. The android application can be written through Android Studio (Figure 3.3).

Figure 3.3: Android Studio

With the collaboration of the data from both OBD-II and smartphone's sensors, the GPS-integrated location prediction model can be performed. The GPS will provide the location when the number of visible satellites is adequate. If the number of satellites detected is not sufficient, the location prediction will be activated to give predicted coordinates of the vehicle.

3.3 Conceptual Framework

The proposed system of smartphone-based GPS-integrated location prediction model for OBD-II-equipped land vehicle localization will work as shown in Figure 3.4. This integration system is loosely coupled. According to Figure 3.4, the system will firstly check the number of satellites. If the number of satellites is more than 4, the GPS latitude and longitude will be displayed. If the number of satellites is less than 4, the location prediction algorithm will take over the task. The location prediction algorithm will compute the next location with the last known coordinate, vehicle's speed and vehicle's

heading direction/bearing. The predicted coordinates are then proceeded to check accuracy and analysis.

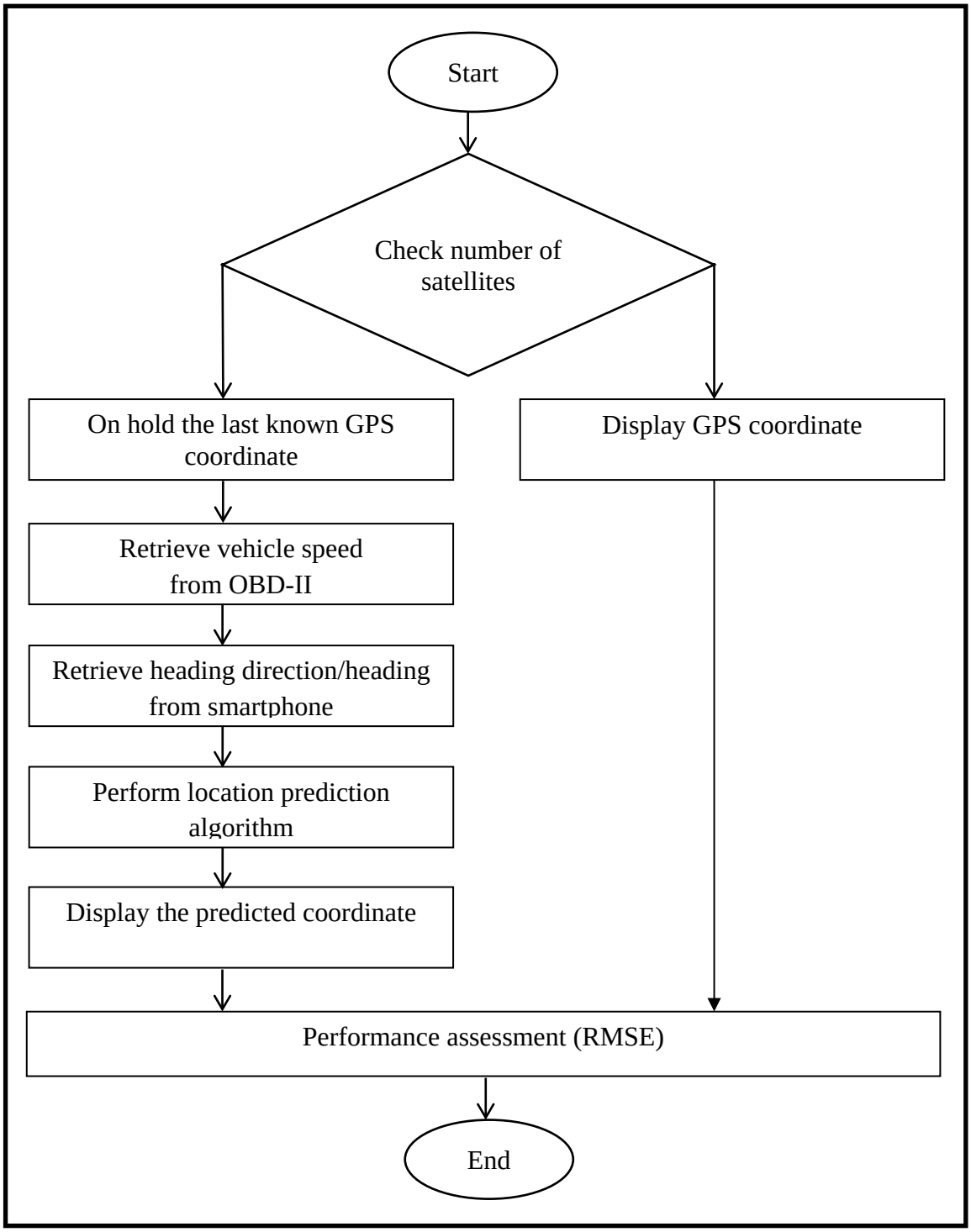

Figure 3.4: Conceptual Framework

3.3.1 Data Retrieval and Manipulation

Prior to the experimental works, an in depth fundamental study on the positioning technologies is carried out to comprehend the theories available. With the comprehensive understanding on GPS and location prediction approaches, OBD-II adaptor ELM 327, OPPO F1 Plus and Samsung Galaxy S2 are selected as experimental devices. The specifications and functionality of these devices are studied in order to be used in the experimental works. Nevertheless, a prediction algorithm is suggested for the location prediction during the GPS signal outage. The devices are to be installed on a personal land vehicle, namely Honda City (as shown in Figure 3.8), for experimental purpose.

The OBD-II adaptor ELM 327 is shown in Figure 3.5 and its specifications are shown in Table 3.2. Its dimension is 48mm x 25mm x 32mm, perfectly light and small. It will be installed in the chosen car, Honda City by just plugging in to the OBD-II socket, which is located under the steering of the car. It communicates and transfers data through Bluetooth connection. The Bluetooth range is 5 m to 15 m. This device can provide a long list of vehicle's parameters including engine RPM, coolant temperature, fuel system status, air flow rate, fuel pressure, and so forth. The number of parameters ranges from 4,000 to 15,000. This device is installed mainly to obtain the vehicle's speed.

Figure 3.5: OBD-II Adaptor ELM 327

Table 3.2: ELM 327 Bluetooth Specifications

	ELM 327 Bluetooth Specifications
Size	48mm x 25mm x 32mm
Supported OBD-II Protocols	J1850 PWM (Ford Vehicles) J1850 VPW (GM Vehicles) ISO9141-2 (Asian, European, Chrysler Vehicles) ISO14230-4 (Keyword Protocol 2000) ISO15765-4 (CAN)
Bluetooth Range	5-15 meters
Baud Rate	9600 or 38400
Operating Voltage	12/24V
Nominal Idle Current	45mA
Operating Temperature	-20º to 55º C
Operating Humidity	10 to 85%

In order to extract data from OBD-II adaptor, a smartphone is needed. The smartphone has to consist of GPS and Bluetooth connectivity in order to obtain GPS data and vehicle's speed. The smartphone OPPO F1 Plus (Figure 3.6) with these two functions is deployed. To be further discussed, this smartphone has accelerometer and gyroscope but does not have compass/magnetometer. These are shown in Table 3.3.

Figure 3.6: OPPO F1 Plus

Table 3.3: OPPO F1 Plus Specifications

	OPPO F1 Plus Specifications	
Size	151.8mm x 74.3mm x 6.6mm	
Processor	2GHz octa-core	
RAM	4GB	
Internal Storage	64GB	
Connectivity	Wi-Fi	Yes
	GPS	Yes
	Bluetooth	Yes
	USB OTG	Yes
	NFC	No
	Infrared	No
Sensors	Compass/ Magnetometer	No
	Proximity sensor	Yes
	Accelerometer	Yes
	Ambient light sensor	Yes
	Gyroscope	Yes

Currently, there is no android application that can log compass value (heading direction/bearing). Thus, a new coding is written to be programmed into a smartphone. Samsung Galaxy S2 is chosen because it has accelerometer, gyroscope and compass/magnetometer. It can provide the data that is needed. The smartphone is illustrated in Figure 3.7 and its specifications are presented in Table 3.4.

Figure 3.7: Samsung Galaxy S2

Table 3.4: Samsung Galaxy S2 Specifications

	Samsung Galaxy S2 Specifications	
Size	125.3mm x 66.1mm x 8.49mm	
Processor	1.2GHz dual-core	
RAM	1GB	
Internal Storage	16GB	
Connectivity	Wi-Fi	Yes
	GPS	Yes
	Bluetooth	Yes
	USB OTG	No
	NFC	Yes
	Infrared	No
Sensors	Compass/ Magnetometer	Yes
	Proximity sensor	Yes
	Accelerometer	Yes
	Ambient light sensor	No
	Gyroscope	Yes

For the road test to be carried out, a land vehicle with ECU and OBD-II port is chosen. Honda City (Figure 3.8) with protocol ISO9141-2 is used in the experiment. The OBD-II adaptor device is installed in this vehicle at OBD-II socket which is under steering. Once the vehicle is initiated, the device will communicate with Bluetooth-paired smartphone immediately.

Figure 3.8: Honda City

Once the device is connected to smartphone through bluetooth, the application (Torque) is able to read the input NMEA sentences from satellites and PIDs information from OBD-II adaptor ELM 327. The application can display the GPS speed, GPS heading direction/bearing, GPS accuracy, number of visible satellites and vehicle's speed (OBD-II speed) and also log the data. The data can be then extracted and analyzed. On the other hand, the vehicle's heading direction/bearing is also logged for location prediction purpose. The aforementioned data are stored in excel file for further analysis purpose.

3.3.2 Prediction Algorithm

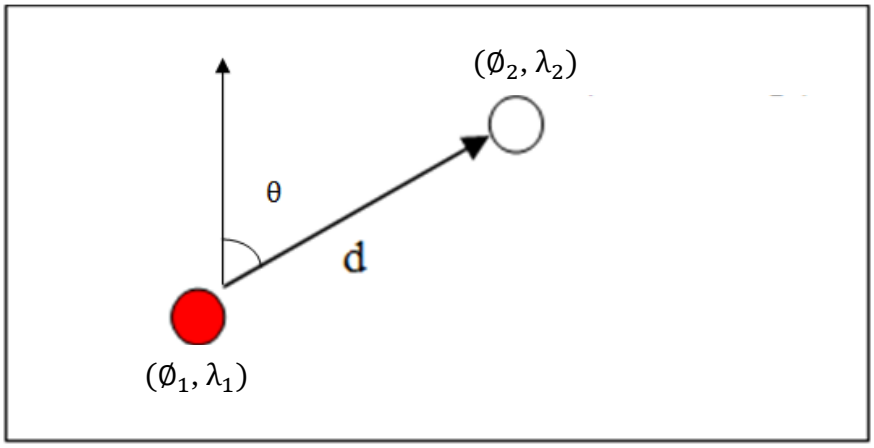

Figure 3.9: Distance between Two Locations

Figure 3.9 illustrates the last known coordinate, $(\emptyset_1, \lambda_1)$, the next coordinate, $(\emptyset_2, \lambda_2)$, the distance between two coordinates, d and also the heading direction/bearing, θ. The heading direction/bearing is the angle between the true north of the last known coordinate to the next coordinate.

The prediction algorithm is derived from the equations below:

$$\text{Difference in latitude } = \frac{\text{d}}{60} \times \cos\theta \tag{3.1}$$

$$\text{Difference in longitude} = \frac{\text{d}}{60} \times \sin\theta \tag{3.2}$$

where d is the distance between two locations in nautical mile and θ is the heading direction/bearing measured from north to that certain location in degree. The distance in nautical mile needs to be divided by 60 because 1° is equals to 60 nautical miles. These equations can be written as in Equation 3.3 and Equation 3.4 where $\emptyset_1$ is latitude of last known coordinate, λ_1 is the longitude of last known coordinate, $\emptyset_2$ is latitude of next coordinate, λ_2 is the longitude of next coordinate,. Then, they can be rearranged as Equation 3.5 and Equation 3.6.

$$\emptyset_2 - \emptyset_1 = \frac{\text{d}}{60} \times \cos\theta \tag{3.3}$$

$$\lambda_2 - \lambda_1 = \frac{\text{d}}{60} \times \sin\theta \tag{3.4}$$

$$\emptyset_2 = \emptyset_1 + \frac{\text{d}}{60} \times \cos\theta \tag{3.5}$$

$$\lambda_2 = \lambda_1 + \frac{\text{d}}{60} \times \sin\theta \tag{3.6}$$

The simplified predicted coordinate is

$$\text{c}_\text{p} = \begin{bmatrix}\emptyset_2 \\ \lambda_2\end{bmatrix} = \begin{bmatrix}\emptyset_1 \\ \lambda_1\end{bmatrix} + 9 \times 10^{-6}\text{v}\begin{bmatrix}\cos\theta \\ \sin\theta\end{bmatrix} \pm \begin{bmatrix}\text{e}_\emptyset \\ \text{e}_\lambda\end{bmatrix} \tag{3.7}$$

where c_p is the predicted coordinate, $\emptyset_2$ is the predicted latitude, λ_2 is the predicted longitude, $\emptyset_1$ is the last known latitude, λ_1 is the last known longitude, 9×10^{-6} is the converting factor, v is the velocity of vehicle per second, θ is the heading direction/bearing, $\text{e}_\emptyset$ is the latitude error, and e_λ is the longitude error.

3.3.3 GPS-integrated Location Prediction Model

A Matlab coding is written to post-process all the collected data, including GPS latitude, GPS longitude, GPS speed, GPS heading direction/bearing, number of satellites, vehicle's speed and vehicle's heading direction/bearing. The functionality of the location prediction algorithm should be validated before proceeds to be integrated with GPS. When the algorithm works, the algorithm should be integrated with GPS through Matlab coding. The functionality of the model will be validated. It is supposed that GPS will work when the GPS signal is available, else, the algorithm will compute predicted coordinates when the GPS signal is lost. The model is able to perform the loosely coupled integration and provide coordinates continuously either under LOS or NLOS conditions.

3.4 System Evaluation and Validation

3.4.1 Data Collection

The data collection for the smartphone-based GPS-integrated location prediction model is planned to be taken place in Kuching, Sarawak, Malaysia (Figure 3.10). Different test trajectories will be chosen to test the capability of the model. The scenarios have to involve slight turning, sharp turning, U-turn and roundabout. Besides the road condition will be different, the duration of data collection will be varied. The duration will be set as 5 minutes and 10 minutes.

During the data collection, the OBD-II adaptor will be plugged in to its socket in the chosen vehicle and it is made sure connected to the smartphone OPPO F1 Plus for the data logging purpose. The smartphone OPPO F1 Plus can be placed at the dashboard of the vehicle. Another smartphone Samsung Galaxy S2 will be placed properly on the dashboard

too. Its position is critical to log accurate compass values. The values are the vehicle's heading direction/bearing per second which is a critical parameter in the location prediction model. Once the devices are placed properly at their positions in the vehicle and initiated, the vehicle can be driven along the set road trajectories for the fixed duration.

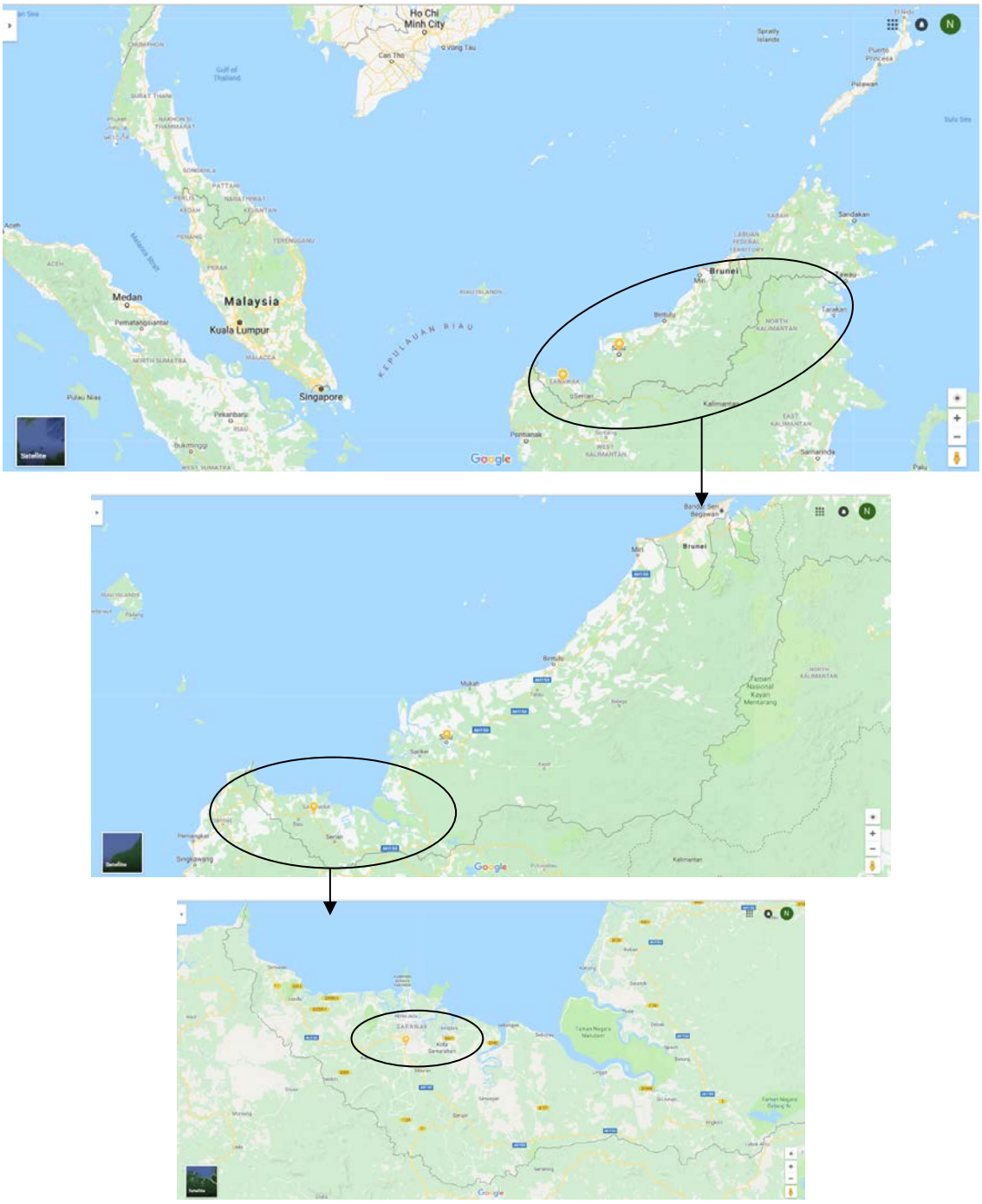

Figure 3.10: Area of Data Collection (Kuching, Sarawak, Malaysia)

3.4.2 Data Analysis

The performance of every experiment will be accessed by using Root Mean Square Error (RMSE). RMSE can be calculated with different ways. The Spherical Law of Cosine (Equation 2.19) can be inserted in Matlab code to compute the distance between the actual coordinates and predicted coordinates. The distance is the RMSE. Then, the average and standard deviation of RMSE can be calculated.

Another method of calculation is shown in Figure 3.11. The logged data is exported into UTM Conversion MS Excel sheet to convert latitude and longitude in degree into UTM format. UTM shows Easting and Northing value in meters. The horizontal and vertical positioning errors can be found by using Equation 3.8 and 3.9. With the values of horizontal and vertical positioning error, RMSE can be calculated according to Equation 2.7.

$$e_{\lambda} = E_a - E_p \tag{3.8}$$

$$e_{\emptyset} = N_a - N_p \tag{3.9}$$

where e_{λ} is the horizontal error/longitude error, $E_a$is the actual easting value, E_p is the predicted easting value, $e_{\emptyset}$ is the vertical error/latitude error, N_a is the actual northing value, N_p is the predicted northing value.

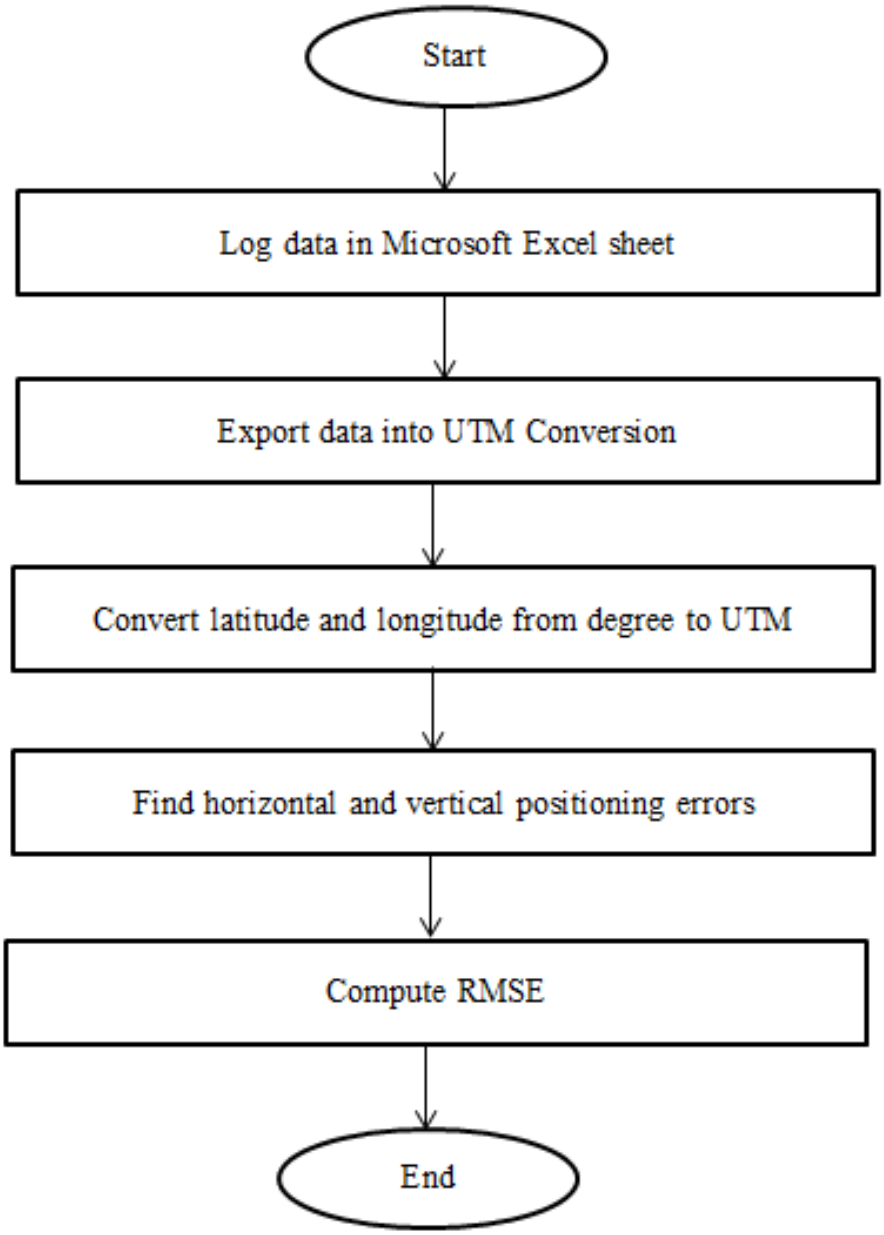

Figure 3.11: Flow Chart to Obtain RMSE

The Spherical Law of Cosine will be chosen to compute the RMSE. The graphs of performance are plotted by using Matlab and Microsoft Excel. The graphs include graph of latitude versus longitude, graph of RMSE versus time, graph of comparison and so on. Through the graphs, the continuity and accuracy of the experiments can be clearly observed.

3.5 Chapter Summary

As aforementioned in Chapter 2, there is no research on smartphone-based GPS-integrated location prediction model for vehicle localization. Therefore, this chapter describes the methods to design the model, the details of data collection and ways of analysis for the results of experiment. The experiment for the vehicle localization is carried out by placing the planned devices on a chosen vehicle and the vehicle will be driven in different conditions/durations to verify the functionality of this model. The data will be saved into database for further analysis. The performance will be validated through its continuity and accuracy, which mainly emphasizes on the RMSE.

CHAPTER 4

RESULTS AND DISCUSSION

4.1 Overview

This chapter addresses the results of the smartphone-based GPS-integrated location prediction model for vehicle localization and provides complementary explanations of the results obtained. The chapter covers the results and analysis of experimental work which was carried out on five different test trajectories. Analysis is done based on one of the discussed performance assessment method, Root Mean Square Error (RMSE). The prediction model is then compared with other prediction formulas/models. The analysis will show the reliability and accuracy of the smartphone-based GPS-integrated location prediction model for OBD-II-equipped vehicle localization.

4.2 Validation of Functionality of Prediction Algorithm

To validate the functionality of the algorithm, data collection was carried out with logged GPS latitude, GPS longitude, GPS speed and GPS heading direction/bearing. The data were logged each second up to 500s to show the reliability and accuracy of the prediction algorithm. By substituting the collected data into the prediction algorithm (written with Matlab and coding as shown in Appendix A), the result of the prediction can be observed through Figure 4.1 to Figure 4.5.

The experimental road tests have been carried out at Jalan Akses FAC on 15 December 2016 (Thursday) and repeated for 5 times in the period of time (2.00pm to 2.50pm). The total duration was 50 minutes which meant averagely 10 minutes per round, providing about 500 to 600 data each round. It was a sunny day with clear sky view. Thus, the number of satellites in Line-of-Sight (LOS) was adequate (minimum 6 and maximum 17). With this number of satellites visible to the data collection device, the GPS can provide location with excellent accuracy.

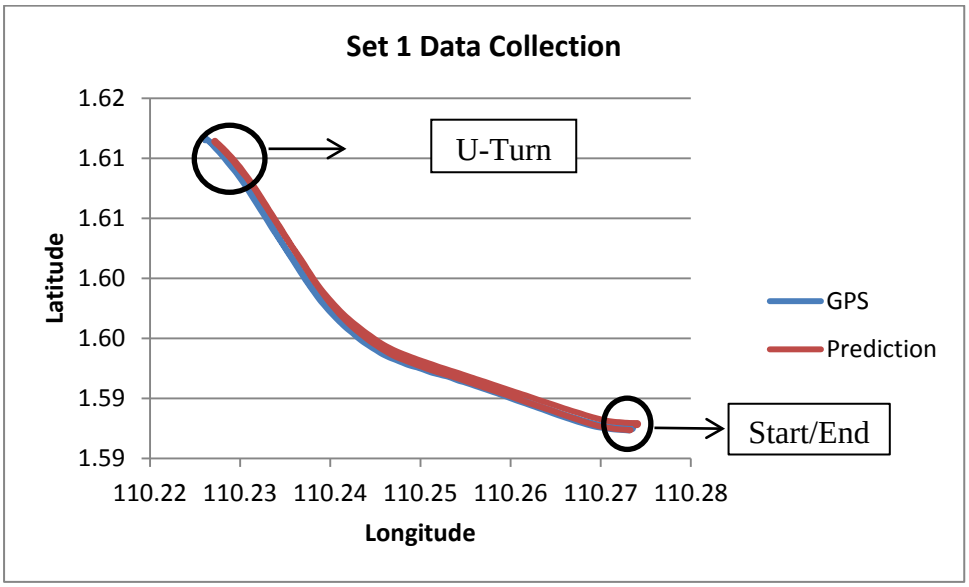

Figure 4.1: Prediction Algorithm Validation 1

Figure 4.1 shows the route plotted by using GPS coordinates (blue line) and a predicted route (red line). The result shows precise and accurate prediction. To be specific, the accuracy is 7.47 m. The accuracy is obtained from the RMSE calculation. The crucial part is the prediction during the 180° turning at the U-turn area, as highlighted in the figure.

The errors were increasing to higher value after the U-turn. When there is a sudden change in the heading value within short period of time, the prediction algorithm could not

provide high accuracy computation. The sensor errors happen in millisecond instead of one second. Thus, the predicted coordinates will deviate from the actual values.

Figure 4.2: Prediction Algorithm Validation 2

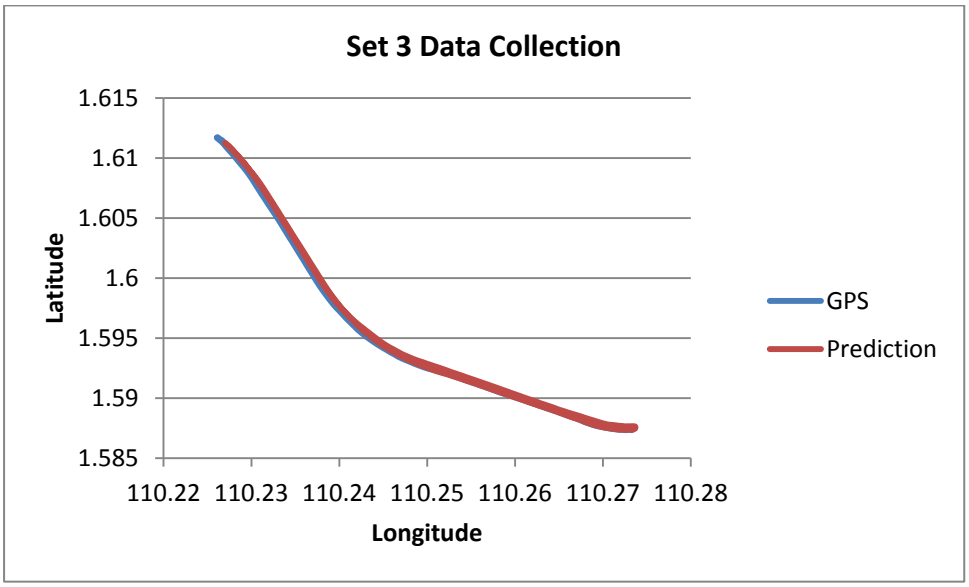

Figure 4.3: Prediction Algorithm Validation 3

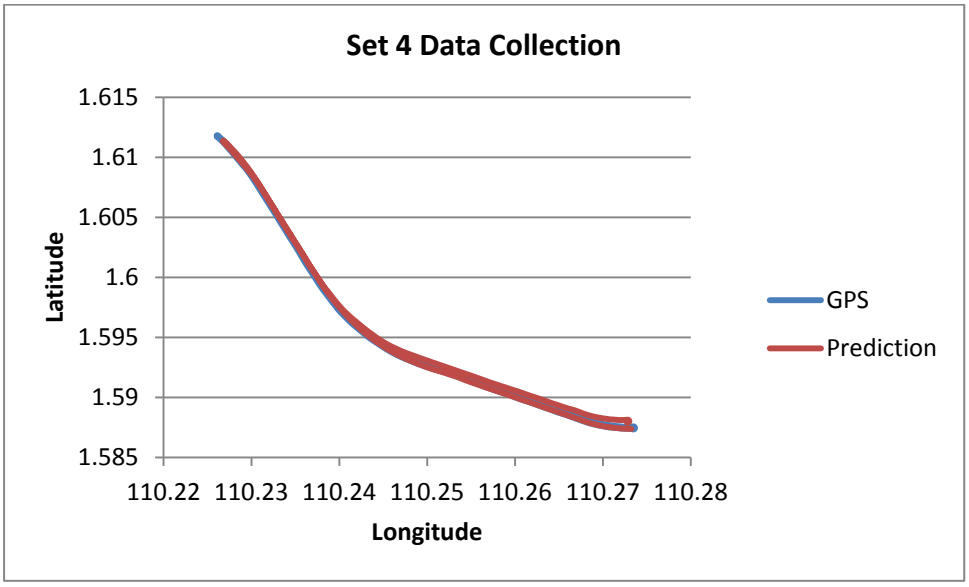

Figure 4.4: Prediction Algorithm Validation 4

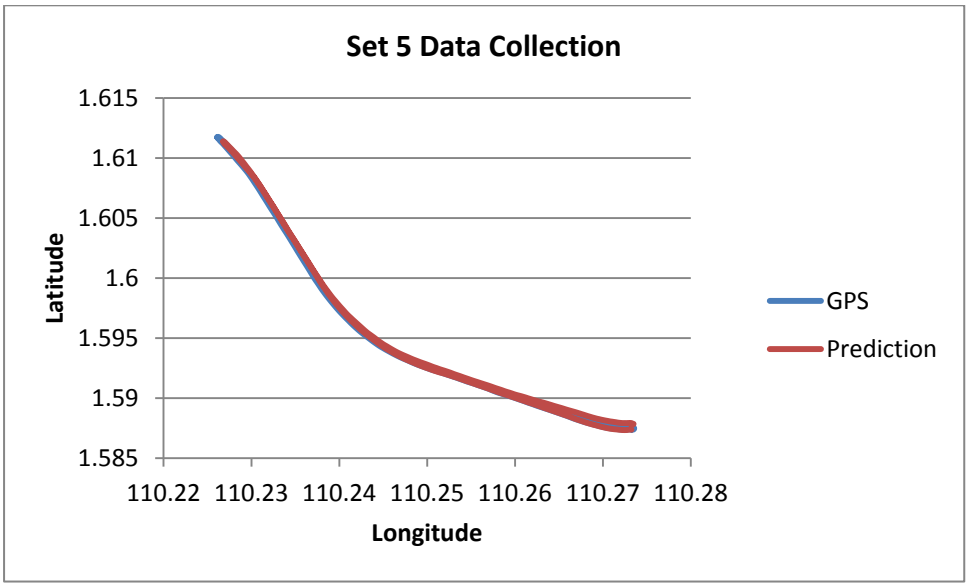

Figure 4.5: Prediction Algorithm Validation 5

From the observation on Figure 4.1 to Figure 4.5, it is verified that the algorithm is works if the obtained parameters (speed and heading direction/bearing) are with certain accuracy. The accuracy calculated were 7.47 m, 5.69 m, 9.80 m, 5.77 m and 8.48 m

respectively and tabulated in Table 4.1. According to the research works regarding positioning, GPS provides position information with accuracy of 10 meters or less [143]. Thus, outdoor positioning with accuracy range of 10 m is acceptable. Figure 4.1 to 4.5 shows slight deviation at U-turn, proving that the prediction will deviate from its actual route when there is a sudden change in direction.

The maximum RMSE ranges from 22.8780 m to 47.7377 m. The errors are higher at two major turning points which are the U-turn and the start/end point (as shown in Figure 4.2). From Table 4.1, it can be observed that Set 2 is showing a better result. It presents the lowest maximum value of RMSE, the least average of RMSE and the smallest standard deviation of RMSE. This is due to the number of visible satellites along the route during data collection is higher if compared to other sets of data collection. On the other hand, Set 5 gives the worst performance because the number of visible satellites is lower during the data collections.

Besides, it is found that the car speed might affect the number of visible satellites. As the speed increases, the number of satellites in LOS may decrease. By observing the raw data, the number of satellites in LOS drop to 10 or less than 10 when the car speed increases up to 80km/h and above, particularly if the car is accelerating up to a speed of 110 km/h. When the speed is increasing and the number of visible satellites is decreasing, the prediction algorithm gives result with less precision and less accuracy.

In Figure 4.6, Set 2 and Set 4 show the better results in terms of either average or standard deviation of RMSE. Standard deviation is a better measurement in analyzing data as it uniquely characterized the dispersion of a distribution. The standard deviation of RMSE is ranging in between 5 m to 10 m. This shows that the accuracy of this prediction

algorithm is excellent as GPS itself defines its accuracy as 6 m to 7 m (as claimed in Section 2.2.1).

Table 4.1: Performance of Prediction Algorithm

	Set 1	**Set 2**	**Set 3**	**Set 4**	**Set 5**
Maximum (m)	35.5926	22.8780	32.9219	28.4206	47.7377
Average (m)	19.2235	10.9820	17.9273	13.2558	21.2553
Standard Deviation (m)	7.5309	5.7089	9.8204	5.7901	8.5231
Average Speed (km/h)	76	83	83	81	84
Average No. of Satellites	11	12	11	11	10

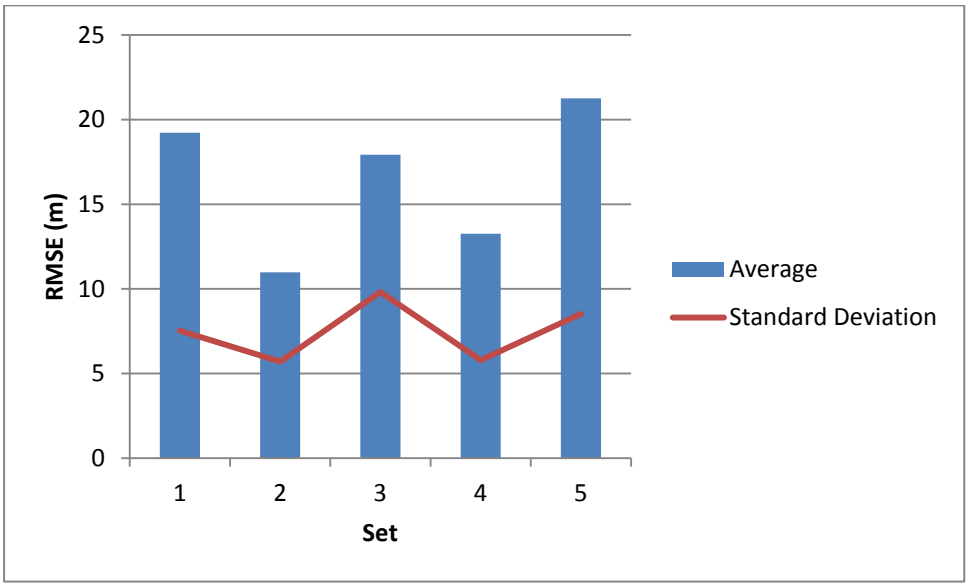

Figure 4.6: Average and Standard Deviation of RMSE of Prediction Algorithm

4.3 Validation of Functionality of Prediction Model

The functionality of the GPS-integrated Dead Reckoning prediction model was validated by insertion of the collected data (GPS latitude, GPS longitude, GPS speed and GPS heading direction/bearing) used in Section 4.2 into the prediction model. The GPS data is integrated with the prediction algorithm through loosely-coupled method. When the GPS signal outage (assuming the satellite signal is lost when the number of satellites is less

than 10), the prediction algorithm will take over the task to perform the location computation and show coordinate of vehicle. While the GPS signal is available, the GPS coordinate will be shown. The coding for this GPS-integrated Dead Reckoning prediction model was written in Matlab (as shown in Appendix B). The result of prediction can be observed through Figure 4.7 to Figure 4.11.

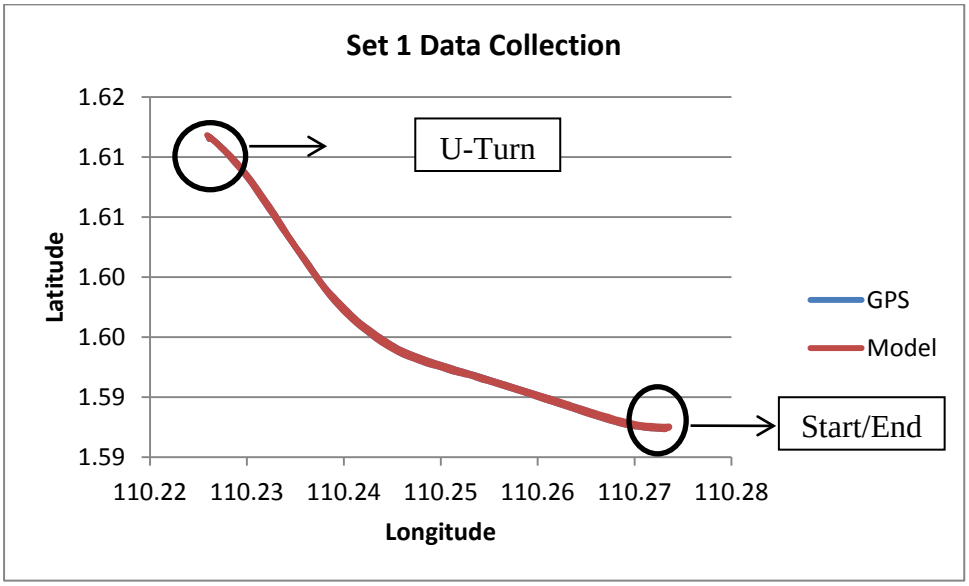

Figure 4.7: Prediction Model Validation 1

The data used to validate the functionality of prediction algorithm is same as the data used to validate the functionality of GPS-Integrated prediction model. In Figure 4.7, the blue line is the route plotted with GPS coordinates while the red line is the route plotted with the predicted coordinates. It can be observed that the test trajectory in this section is same as the route in Section 4.2, with the same Start/End point and a U-Turn. The only difference is the predicted route of the integrated model is more precise and accurate if compared to the prediction by stand-alone prediction algorithm.

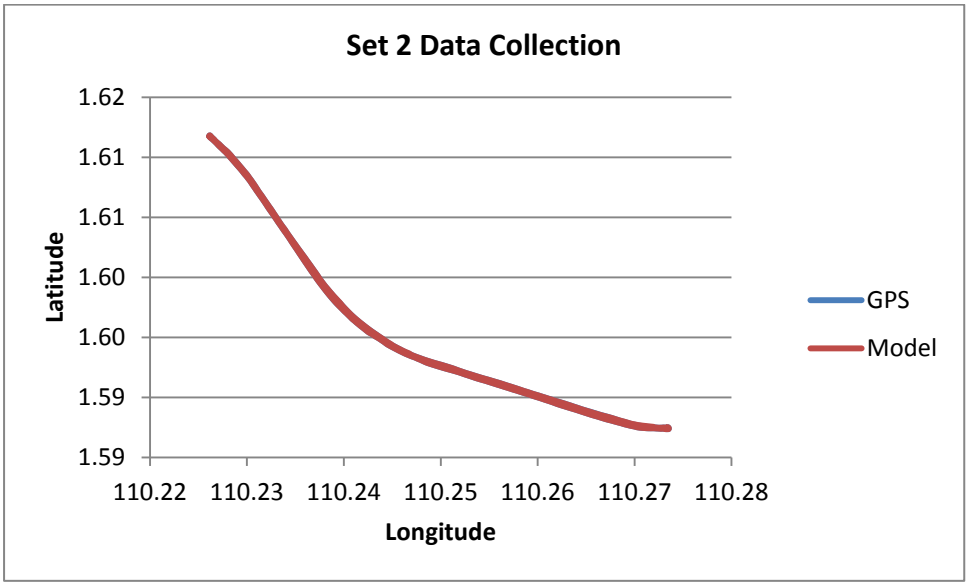

Figure 4.8: Prediction Model Validation 2

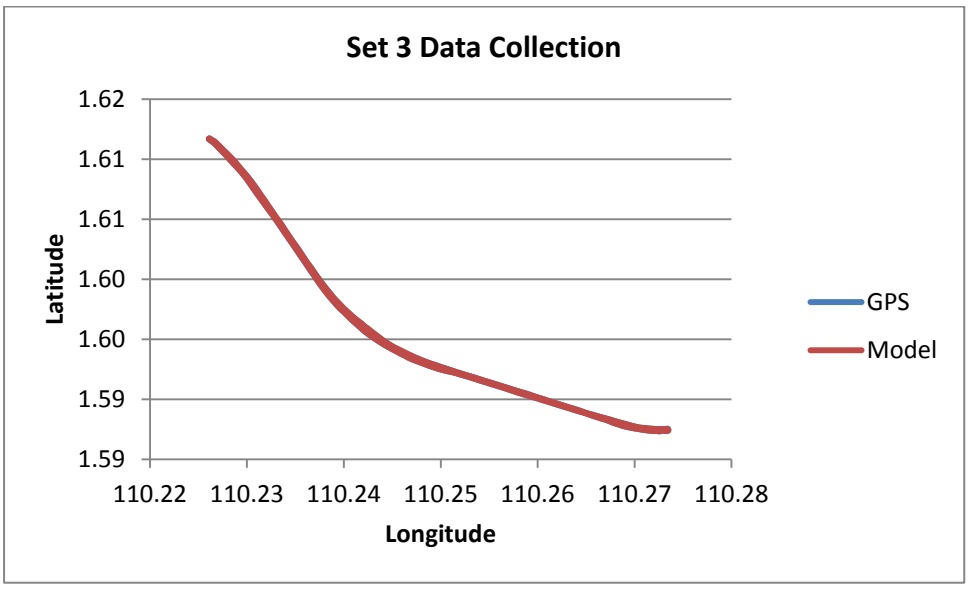

Figure 4.9: Prediction Model Validation 3

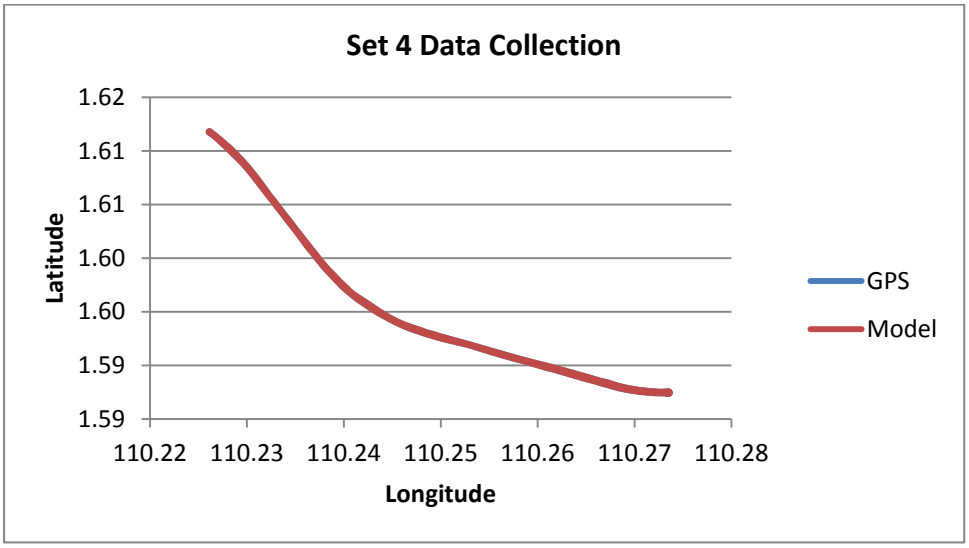

Figure 4.10: Prediction Model Validation 4

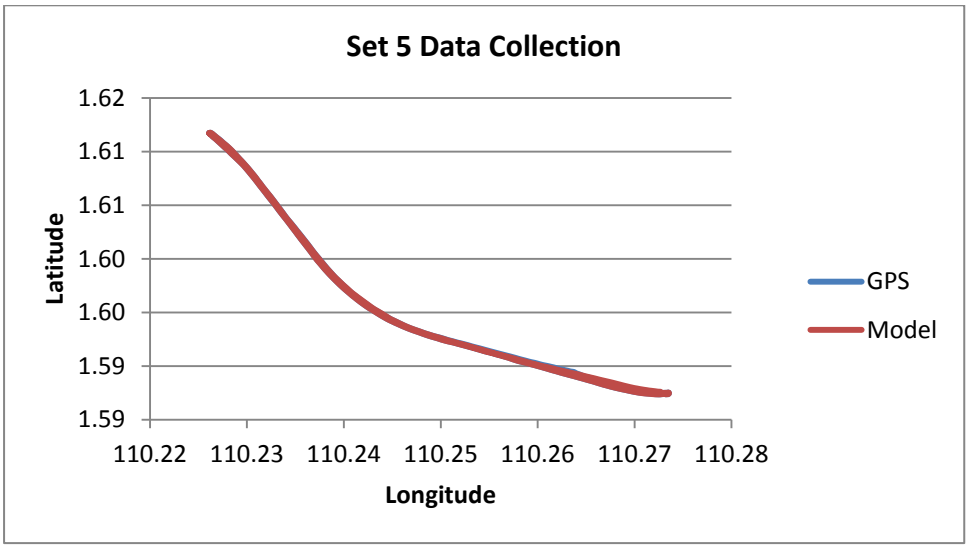

Figure 4.11: Prediction Model Validation 5

The results in Figure 4.7 to Figure 4.11 proved that the prediction model performed well with the provided parameters (speed and heading direction/bearing). The accuracy calculated were 3.96 m, 1.18 m, 1.53 m, 1.99 m and 8.41 m respectively and tabulated in Table 4.2. These results show excellent improvement compared to standalone prediction algorithm.

The maximum RMSE ranges from 5.87 m to 44.17 m. These values are averagely lower than the maximum RMSE in previous section. In term of average and standard deviation of RMSE, Set 2 gives the best results while Set 5 gives the worst results. The highest maximum RMSE in Set 5 is due to the outage of GPS signal for about 100s and the prediction errors accumulate up to high value in this period of time. During this period of time, the car speed is high (above 100 km/h) and the number of visible satellites is low (6 to 10). This is the reason of the poor accuracy.

Since the prediction algorithm only performs when the number of satellites detected is less than or equal to 10, the number of prediction in each set is observed. The prediction data in Set 1 is 202, Set 2 is 128, Set 3 is 150, Set 4 is 189 and Set 5 is 250. This data is plotted in Figure 4.12. From Figure 4.12, it can be observed that the more the data of prediction, the higher the standard deviation of RMSE. When more predictions are performed in a set of data, it has higher probability to get cumulative prediction errors, which in turns reduces the accuracy.

To conclude the overall data in this prediction model, the data is satisfying as it gives an average data that is less than 10 m of RMSE. It only gives poor prediction when the vehicle stopped and waited for U-turn or when the prediction algorithm runs for longer term.

Table 4.2: Performance of GPS-integrated Location Prediction Model

	Set 1	**Set 2**	**Set 3**	**Set 4**	**Set 5**
Maximum (m)	25.4086	5.8653	8.6792	11.7152	44.1727
Average (m)	1.4454	0.5289	0.7178	0.9667	3.9050
Standard Deviation (m)	3.6781	1.1787	1.5302	1.9915	8.4055
Number of Prediction	202	128	150	189	250

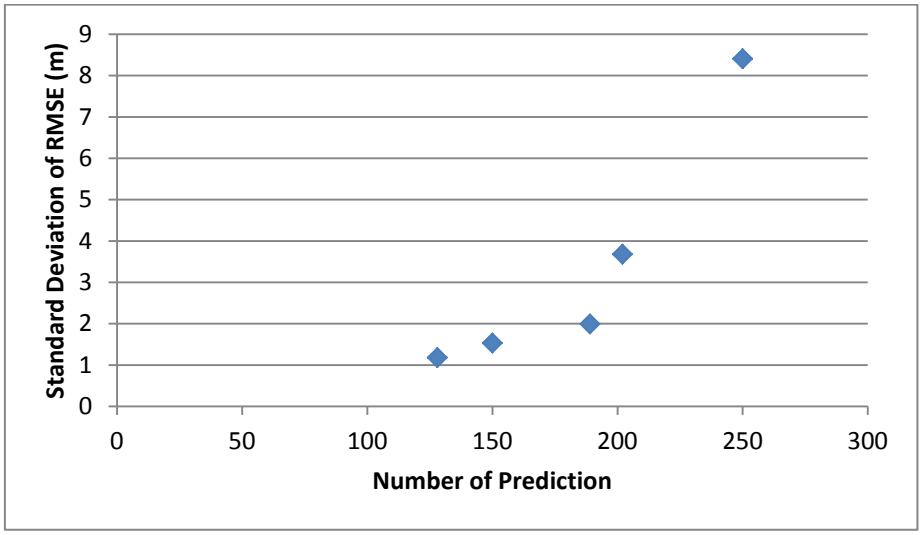

Figure 4.12: Standard Deviation of RMSE versus Number of Prediction

In term of average and standard deviation of RMSE, prediction algorithm shows higher average value than standard deviation. In contrast, prediction model shows higher standard deviation than average value (Figure 4.13). This is due to the reason that when no prediction error will be detected in prediction model when GPS signal is excellent and thus those zero positioning errors will make the average value lower. Standard deviation characterizes each data uniquely so the value is higher if compared to the average value.

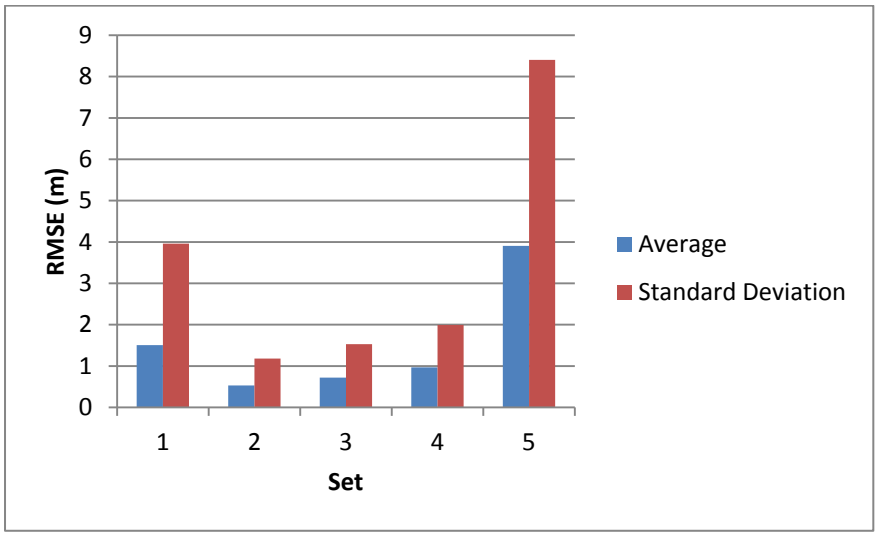

Figure 4.13: Average and Standard Deviation of RMSE of Prediction Model

4.4 Performance Assessment of GPS-Integrated Prediction Model

The required parameters for the GPS-Integrated prediction model are collected through a smartphone OPPO F1 Plus, a smartphone Samsung Galaxy S2 and On-Board-Diagnostic-II (OBD-II) Bluetooth device ELM 327. The OBD-II bluetooth adaptor is installed on a vehicle namely Honda. A smartphone application, Torque (Lite) (as circled in Figure 4.14) is installed in OPPO F1 Plus to read the data from the OBD-II through Bluetooth connection. The logged data is saved in .csv file, as shown in Figure 4.15. The data consists of date, time, GPS latitude, GPS longitude, GPS heading direction/bearing, GPS speed, speed (OBD), gyroscope data, accelerometer data and number of satellites. The data is comprehensive and adequate for the experiment.

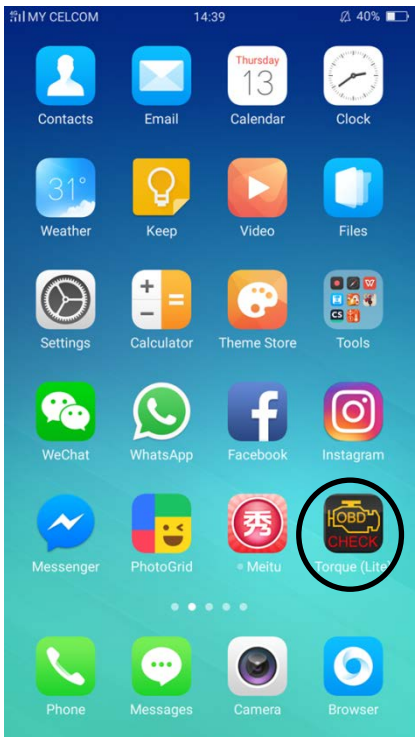

Figure 4.14: Torque Installed in OPPO F1 Plus

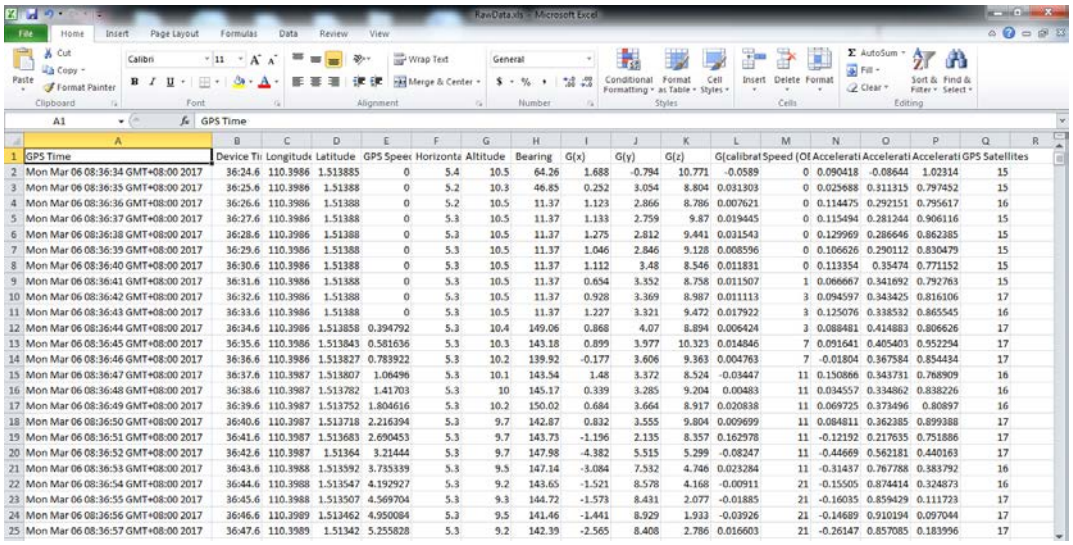

	A	B	C	D	E	F	G	H	I	J	K	L	M	N	O	P	Q	R
1	GPS Time	Device Ti	Longitude	Latitude	GPS Speed	Horizonta	Altitude	Bearing	G(x)	G(y)	G(z)	G(calibrat	Speed (Of	Accelerati	Accelerati	Accelerati	GPS Satellites	
2	Mon Mar 06 08:36:34 GMT+08:00 2017	36:24.6	110.3986	1.513885	0	5.4	10.5	64.26	1.688	-0.794	10.771	-0.0589	0	0.090418	-0.08644	1.02314	15	
3	Mon Mar 06 08:36:35 GMT+08:00 2017	36:25.6	110.3986	1.51388	0	5.2	10.3	46.85	0.252	3.054	8.804	0.031303	0	0.025688	0.311315	0.797452	15	
4	Mon Mar 06 08:36:36 GMT+08:00 2017	36:26.6	110.3986	1.51388	0	5.2	10.5	11.37	1.123	2.866	8.786	0.007621	0	0.114475	0.292151	0.795617	16	
5	Mon Mar 06 08:36:37 GMT+08:00 2017	36:27.6	110.3986	1.51388	0	5.3	10.5	11.37	1.133	2.759	9.87	0.019445	0	0.115494	0.281244	0.906116	15	
6	Mon Mar 06 08:36:38 GMT+08:00 2017	36:28.6	110.3986	1.51388	0	5.3	10.5	11.37	1.275	2.812	9.441	0.031543	0	0.129969	0.286646	0.862385	15	
7	Mon Mar 06 08:36:39 GMT+08:00 2017	36:29.6	110.3986	1.51388	0	5.3	10.5	11.37	1.046	2.846	9.128	0.008596	0	0.106626	0.290112	0.830479	15	
8	Mon Mar 06 08:36:40 GMT+08:00 2017	36:30.6	110.3986	1.51388	0	5.3	10.5	11.37	1.112	3.48	8.546	0.011831	0	0.113354	0.35474	0.771152	15	
9	Mon Mar 06 08:36:41 GMT+08:00 2017	36:31.6	110.3986	1.51388	0	5.3	10.5	11.37	0.654	3.352	8.758	0.011507	1	0.066667	0.341692	0.792763	15	
10	Mon Mar 06 08:36:42 GMT+08:00 2017	36:32.6	110.3986	1.51388	0	5.3	10.5	11.37	0.928	3.369	8.987	0.011113	3	0.094597	0.343425	0.816106	17	
11	Mon Mar 06 08:36:43 GMT+08:00 2017	36:33.6	110.3986	1.51388	0	5.3	10.5	11.37	1.227	3.321	9.472	0.017922	3	0.125076	0.338532	0.865545	16	
12	Mon Mar 06 08:36:44 GMT+08:00 2017	36:34.6	110.3986	1.513858	0.394792	5.3	10.4	149.06	0.868	4.07	8.894	0.006424	3	0.088481	0.414883	0.806626	17	
13	Mon Mar 06 08:36:45 GMT+08:00 2017	36:35.6	110.3986	1.513843	0.581636	5.3	10.3	143.18	0.899	3.977	10.323	0.014846	7	0.091641	0.405403	0.952294	17	
14	Mon Mar 06 08:36:46 GMT+08:00 2017	36:36.6	110.3986	1.513827	0.783922	5.3	10.2	139.92	-0.177	3.606	9.363	0.004763	7	-0.01804	0.367584	0.854434	17	
15	Mon Mar 06 08:36:47 GMT+08:00 2017	36:37.6	110.3987	1.513807	1.06496	5.3	10.1	143.54	1.48	3.372	8.524	-0.03447	11	0.150866	0.343731	0.768909	16	
16	Mon Mar 06 08:36:48 GMT+08:00 2017	36:38.6	110.3987	1.513782	1.41703	5.3	10	145.17	0.339	3.285	9.204	0.00483	11	0.034557	0.334862	0.838226	16	
17	Mon Mar 06 08:36:49 GMT+08:00 2017	36:39.6	110.3987	1.513752	1.804616	5.3	10.2	150.02	0.684	3.664	8.917	0.020838	11	0.069725	0.373496	0.80897	16	
18	Mon Mar 06 08:36:50 GMT+08:00 2017	36:40.6	110.3987	1.513718	2.216394	5.3	9.7	142.87	0.832	3.555	9.804	0.009699	11	0.084811	0.362385	0.899388	17	
19	Mon Mar 06 08:36:51 GMT+08:00 2017	36:41.6	110.3987	1.513683	2.690453	5.3	9.7	143.73	-1.196	2.135	8.357	0.162978	11	-0.12192	0.217635	0.751886	17	
20	Mon Mar 06 08:36:52 GMT+08:00 2017	36:42.6	110.3987	1.51364	3.21444	5.3	9.7	147.98	-4.382	5.515	5.299	-0.08247	11	-0.44669	0.562181	0.440163	17	
21	Mon Mar 06 08:36:53 GMT+08:00 2017	36:43.6	110.3988	1.513592	3.735339	5.3	9.5	147.14	-3.084	7.532	4.746	0.023284	11	-0.31437	0.767788	0.383792	16	
22	Mon Mar 06 08:36:54 GMT+08:00 2017	36:44.6	110.3988	1.513547	4.192927	5.3	9.2	143.65	-1.521	8.578	4.168	-0.00911	21	-0.15505	0.874414	0.324873	16	
23	Mon Mar 06 08:36:55 GMT+08:00 2017	36:45.6	110.3988	1.513507	4.569704	5.3	9.3	144.72	-1.573	8.431	2.077	-0.01885	21	-0.16035	0.859429	0.111723	17	
24	Mon Mar 06 08:36:56 GMT+08:00 2017	36:46.6	110.3989	1.513462	4.950084	5.3	9.5	141.46	-1.441	8.929	1.933	-0.03926	21	-0.14689	0.910194	0.097044	17	
25	Mon Mar 06 08:36:57 GMT+08:00 2017	36:47.6	110.3989	1.51342	5.255828	5.3	9.2	142.39	-2.565	8.408	2.786	0.016603	21	-0.26147	0.857085	0.183996	17	

Figure 4.15: Data Logged via Torque (Lite)

Another parameter, heading direction/bearing is collected through a newly-programmed logging phone application (programmed with Android Studio 2.1.2) that is installed in Samsung Galaxy S2 (its icon and name are as shown in Figure 4.16). It is an android compass application (its interface is as shown in Figure 4.17) which can log the reading value of the compass per second in text file (as shown in Figure 4.18). The data is post-processed to obtain the predicted coordinates. The post-processed solutions are presented in the following section.

Figure 4.16: Icon and Name of Apps

Figure 4.17: Interface of Apps

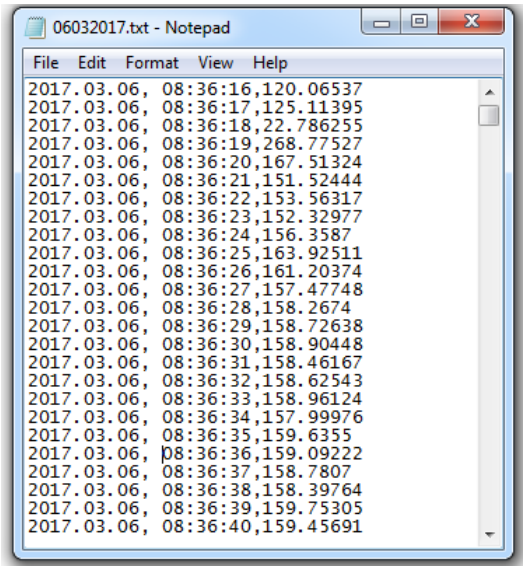

Figure 4.18: Logged Compass Values with Date and Time

The comprehensive data collection of five test trajectories were carried out and evaluated in this section. The total duration of field test was about 5013 seconds, which indicates 83 minutes and 33 seconds or 1 hour, 23 minutes and 33 seconds. During the data collection, it was a sunny day with clear blue sky view and the traffic was smooth as few vehicles were seen on the test trajectories.

4.4.1 Scenario 1

In Scenario 1, the first test trajectory is in Samajaya Free Industrial Zone. It is a rectangular path with five major left turnings, involving right-angle turning (90°) and non-right-angle turning (< 90°). The starting and ending point is at the same point as shown in Figure 4.19 and the black arrow shows the direction of the vehicle (facing south east) before it starts.

The data collection is carried out on 6 March 2017 (Monday), starting from 8.36 am and ending at 8.56 am. This is the duration for 5 set data collection, which means there is a total of 20 minutes driving and collected about 1200 data. The average driving time for a round is 4 minutes, which is 240 seconds and giving 240 data. Three sets of data will be shown as following. During the data collection, it was a sunny day with clear sky view and clear traffic.

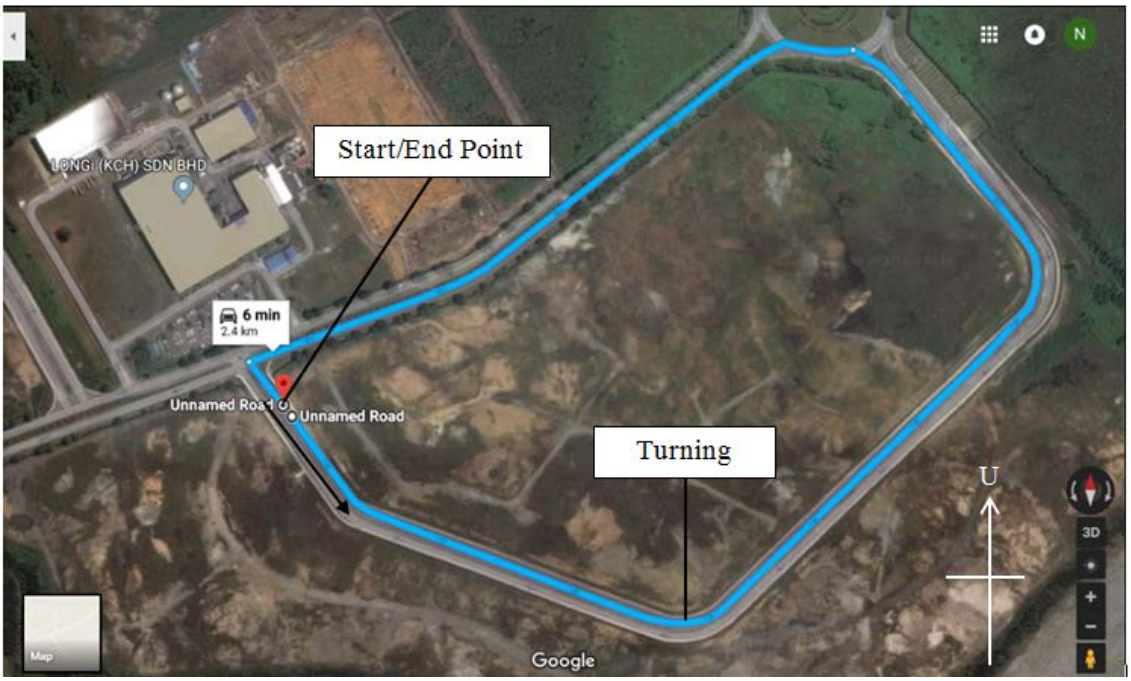

Figure 4.19: First Test Trajectory Plotted on Google Map

The GPS signal outage is intentionally introduced into the model during the experiment. There are 10 times of 10 seconds outage in this scenario. Among these 10 times of outage in Set 1 data, there are only 3 outages with major errors that more than 50 m RMSE while others' errors remain below 20 m. The major errors can be seen as labeled in Figure 4.20 and Figure 4.21. The 3 major errors of the prediction happened at the major turning point and on the path after the major turning. The major turn makes the compass

drift and could not calibrate itself in time right after the turn. Thus, the errors accumulate and make the prediction inaccurate.

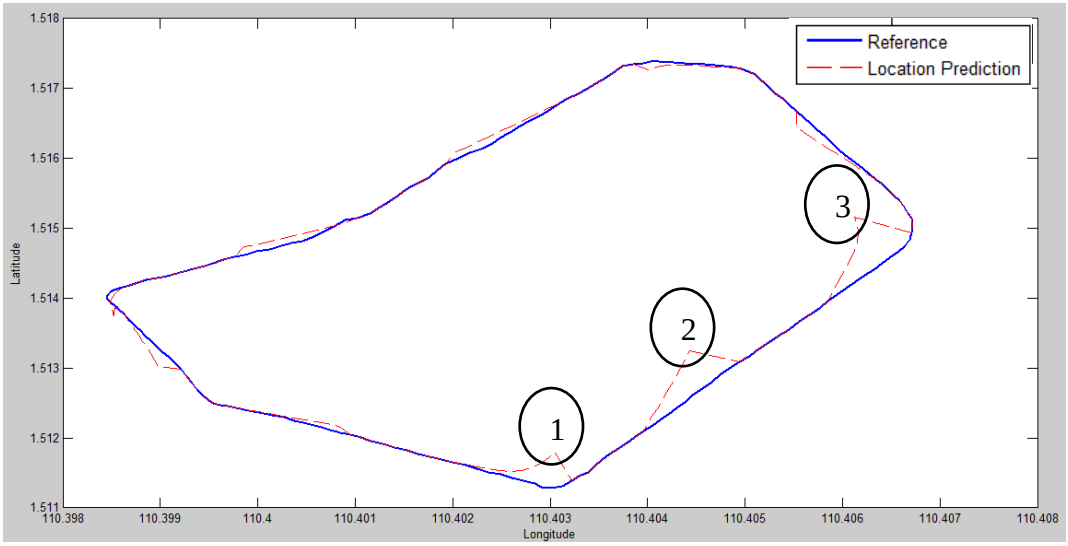

Figure 4.20: Comparison between Reference and Location Prediction (Scenario 1 Set 1)

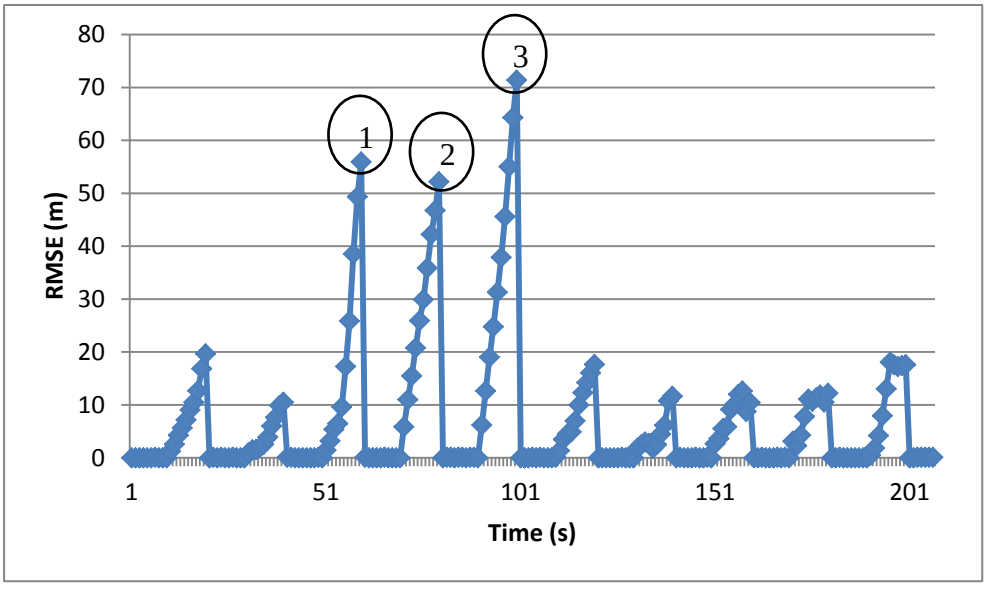

Figure 4.21: RMSE versus Time (Scenario 1 Set 1)

In the set 2 of Scenario 1, the major errors happened twice among the 10 outages, which peaking 50 m and 60 m. The other errors remain below 20 m. The major errors

happened at the same place, right after the first major turning. The collected heading direction/bearing deviated from its actual value after the turn and could not align back to the actual value immediately. Therefore, the prediction is imprecise and the RMSE is higher.

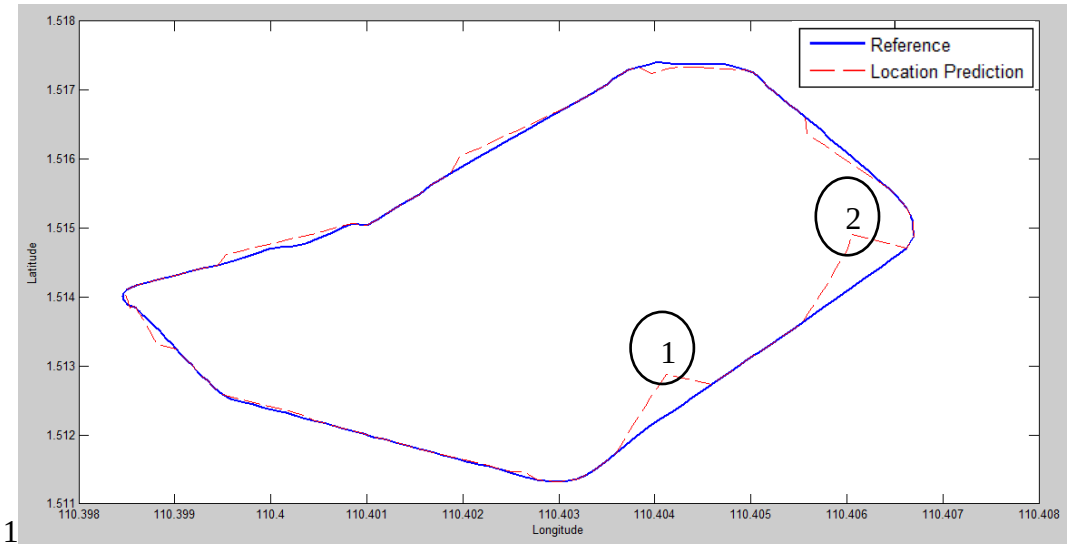

Figure 4.22: Comparison between Reference and Location Prediction (Scenario 1 Set 2)

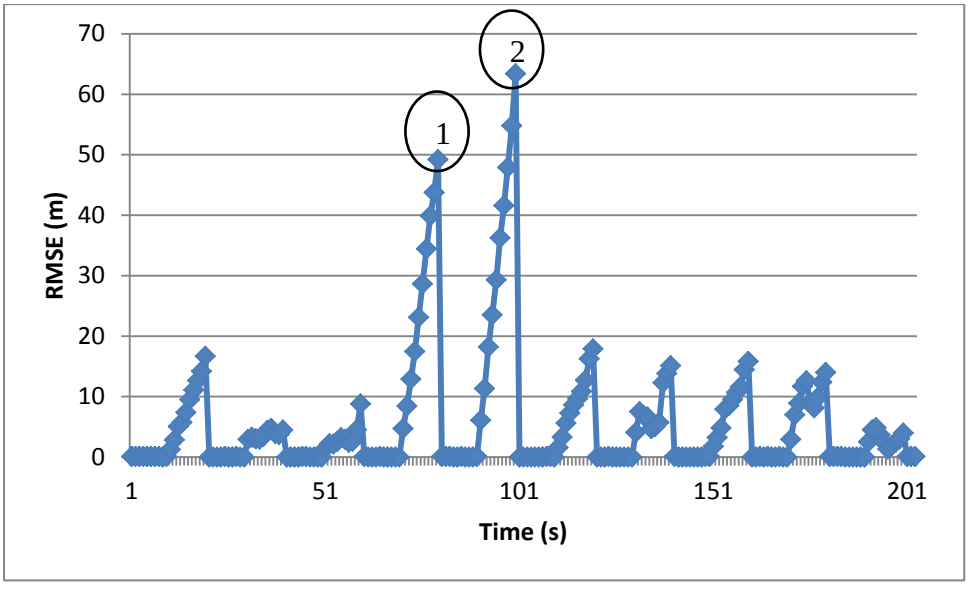

Figure 4.23: RMSE versus Time (Scenario 1 Set 2)

Set 3 data is alike with Set 1 which has 3 major errors after the first major turn. The errors are as high as 50 m and approaching 65 m. The measured and logged compass values are not accurate after the turn, making the predicted coordinates deviate to the left. However, the error is minimized after the second major turn as the compass started to calibrate itself to correct value. The other error to be mentioned is during the first outage, which giving an error of 18 m. The error might due to the compass have not been adjusted to its best position before the experiment started.

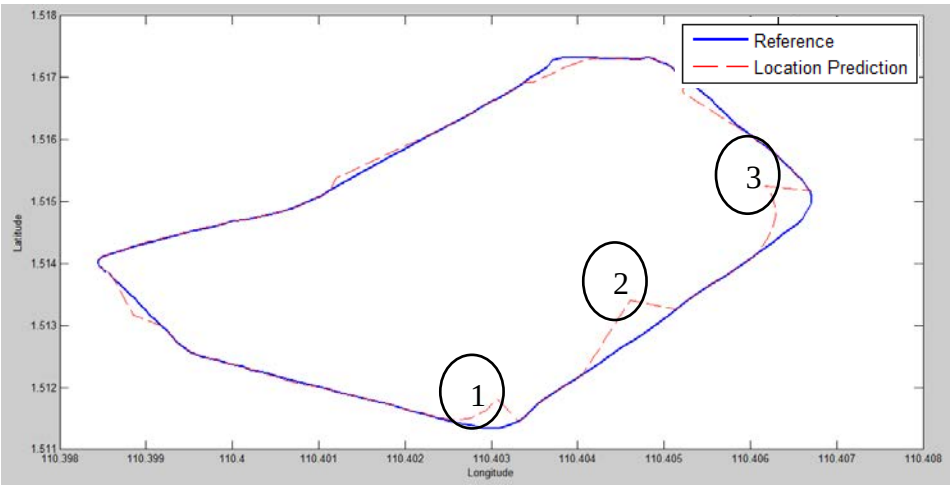

Figure 4.24: Comparison between Reference and Location Prediction (Scenario 1 Set 3)

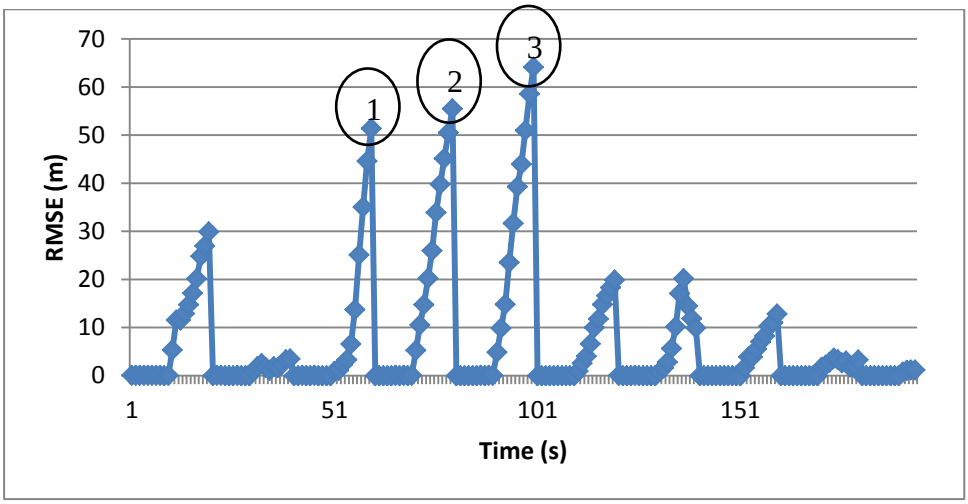

Figure 4.25: RMSE versus Time (Scenario 1 Set 3)

Figure 4.26 is comparison of the error performance of 3 sets of data. They are showing similar pattern of errors, except set 2 has lower error at 51 s and set 3 has higher error at 11 s. Set 1 has higher error at 31 s and 191 s if compared to the other 2 sets.

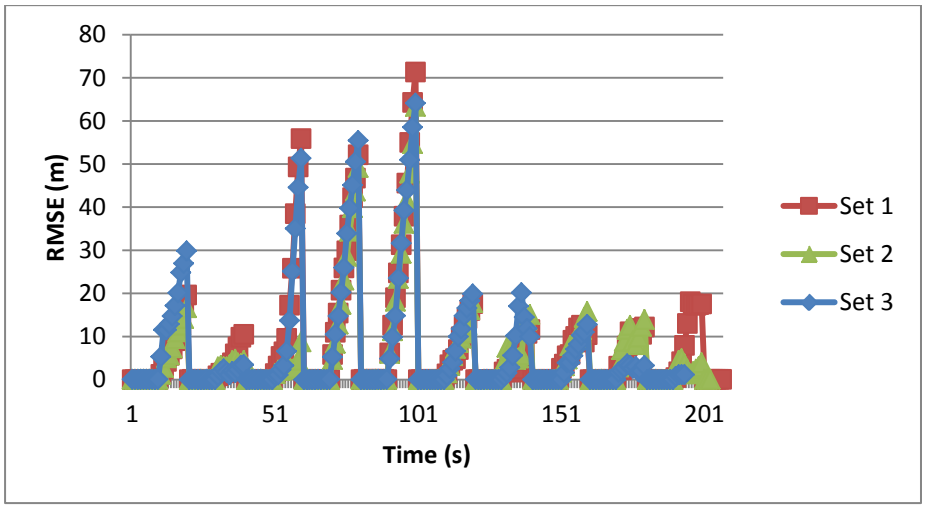

Figure 4.26: Comparison of RMSE in Scenario 1

In Table 4.3, the minimum, maximum, average and standard deviation of RMSE in meters is presented. The minimum RMSE value will be zero while the maximum RMSE value is approaching 71.3837 m. This maximum RMSE is high but the overall performance of the GPS-integrated prediction model is great as the average RMSE is between 5.6377 m to 6.8875 m, which is lower than 10 m. On the other hand, the standard deviation of RMSE for total 100s of outage can be remained below 15 m shows a good performance.

Table 4.3: Comparison of RMSE in Scenario 1

RMSE (m)	Route 1		
	Set 1	**Set 2**	**Set 3**
Maximum	71.3837	63.4060	64.1347
Average	6.8875	5.6377	6.8079
Standard Deviation	12.6611	10.4699	12.9271

In comparison with the smartphone-based inertial navigation system in [144], the location is predicted according to gyroscope-based heading and magnetometer-based heading. The maximum errors obtained are 211.86 m and 296.16 m. If using the magnetometer-based heading prediction as example, the mean error is 111.64 m while the standard deviation is 82.80 m. The error is higher than the RMSE in this road test result and it happens in a real distance of 183 m which is comparable with the distance in this experiment.

4.4.2 Scenario 2

Scenario 2 is the second test trajectory in Samajaya Free Industrial Zone. It is another rectangular path but with only four major left turnings, involving two right-angle turnings (90°) and two non-right-angle turnings (< 90°). The starting and ending point is at the same destination as shown in Figure 4.27 and the white arrow shows that the vehicle is facing south west before the experiment is carried out.

The data collection of Scenario 2 is carried out on 6 March 2017 (Monday), from 9.05 am to 9.21 am with total of 5 set data. The total of 16 minutes' drive has collected about 960 data. Each round of driving contributes about 192 data in 192 seconds. The performance of the three sets of data will be presented. The weather is good during data collection and without traffic congestion.

Figure 4.27: Second Test Trajectory Plotted on Google Map

There are 12 GPS signal outages which is intentionally substitute into the GPS-integrated model during the field test. In Scenario 2 Set 1, when the vehicle was facing south west, the errors are smaller and below 10 m. There are 4 out of 12 outages with low error. After the first corner, each outage shows larger error that more than 20 m. Among the 8 high errors prediction, the highest is at 151 s where the error increases up to 80 m.

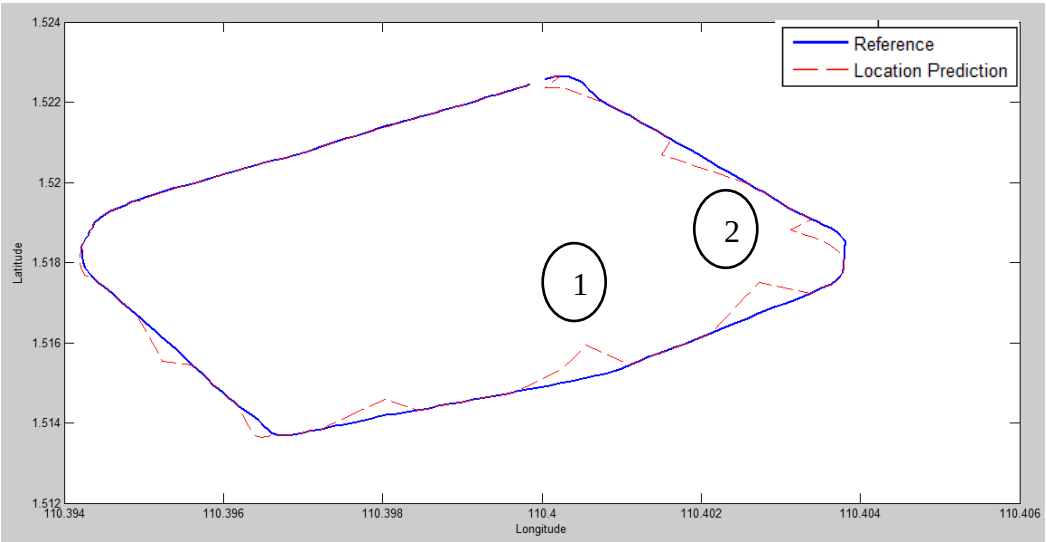

Figure 4.28: Comparison between Reference and Location Prediction (Scenario 2 Set 1)

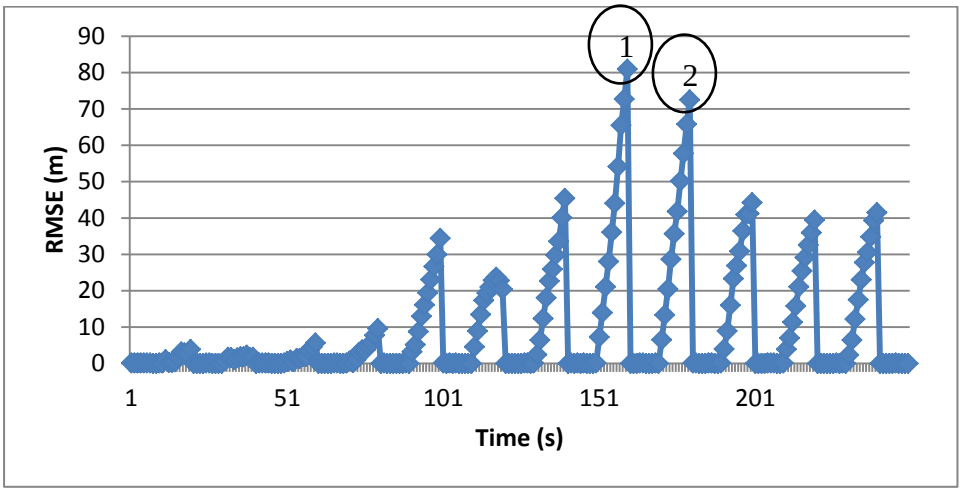

Figure 4.29: RMSE versus Time (Scenario 2 Set 1)

In Scenario 2 Set 2, there are 3 prediction errors that are more than 50 m, 5 prediction errors that are in the range of 20 m to 50 m while other 4 predictions have error less than 10 m (at the beginning and when vehicle was facing south west). The predicted route deviated to the right when the vehicle was facing south east and deviated to the left when facing north east and north west. Comparative to the performance in Scenario 1 whereas the errors tend to increase to higher point when the vehicle was facing to the north east.

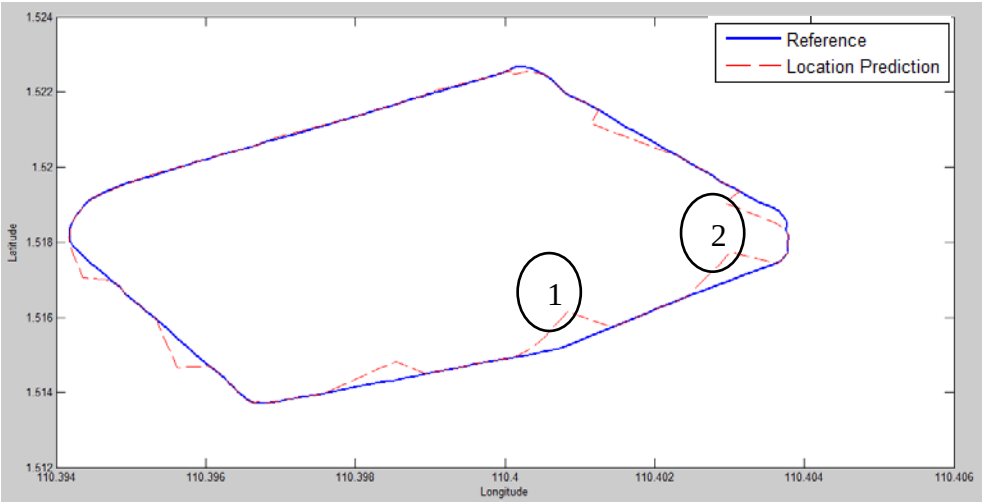

Figure 4.30: Comparison between Reference and Location Prediction (Scenario 2 Set 2)

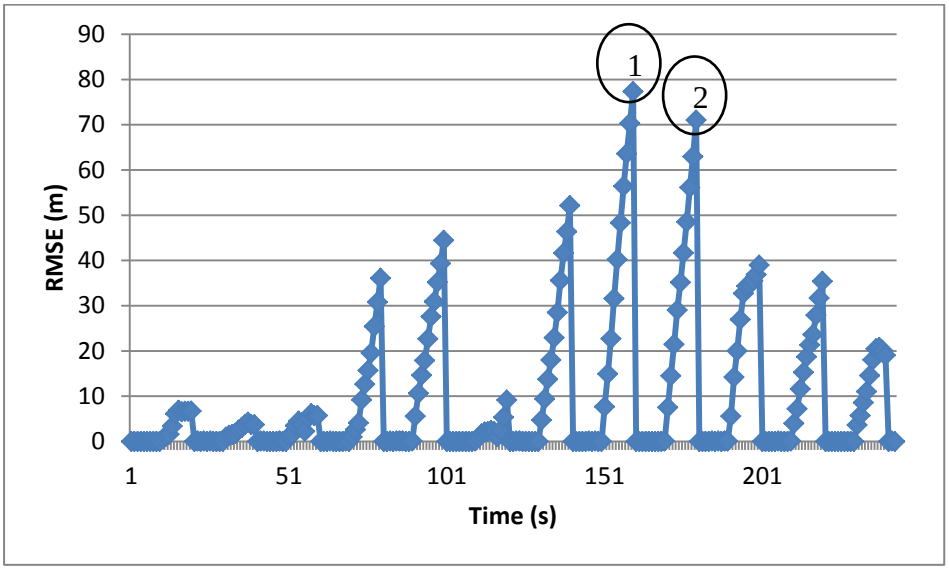

Figure 4.31: RMSE versus Time (Scenario 2 Set 2)

In comparison with Scenario Set 1 and Set 2 data, Set 3 performs the best which it has only 2 major prediction errors. The 2 major errors are about 48 m and 62 m when the vehicle was facing south east. The other errors are about 22 m or below. The 2 major errors happened when the measured heading direction/bearing is about 20° different from the actual value.

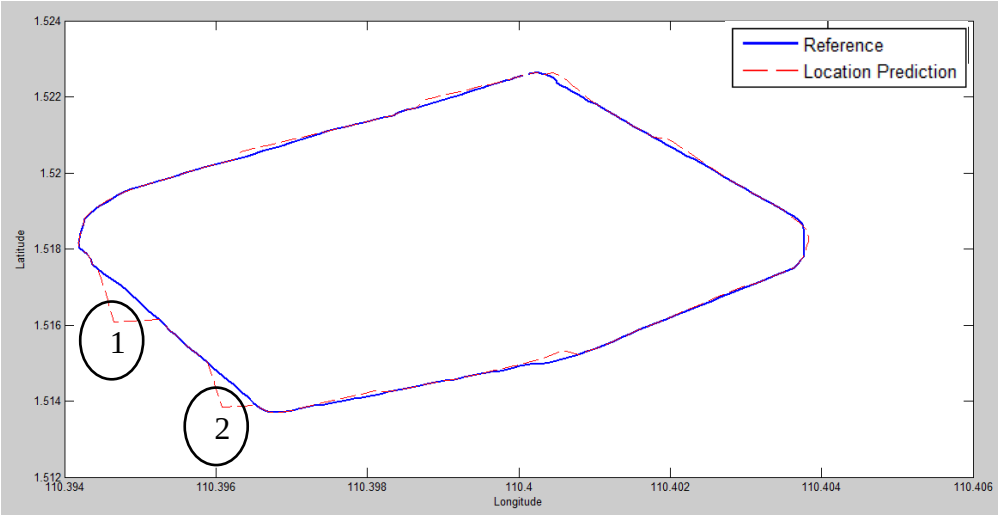

Figure 4.32: Comparison between Reference and Location Prediction (Scenario 2 Set 3)

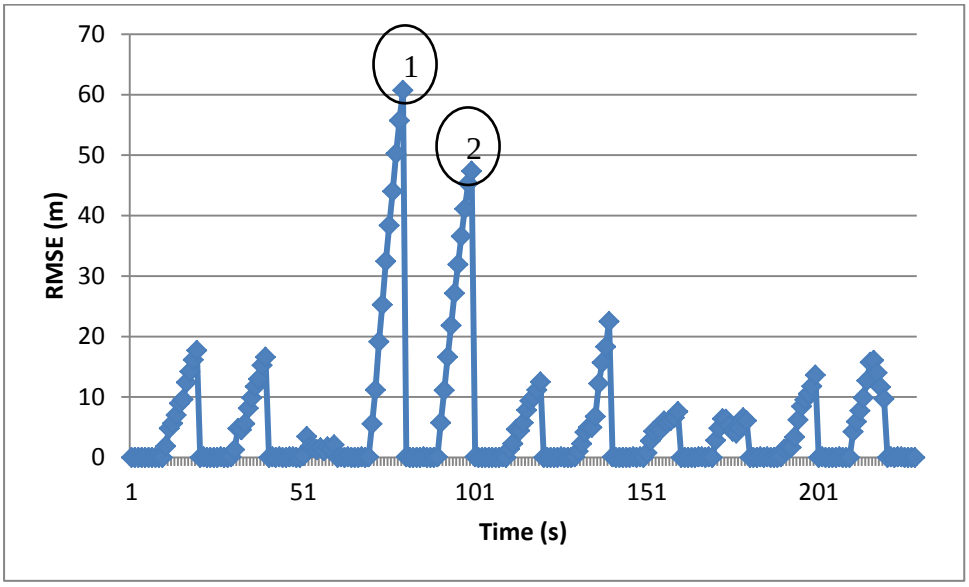

Figure 4.33: RMSE versus Time (Scenario 2 Set 3)

Referring to Figure 4.34, the errors of Set 1 and Set 2 are more similar. Both sets of data have the highest errors at the 151 s and 171 s with errors in the range of 70 m and 80 m. The large errors at these 2 outages are due to the deviation of compass values for more than 20°.

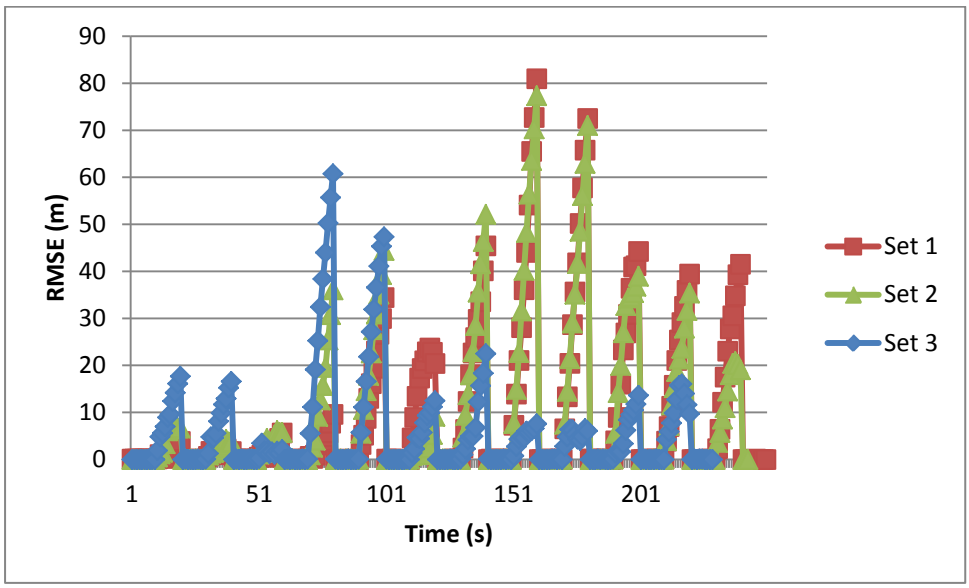

Figure 4.34: Comparison of RMSE in Scenario 2

The minimum error values are 0 m while the maximum error values range from 60 m to 80 m. In total of 250 data, there are 12 outages which involve 120 s of prediction. In average, the prediction has RMSE of 8.94 m, 9.31 m and 5.56 m. The prediction errors can be maintained below 10 m is good. The standard deviations of RMSE are about 10 m and 15 m. The results of the outperforming set 3 can be seen from Table 4.4 as well. Its maximum, average and standard deviation of RMSE is the lowest among the 3 set of data collections.

Table 4.4: Comparison of RMSE in Scenario 2

RMSE (m)	Route 2		
	Set 1	**Set 2**	**Set 3**
Maximum	80.9471	77.3509	60.7309
Average	8.9395	9.3090	5.5644
Standard Deviation	15.7659	15.7512	10.3887

Dynamic neural network is introduced into GPS/INS navigation and the authors mainly focus on IDNN technique [39]. The authors compare the results of IDNN with INS (raw), RBFNN and KF. IDNN gives RMSE of 11.89 m while others are larger than this value. Therefore, the average RMSE in Table 4.4 is good if compared to the result in [39].

4.4.3 Scenario 3

The third test trajectory was in Samajaya Free Industrial Zone. It is another rectangular path with four major left turnings, involving two right-angle turnings (90°) and two non-right-angle turnings (< 90°). The start/end point is indicated in Figure 4.35. The black arrow shows that the vehicle is facing south east before the experiment is carried out and the vehicle turned left after the experiment started for a few seconds.

The date of data collection for Scenario 3 was on 6 March 2017 (Monday) and the time was from 9.36 am to 9.53 am. There is a total of 4 set data in this 17 minutes' drive, contributing about 1020 data. Each round of driving contributes about 192 data in 192 seconds. The performance of the three sets of data collected under clear sky view and clear traffic will be presented, as following.

Figure 4.35: Third Test Trajectory Plotted on Google Map

The third test trajectory obtained the best measured heading direction/bearing as the data showed better prediction results if compared to other test trajectories. The largest error is 30 m and the second largest error is 20 m. These values are much lower than the maximum errors in previous scenarios. The major errors start to happen at the third turning corner, which involving twice 45° turns. After the forth turn, the compass was able to calibrate itself to make the logged heading direction/bearing accurate.

This trajectory has 10 GPS signal outages that was intentionally injected into the prediction model. Excluding the 2 major errors, there are 8 outages with prediction errors less than 20 m and 6 of them gives errors of 10 m or less than 10 m.

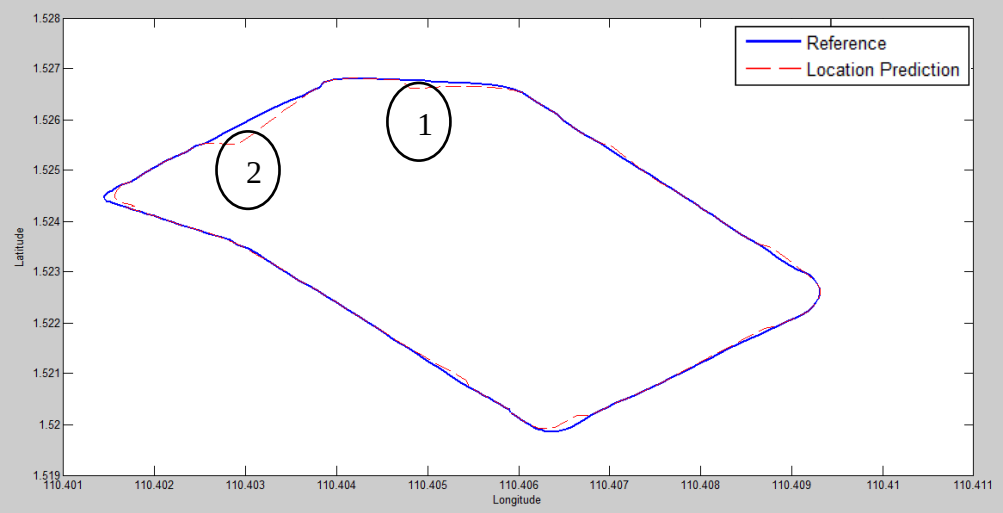

Figure 4.36: Comparison between Reference and Location Prediction (Scenario 3 Set 1)

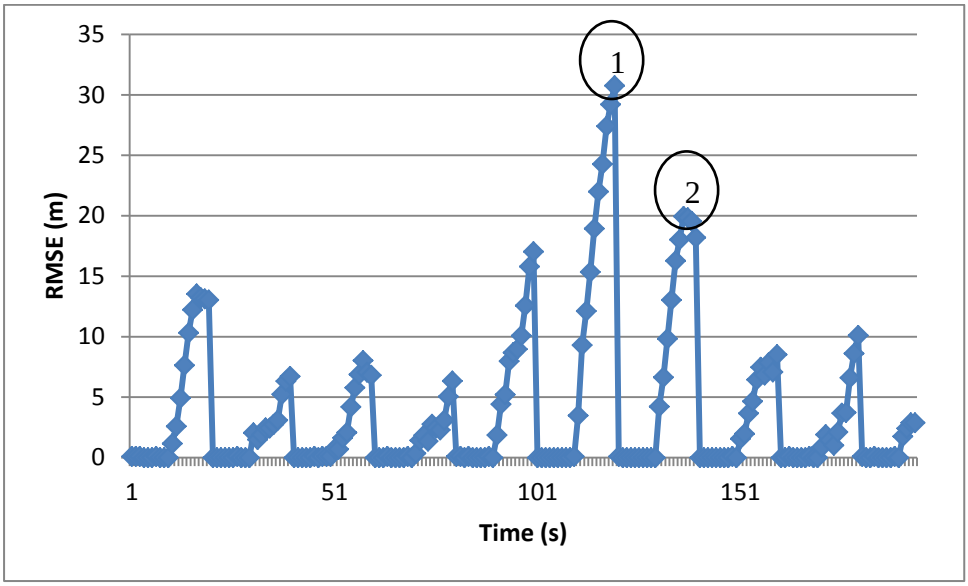

Figure 4.37: RMSE versus Time (Scenario 3 Set 1)

Scenario 3 Set 2 also gives great performance where the major errors only happened twice. The major errors are about 35 m while minor errors are below 15 m with 6 out of 8 are below 10 m of RMSE. The prediction is precise and accurate according to this performance.

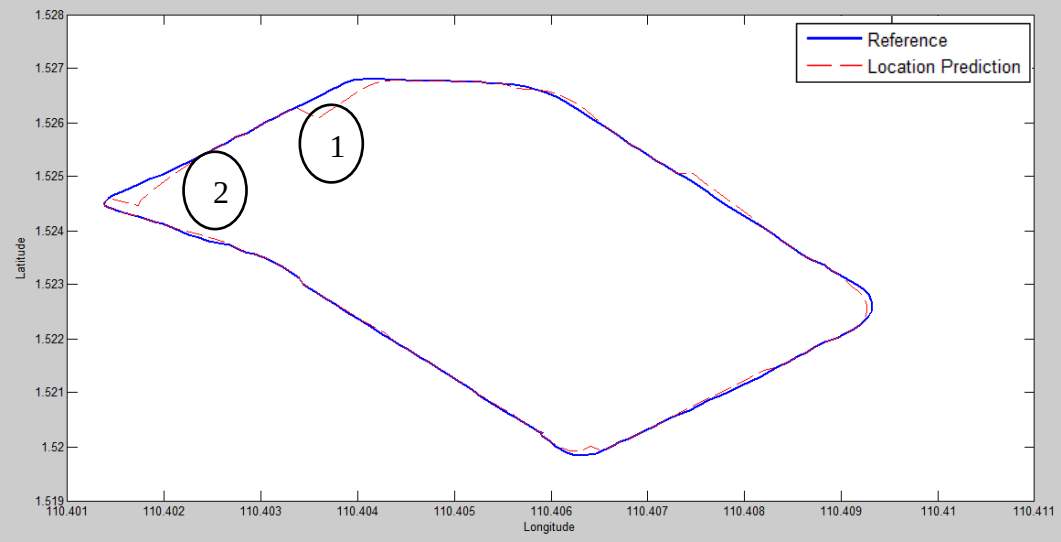

Figure 4.38: Comparison between Reference and Location Prediction (Scenario 3 Set 2)

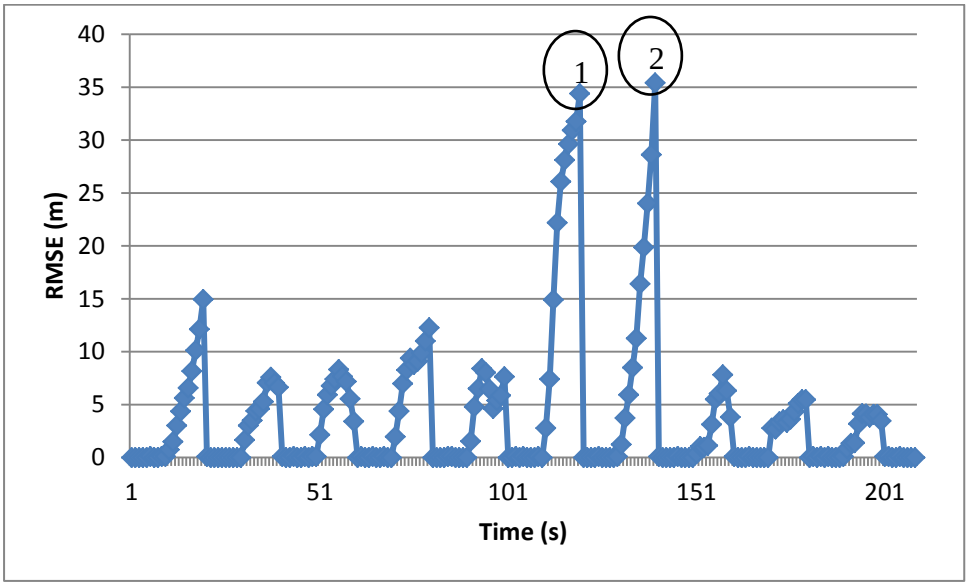

Figure 4.39: RMSE versus Time (Scenario 3 Set 2)

According to Figure 4.40, the major errors (29 m and 36 m) happened twice as indicated. There are 7 other outages which give prediction errors of less than 20 m. Among these 7 outages, 5 of them are with RMSE less than 15 m.

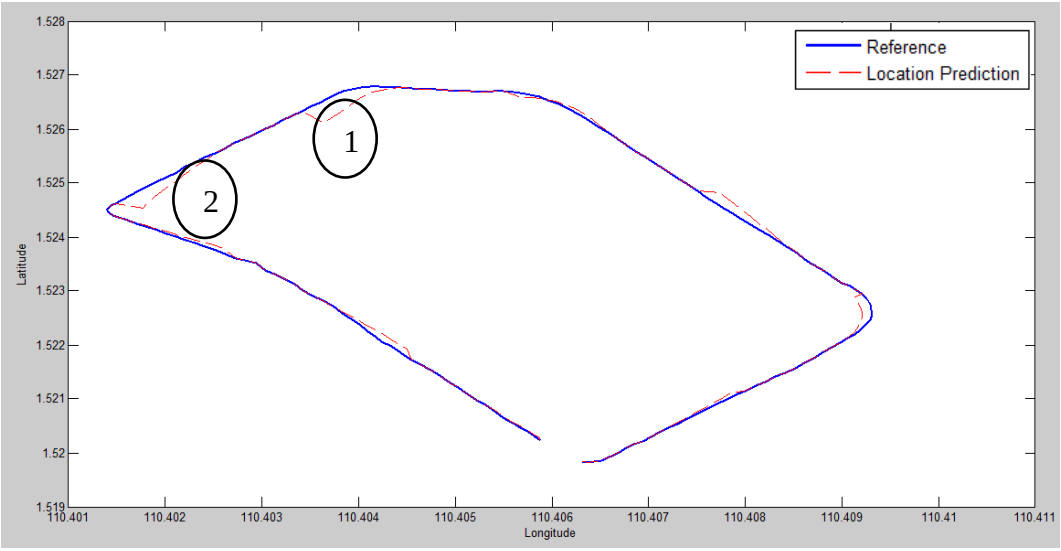

Figure 4.40: Comparison between Reference and Location Prediction (Scenario 3 Set 3)

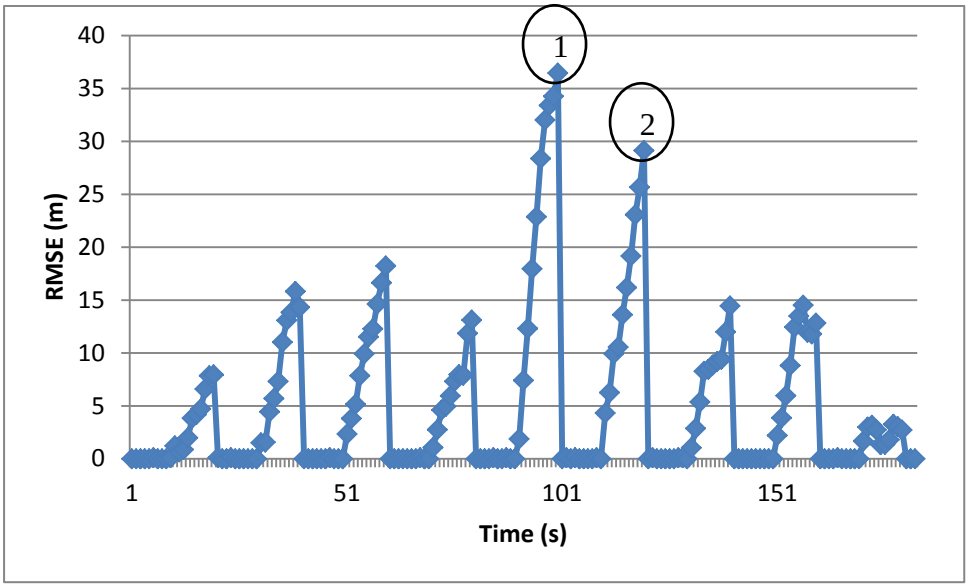

Figure 4.41: RMSE versus Time (Scenario 3 Set 3)

The performance of this 3 set of data in Scenario 3 is slightly different from each other. Set 3 performed the best at the 1st and 9th outages while performed the worst at 2nd, 3rd, 5th and 8th outages especially the 5th outage. Set 2 only performed the worst at 6th and 7th outage while it performed well during other outages. Set 1 performed moderately.

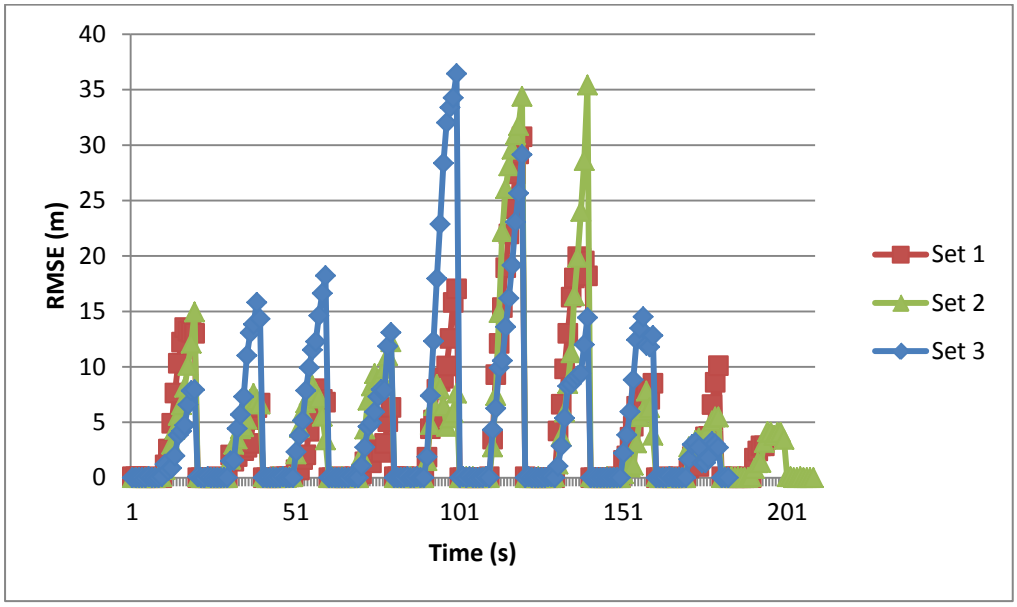

Figure 4.42: Comparison of RMSE in Scenario 3

The minimum value of RMSE is 0 m while the maximum value of RMSE is about 30 m to 36 m. However, judging at the average RMSE, the performance of prediction model in this scenario is the best among the 5 scenarios. The average RMSE of the data maintains below 5 m. The 210 data in this scenario gives 6.18 m, 6.81 m and 7.59 m standard deviation of RMSE respectively. The values of standard deviation also the lowest if compared to other 4 scenarios.

Table 4.5: Comparison of RMSE in Scenario 3

RMSE (m)	Route 3		
	Set 1	**Set 2**	**Set 3**
Maximum	30.7564	35.4105	36.4485
Average	3.7949	3.8773	4.8420
Standard Deviation	6.1844	6.8054	7.5872

An advanced GPS/INS using extended KF and integrating vector observations was described [145]. The different duration of GPS outages was inserted during the experiment.

During the total of 235 seconds of GPS outage, the average RMSE was 7.975 m according to calculation. This value was higher than the average RMSE obtained through the experiment, which is below 5 m.

4.4.4 Scenario 4

Scenario 4 was happened in Samajaya Free Industrial Zone but it is a long straight road with 2 roundabouts. There is a big roundabout and a smaller roundabout. The second roundabout indicates a 180° turning. The vehicle is facing north east at the start/end point as shown by the black arrow in Figure 4.43.

Scenario 4 data collection is carried out on 6 March 2017 (Monday), from 9.56 am to 10.10 am. The 3 sets of data were collected within 14 minutes with about 840 data. Averagely each set of data is 280 seconds and 280 data. The data shows good performance as the weather and traffic was excellent during the experiment.

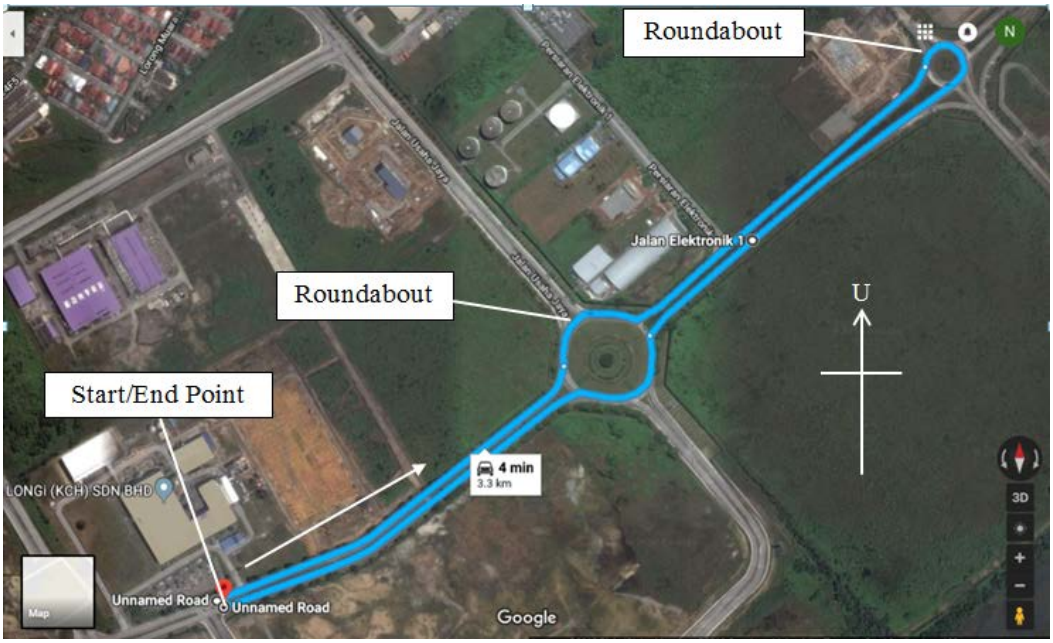

Figure 4.43: Forth Test Trajectory Plotted on Google Map

The difference between this scenario and previous 3 scenarios is that this is not a rectangular path with a few of left turnings but is a long straight round with 2 roundabouts and they are right turning roundabouts. In Figure 4.44, it can be observed that the predicted coordinates of the vehicles shifted to the left when the vehicle is moving towards north east while the predicted coordinates also shifted to the left after 2 roundabouts and facing south west.

The set 1 data shows about 13 times of 10 s GPS signal outages were inserted into the prediction model. There are 4 positioning errors that more than 35 m. Other than RMSE of 21 m and 27 m, other RMSE are below 15 m. The RMSE increases after the 180° turning at the second roundabouts.

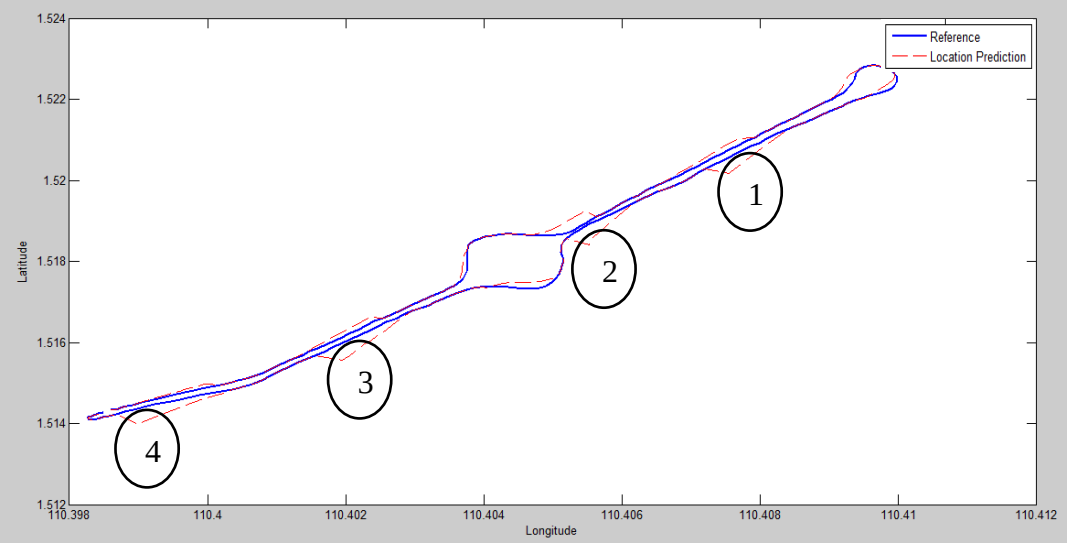

Figure 4.44: Comparison between Reference and Location Prediction (Scenario 4 Set 1)

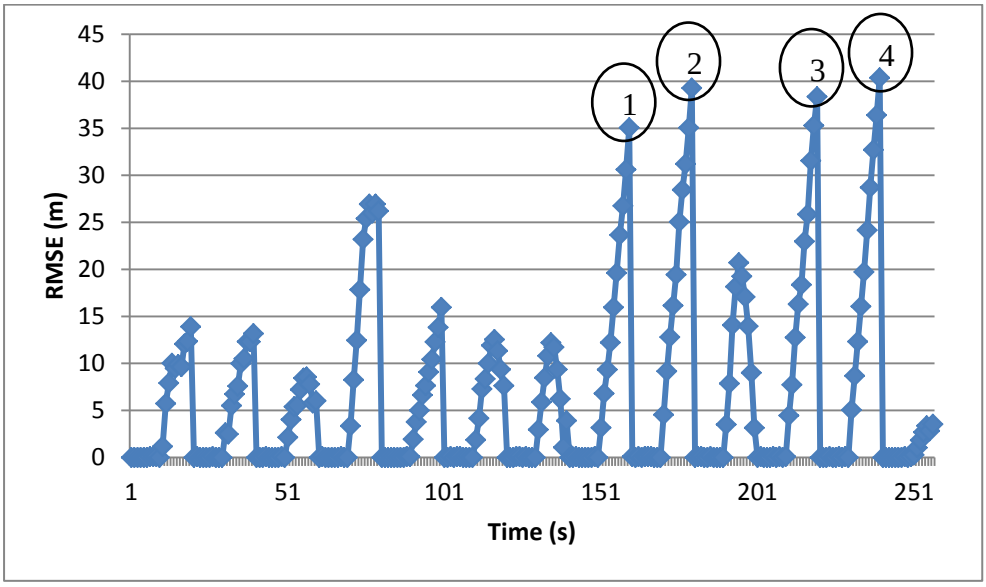

Figure 4.45: RMSE versus Time (Scenario 4 Set 1)

For Scenario 4 set 2, the error goes high to 25 m right after the first roundabout. The error is then minimized until it approached the second roundabout. Its error is about 32 m. Other than that, most of the errors remain in the range of 20 m.

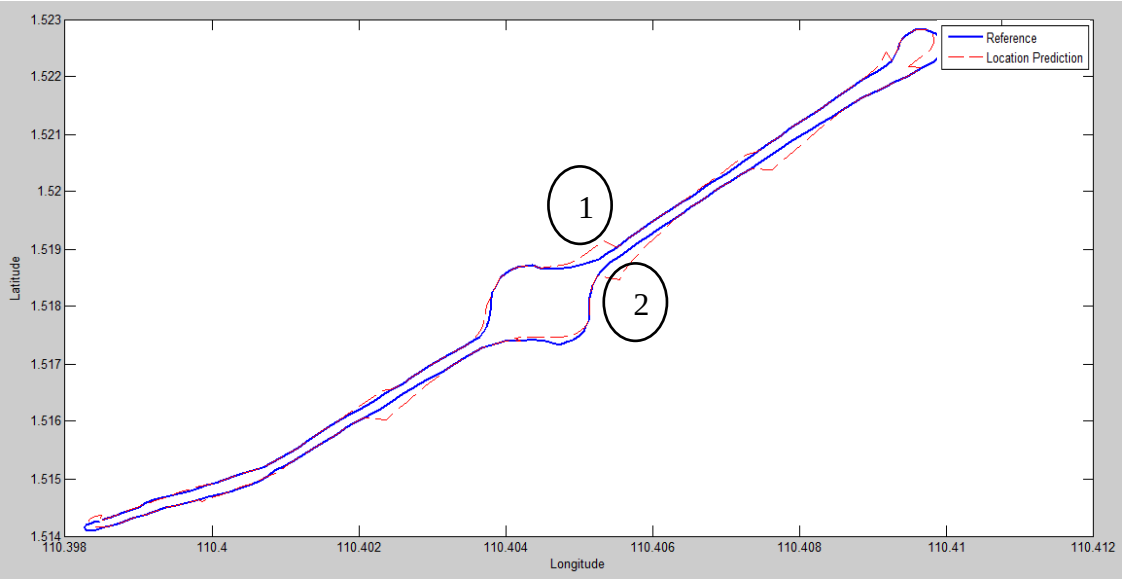

Figure 4.46: Comparison between Reference and Location Prediction (Scenario 4 Set 2)

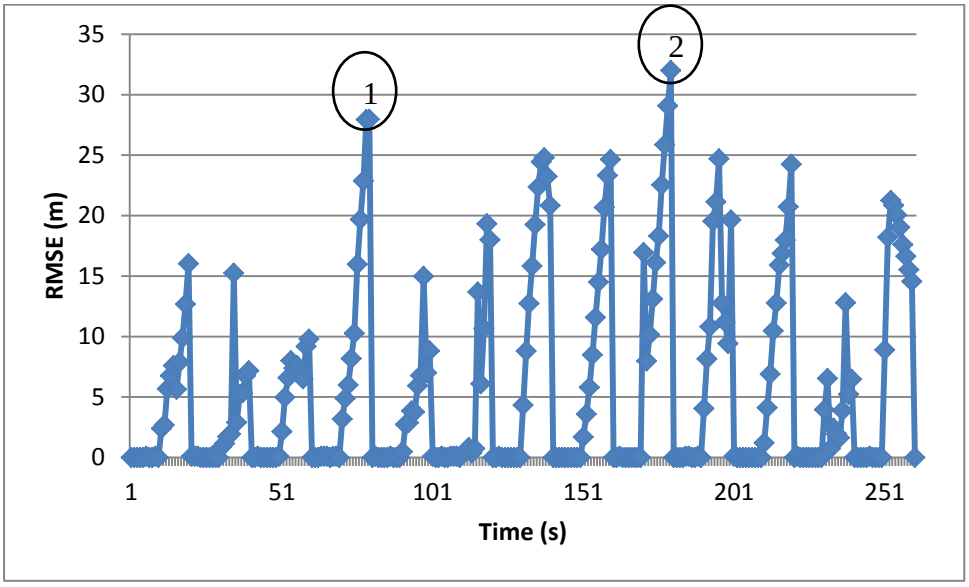

Figure 4.47: RMSE versus Time (Scenario 4 Set 2)

The 4 highest prediction errors during outages are as shown in Figure 4.48 and Figure 4.49. The highest error is during the turning at the second roundabout which is relatively smaller and needs more change in the direction of vehicle. The other 3 errors are high is due to the failure of compass adjustment after the 180° turning at the roundabout.

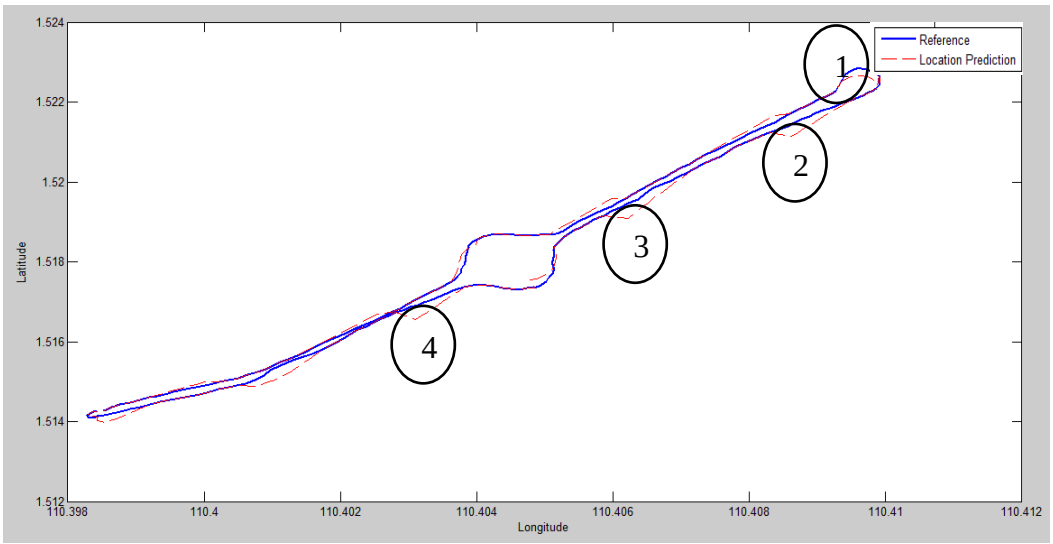

Figure 4.48: Comparison between Reference and Location Prediction (Scenario 4 Set 3)

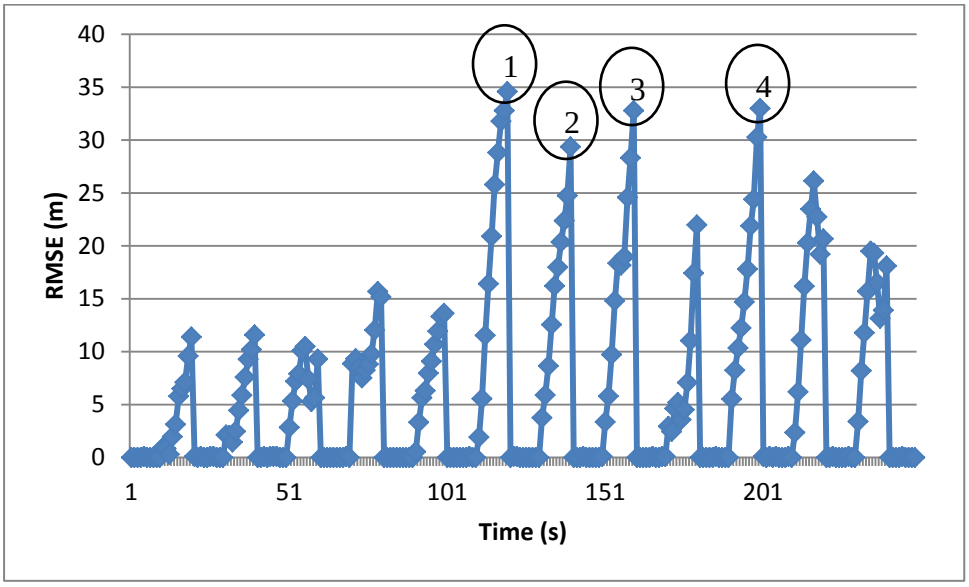

Figure 4.49: RMSE versus Time (Scenario 4 Set 3)

To conclude the overall performance of prediction model in Scenario 4, Figure 4.50 is plotted. The RMSE of 2 set data are presented in graph form. Set 3 performed better at the 4th, 8th, 11th and 12th outage but performed poorer at 6th and 10th outages. From figure, it can be observed that set 1 performed the worst as it contributed a few highest error values. Meanwhile, set 2 gives good performance in term of RMSE as it has only 2 large errors.

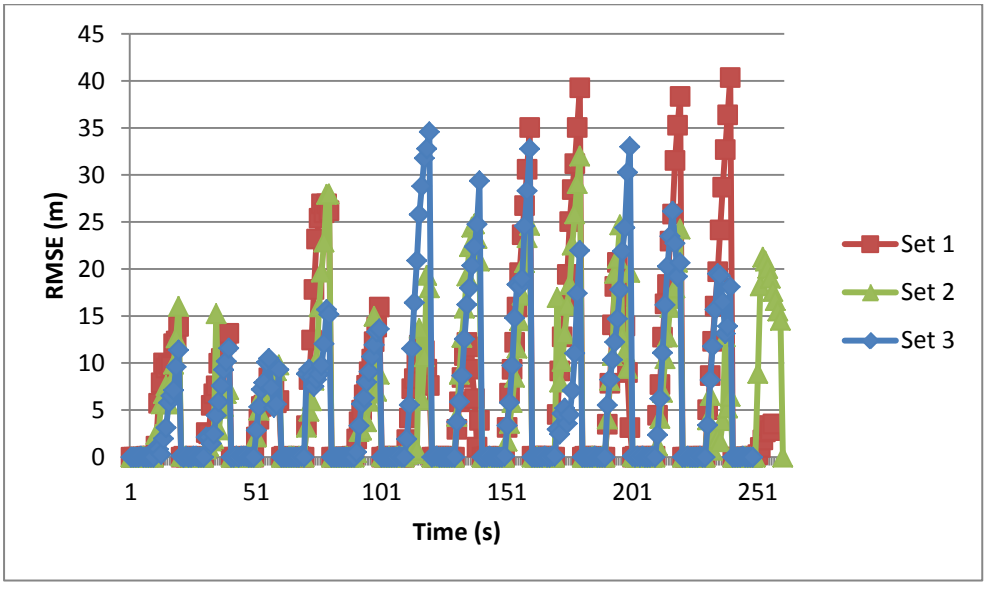

Figure 4.50: Comparison of RMSE in Scenario 4

The minimum value for the data is 0 m. Set 1 has the highest maximum RMSE which is 40.36 m. This raises the average RMSE of set 1 to 6.47 m and its standard deviation to 9.47 m. Set 2 has the lowest maximum, average and standard deviation of RMSE. Its performance is the best. Set 3 has a moderate performance if compared to set 1 and set 2. To conclude the results of the prediction model, the average and standard deviation of RMSE are all below 10 m. This is considered as a successful prediction model.

Table 4.6: Comparison of RMSE in Scenario 4

RMSE (m)	Route 4		
	Set 1	**Set 2**	**Set 3**
Maximum	40.3595	32.0080	34.5755
Average	6.4738	5.6031	5.9381
Standard Deviation	9.4696	7.8881	8.5114

To compare with the results of this scenario, MEMS-based INS/GPS integration for low-cost navigation applications [110] will be discussed. This paper focuses on improving the performance of navigation through the implementation of KF-auto-regressive (KF-AR) model and KF-adaptive-neuro-fuzzy (KF-ANF) module. Within the stimulated 45 s GPS outages, the highest RMSE presented by KF-AR is approaching 60 m. KF-ANF is utilized to enhance the performance of KF-AR by reducing the RMSE to below 20 m and 8 of 9 of the RMSE are below 10 m.

4.4.5 Scenario 5

The fifth test trajectory is at Jalan Akses FAC. It is a long straight road with a main U-turn (180°). The total length of road is 12 km and the driving time is about 10 minutes. The field test was carried out on 6 March 2017 (Monday) in between 1.48 pm and 2.36 pm.

The starting and ending point is as shown in Figure 4.51 and the white arrow shows that the vehicle was facing north west before it departed.

The vehicle mainly faced north west after started the journey and faced south east after make a U-turn. According to the total duration of 48 minutes data collection, there is a total of 2880 data obtained from the 5 rounds of driving. This indicates there is a mean of 576 data per set. The sun was bright and shines while the traffic was smooth during the data collection. The best 3 sets are presented as below.

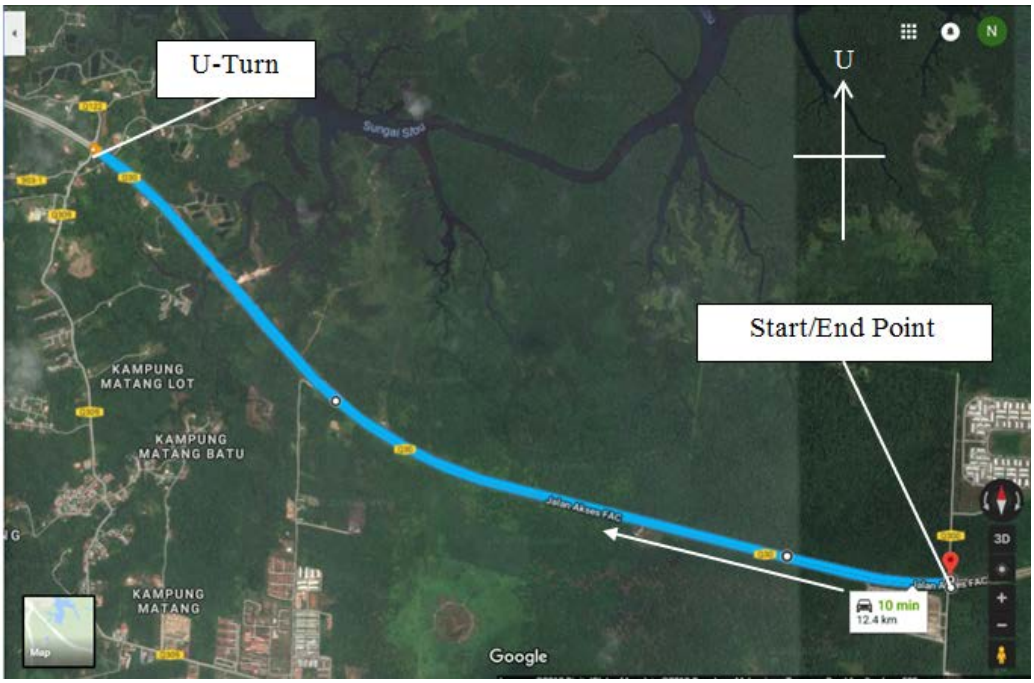

Figure 4.51: Fifth Test Trajectory Plotted on Google Map

This test trajectory is purposely set to a long distance and long duration data collection. With an interval of 10 s, a 10 s GPS signal outage will be programmed into the prediction model. The total number of GPS signal outage is 28. Within these 28 times of outages, the prediction data is about 280.

From Figure 4.52, the prediction errors cannot be seen clearly but the errors can be check in Figure 4.53. Out of 28 outages, there are 9 outages gave errors that more than 30 m while another 19 gave errors that less than 30 m. The errors happened at 7th to 13th outage. This error increasing during vehicle was speeding on a road while there is a small curve on the straight road. The curve means there is a slight change in the heading of vehicle during the driving. However, the small changes are hardly detected and measured by the compass logger especially during high speed.

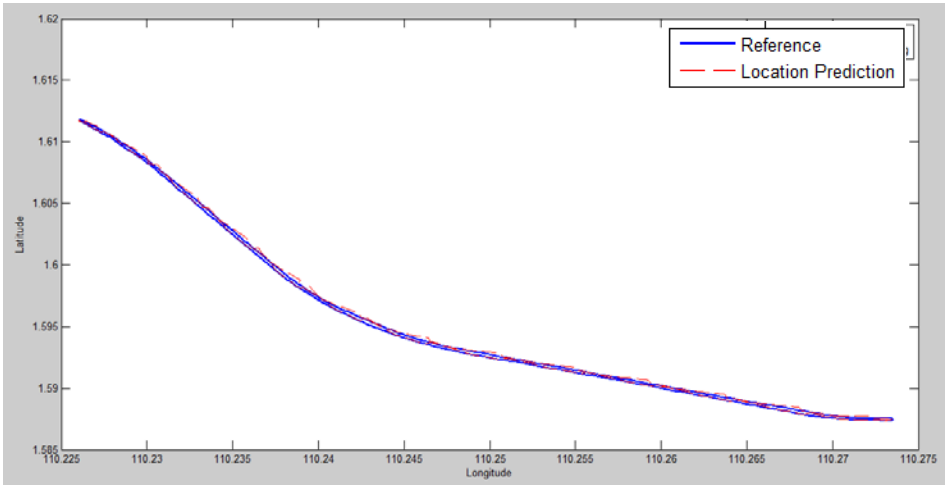

Figure 4.52: Comparison between Reference and Location Prediction (Scenario 5 Set 1)

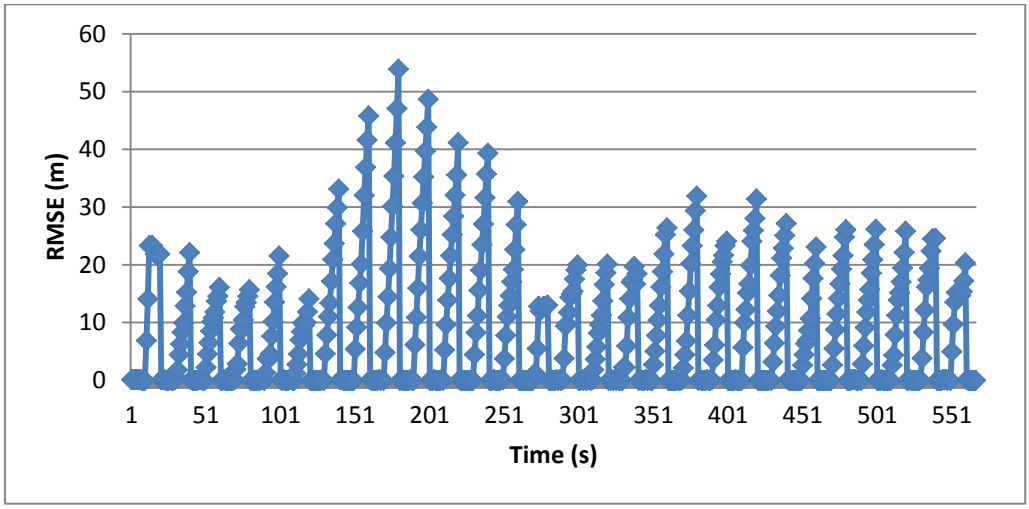

Figure 4.53: RMSE versus Time (Scenario 5 Set 1)

Figure 4.54 shows the test results of scenario 5 set 2 and Figure 4.55 shows the RMSE versus time. There are 24 outages inserted into the prediction model. The performance is better since the errors do not more than 40 m. 24 out of 28 predictions give errors less than 35 m and 33.33% of them give errors that less than 10 m.

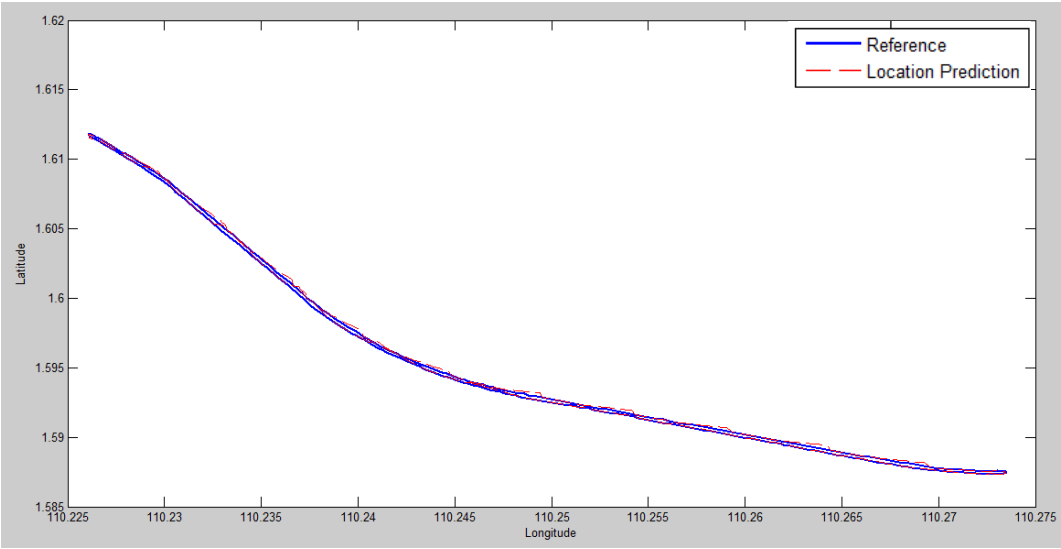

Figure 4.54: Comparison between Reference and Location Prediction (Scenario 5 Set 2)

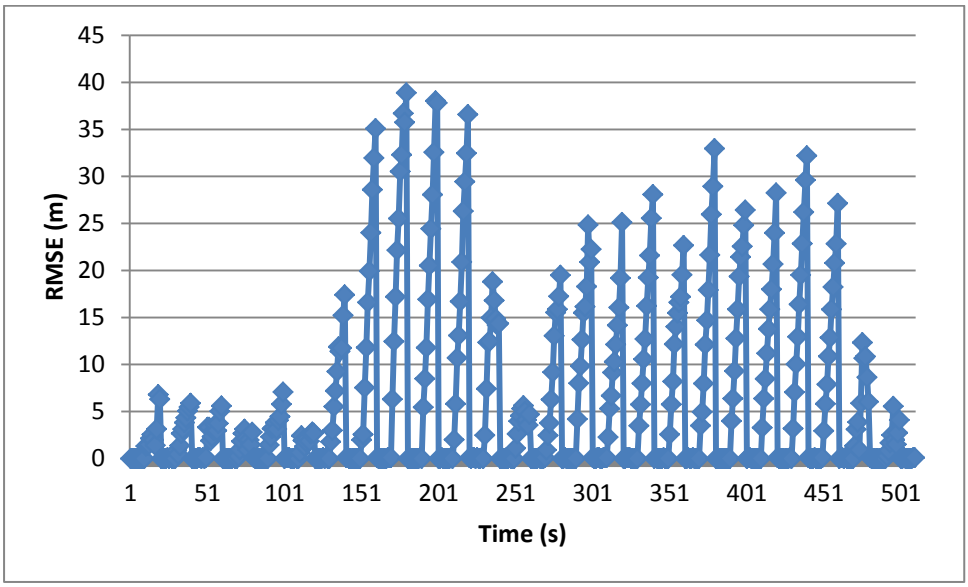

Figure 4.55: RMSE versus Time (Scenario 5 Set 2)

Figure 4.56 and Figure 4.57 show the results of scenario 5 set 3. There are 25 GPS signal outages that are purposely introduced to the prediction model. There are 4 out of 25 outages give errors more than 40 m. Other errors maintained below 30 m with only 2 errors below 10 m.

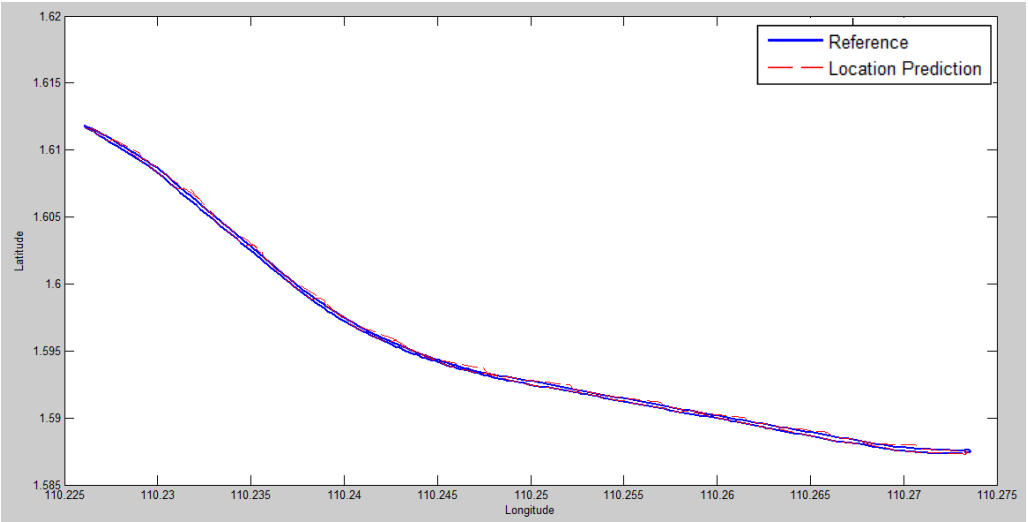

Figure 4.56: Comparison between Reference and Location Prediction (Scenario 5 Set 3)

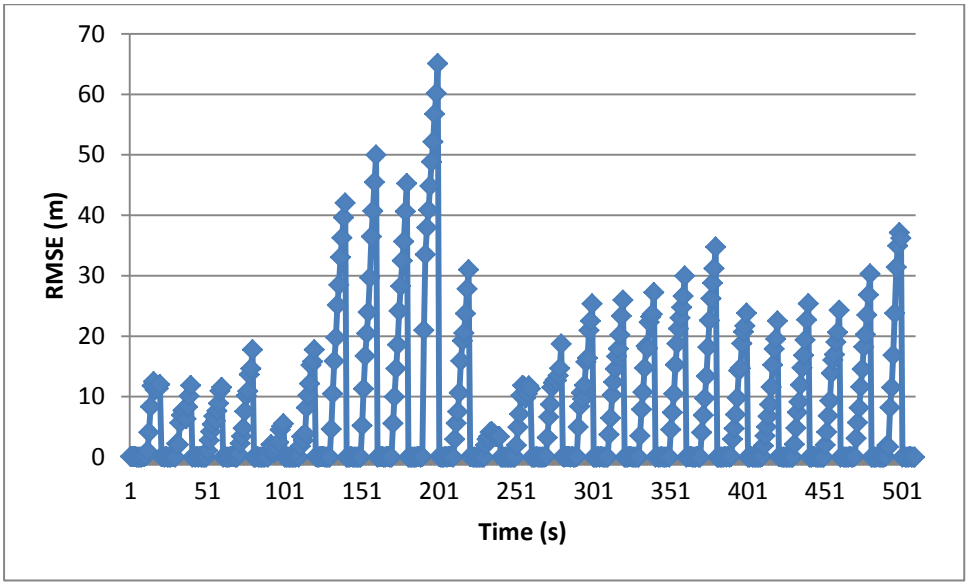

Figure 4.57: RMSE versus Time (Scenario 5 Set 3)

Set 1 spent the most time on data collection and provided more data. Its accuracy from the beginning is much higher than the other 2 sets of data. It has the highest errors from 1st to 5th outage, 9th outage, 11th to 13th outage and 21st outage. Set 1 has the worst performance. Set 2 gives good performance as it only shows the highest errors at 22nd and 23rd outages while has more errors that less than 10 m. Set 3 is the set with moderate results as it has 6 highest errors which is less if compared to set 1's 10 highest errors.

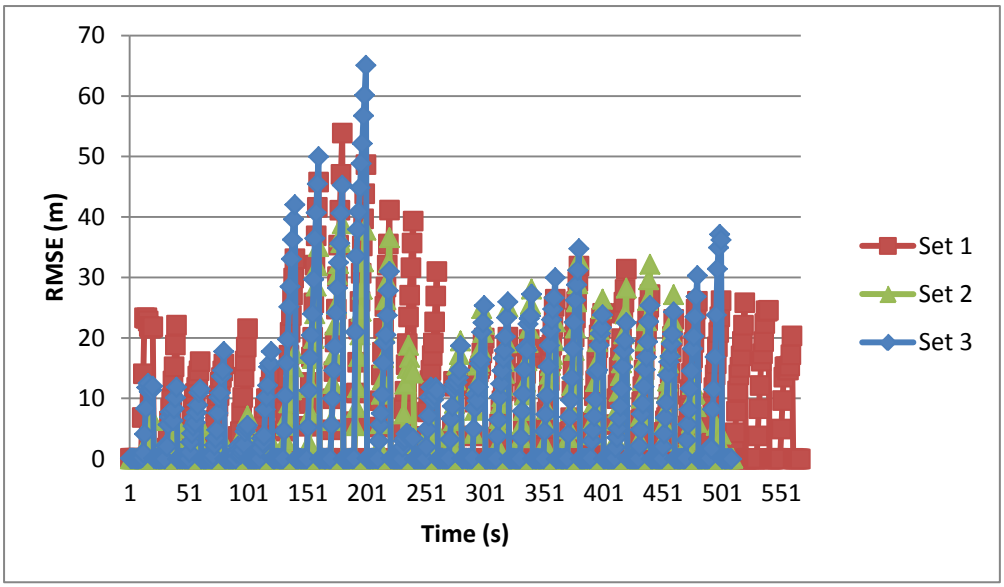

Figure 4.58: Comparison of RMSE in Scenario 5

The minimum values of the RMSE in scenario 5 are 0 m. The maximum values of RMSE in scenario 5 are 53.90 m, 38.88 m and 65.08 m. These maximum values are lower than scenario 1 and scenario 2. The average values of RMSE are below 10 m, which is good as prediction result. The standard deviations of RMSE are 10.52 m, 8.84 m and 11.42 m. These values are comparative with the values in scenario 1 and scenario 2.

Table 4.7: Comparison of RMSE in Scenario 5

RMSE (m)	Route 5		
	Set 1	**Set 2**	**Set 3**
Maximum	53.8965	38.8826	65.0795
Average	7.8452	5.5953	7.4919
Standard Deviation	10.5168	8.8427	11.4183

Various filters are introduced into INS/GPS integration system [146]. The author proposes that adaptive filter is more effective than EKF in terms of estimating position and heading. The on-vehicle road tests are carried out with additional position errors are stimulated into the system within 20 s. Subsequently, simulations are performed to compare the performance of EKF and adaptive filter. The adaptive filter is outperforming and shows RMSE of 12.23 m (latitude error of 8.85 m and longitude error of 8.44 m). The RMSE in this dissertation has better performance than the results in [146].

4.5 Comparison with Other Methods

To further verify the smartphone-based GPS-integrated location prediction model, the results of the model is compared with other works. The other methods that available for location prediction include Vincenty's formula and Haversine formula.

Vincenty's formula is developed by Thaddeus Vincenty in 1975 [147]. The assumption that the figure of the earth is an oblate spheroid is made. Thaddeus Vincenty developed direct problem and inverse problem. The direct problem can be used to compute coordinates while the inverse problem can be used to compute distance and azimuth. The computation is complex. It involves a lot of intermediate parameters and iterations. This method requires longer computational time.

Haversine formula is an equation that is developed according to the law of haversine which relates the sides and angles of spherical triangles [148]. The formulas can be used to calculate great-circle distances between two points on a sphere or calculate the coordinate based on the distance and azimuth.

Vincenty's formula and Haversine formula are programmed by using Matlab (Appendix C and Appendix D). The results of these two formulas are presented in graphical form and in term of RMSE to compare with the results of the model.

The condition of satellite signal lost is assumed as happens when the number of satellites is less than 15 (can be other random number). This condition is intentionally added to the Matlab codes to test the formulas. From Figure 4.59 to Figure 4.63, it can be observed that the location prediction is performed occasionally and randomly.

However, the similarity is that the predicted coordinates by Vincenty's formula, Haversine formula and the prediction model are close to each other. According to the data, they only slightly differ. Thus, Table 4.8 to Table 4.12 show the difference between the computed average RMSE and standard deviation of RMSE in all scenarios.

Figure 4.59 shows the reference route of Scenario 1 and its predicted routes by Vincenty's formula, Haversine formula and the prediction model. The blue route is the reference route. The red and green line covered by the purple line as they are too close to each other's values. The small differences can only be observed from Table 4.8.

The three different methods can give similar performance in terms of RMSE. The highlighted boxes in Table 4.8 are the lowest values if compared to the other two techniques. By this, it can be concluded that Vincenty's formula with the most complex

computation and consideration is not necessary give the best performance. The other two equations can give better accuracy as well.

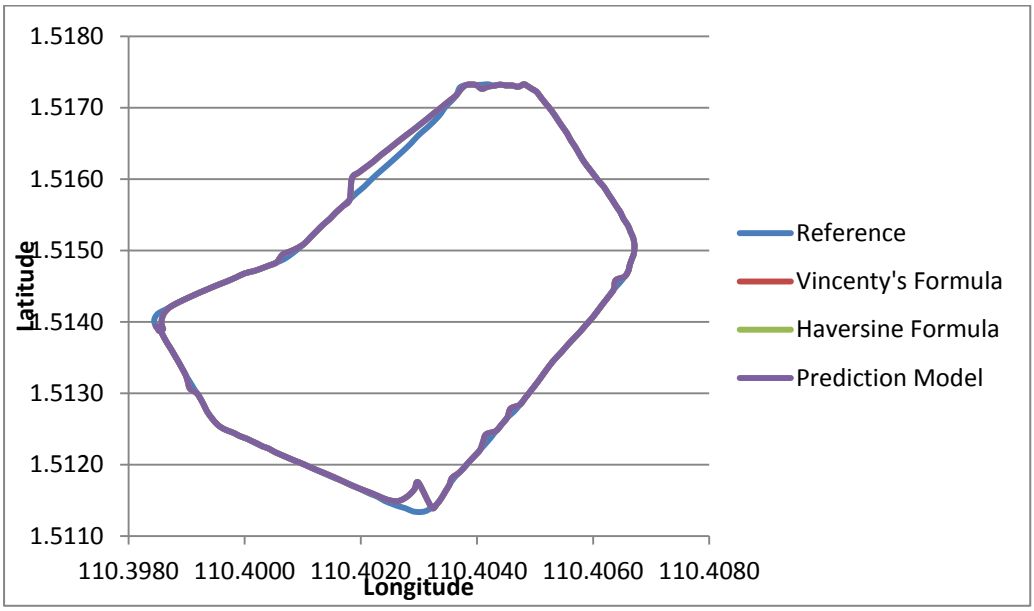

Figure 4.59: Comparison of the Results of Formulas (Scenario 1)

Table 4.8: Comparison of the RMSE of Formulas (Scenario 1)

RMSE	Vincenty's Formula	Haversine Formula	Prediction Model
Average	7.6181	7.5823	7.5831
	5.6272	5.6083	5.6075
	2.8723	2.9033	2.8975
Standard Deviation	21.7734	21.6412	21.6501
	13.1109	13.0169	13.0228
	6.7804	6.8563	6.8467

Figure 4.60 is the comparison of the results of formulas for Scenario 2. The performance of three prediction formulas is as expected, consistent and similar. The red, green and purple lines are predicted routes. They deviate from the blue reference route at the same points and same timing. The magnitude of deviation is slightly different from

each other. The RMSE of Haversine formula and prediction model is closer if compared to RMSE of Vincenty's formula.

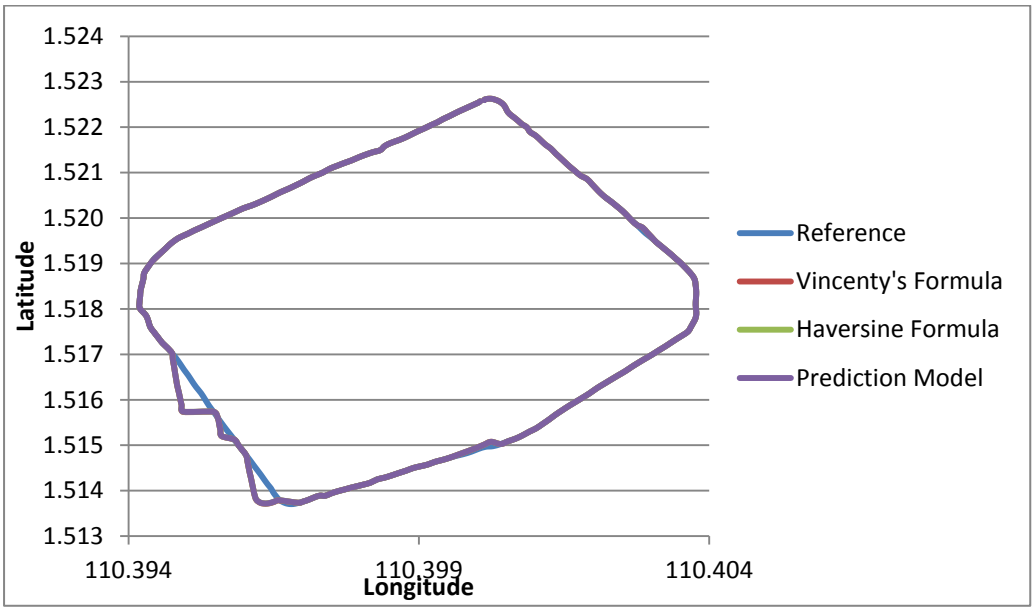

Figure 4.60: Comparison of the Results of Formulas (Scenario 2)

Table 4.9: Comparison of the RMSE of Formulas (Scenario 2)

RMSE	Vincenty's Formula	Haversine Formula	Prediction Model
Average	8.6345	8.6116	8.6118
	6.3059	6.3159	6.3139
	3.4120	3.3927	3.3936
Standard Deviation	16.6007	16.5536	16.5534
	17.7782	17.6876	17.6950
	9.6506	9.6105	9.6122

Scenario 3 has fewer errors if compared to Scenario 1 and Scenario 2. The obvious and major errors happen at the first and forth turnings. The average RMSE values are less than 10 m. Each prediction method can achieve similar RMSE performance. The lowest RMSE values are highlighted in Table 4.10. There is no prediction formula that always

provides the most precise and accurate prediction. The performance of these three methods is comparable.

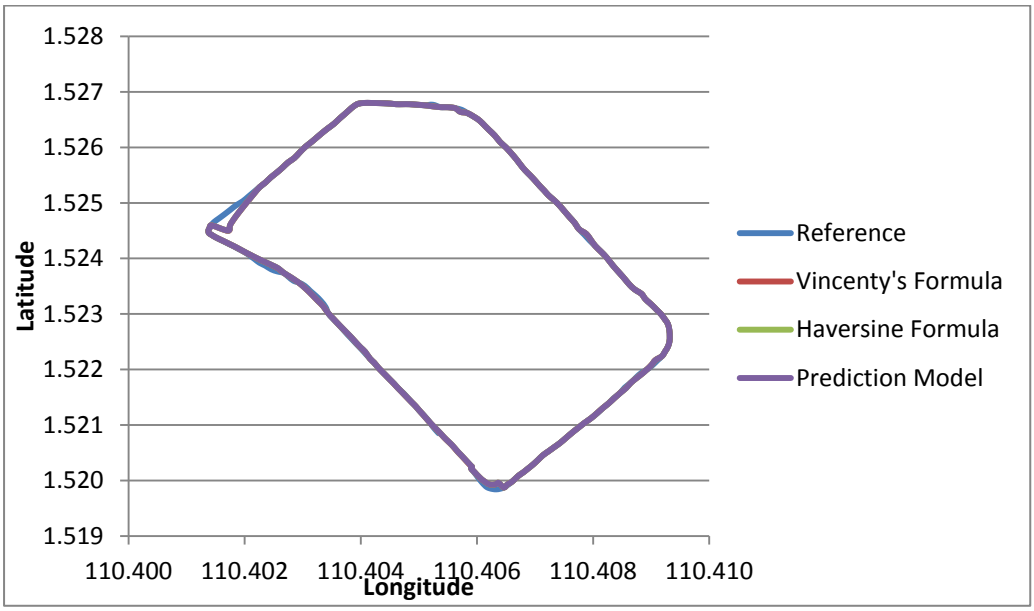

Figure 4.61: Comparison of the Results of Formulas (Scenario 3)

Table 4.10: Comparison of the RMSE of Formulas (Scenario 3)

RMSE	Vincenty's Formula	Haversine Formula	Prediction Model
Average	6.0447	6.2279	6.2097
	1.9021	1.9224	1.9207
	4.9710	4.8987	4.9016
Standard Deviation	9.8151	9.9776	9.9637
	3.9333	3.9204	3.9197
	14.2957	14.0962	14.1048

Among the scenarios, Scenario 4 has the minimal RMSE especially in terms of standard deviation. The standard deviation of RMSE from three prediction methods does not have difference even up to ten thousandth. The complex Vincenty's formula does not outperform in this case. Haversine formula and prediction model provides RMSE with minimal difference and they have better performance if compared to Vincenty's formula.

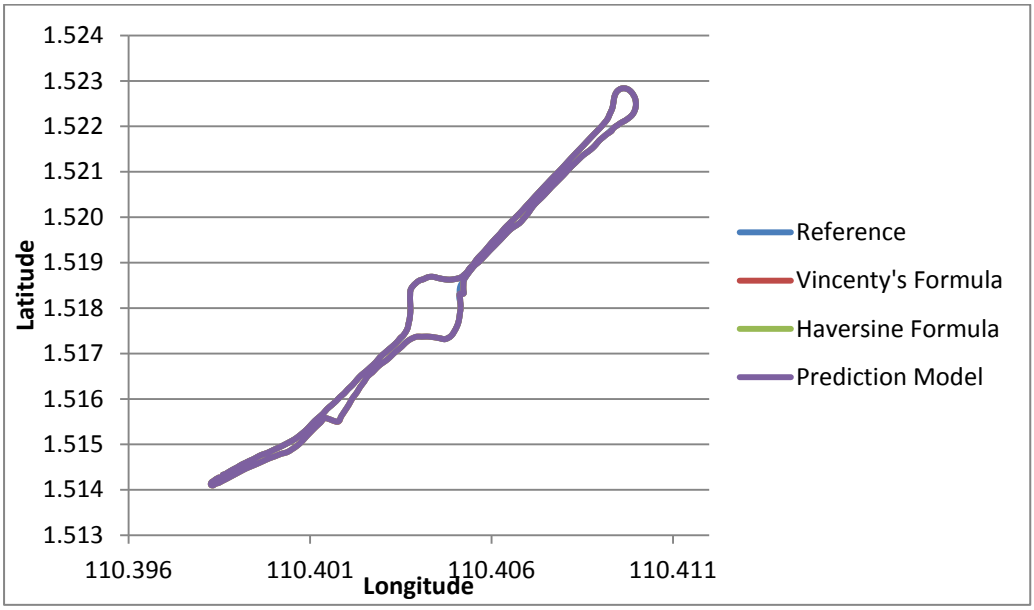

Figure 4.62: Comparison of the Results of Formulas (Scenario 4)

Table 4.11: Comparison of the RMSE of Formulas (Scenario 4)

RMSE	Vincenty's Formula	Haversine Formula	Prediction Model
Average	0.7293	0.7209	0.7213
	3.1441	3.1124	3.1121
	1.3533	1.3276	1.3280
Standard Deviation	0.0027	0.0027	0.0027
	0.0027	0.0027	0.0027
	0.0027	0.0027	0.0027

Scenario 5 is the longest route with the longest duration. Vincenty's formula gives the best RMSE in this case either in term of average or standard deviation. The RMSE values of three methods are comparable. The percentage of difference of RMSE between these three techniques is less than 2%. The small percentage of difference shows the trustworthiness of prediction model.

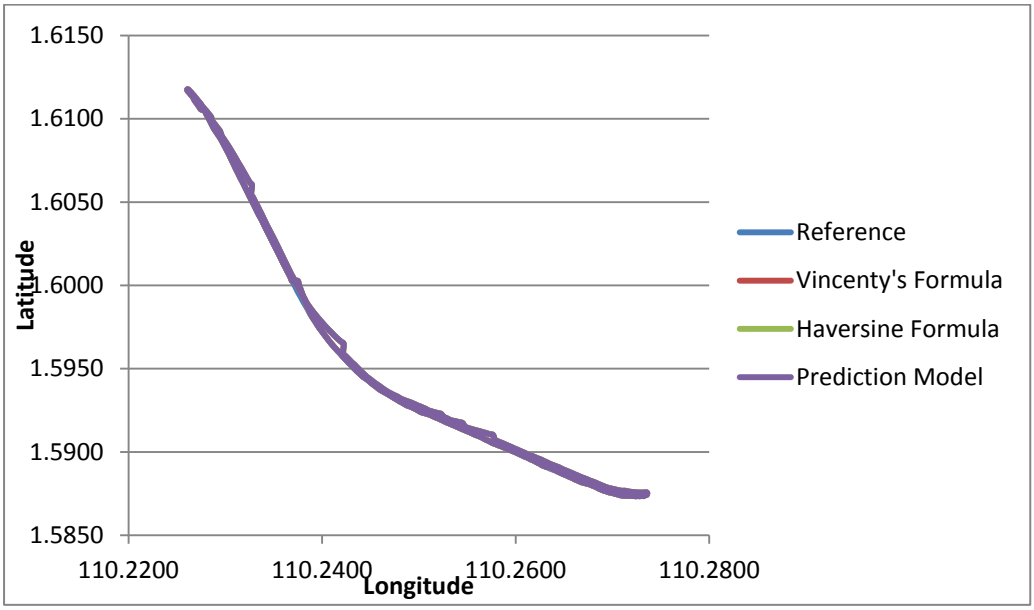

Figure 4.63: Comparison of the Results of Formulas (Scenario 5)

Table 4.12: Comparison of the RMSE of Formulas (Scenario 5)

RMSE	Vincenty's Formula	Haversine Formula	Prediction Model
Average	9.4117	9.5519	9.5406
	5.4217	5.4465	5.4440
	3.1249	3.1827	3.1777
Standard Deviation	20.3703	20.7001	20.6761
	16.0942	16.2139	16.2052
	8.9769	9.1679	9.1537

4.6 Chapter Summary

The functionality of the prediction algorithm and prediction model had been validated with the collected GPS data. For prediction algorithm, the standard deviation of RMSE is ranging in between 5 m to 10 m. For prediction model, the standard deviation of RMSE is ranging in between 1 m to 9 m. The range of RMSE validates the functionality of the prediction algorithm and prediction model.

The smartphone-based GPS-integrated location prediction model for OBD-II-equipped land vehicle localization was developed. Then, the experimental works were carried out in five chosen scenarios. For Scenario 1, the standard deviation of RMSE ranges from 10 m to 13 m. For Scenario 2, the standard deviation of RMSE ranges from 10 m to 16 m. For Scenario 3, the standard deviation of RMSE ranges from 6 m to 8 m. For Scenario 4, the standard deviation of RMSE ranges from 7 m to 10 m. For Scenario 5, the standard deviation of RMSE ranges from 8 m to 12 m. Thus, the minimum value is 6 m and the maximum value is 16 m. This result is satisfying for location prediction.

The location prediction model was further compared with other methods, Vincenty's formula and Haversine formula. The results of these three methods are comparable and is verified that this prediction model is reliable. The RMSE of Haversine formula is closer to the RMSE of prediction model and they are not much different from the RMSE of Vincenty's formula.

CHAPTER 5

CONCLUSION

5.1 Research Summary

The major findings of the study are as follows:

i. The current positioning technologies are compiled, categorized and evaluated in Chapter 2. Throughout the studies on various kinds of positioning technologies, it is found that no research work is done on integrating satellite-based positioning and location prediction for vehicle localization by using smartphone and OBD-II function. Thus, a smartphone-based GPS-integrated location prediction model for OBD-II-equipped vehicle localization is proposed. GPS is chosen as it is a mature and promising satellite-based positioning approach while prediction algorithm can support the positioning of vehicle whenever GPS has NLOS problem. Smartphone is selected as it is portable and convenient. In addition, OBD-II is deployed due to it is mandatory installed in most of Asian vehicles, its adaptor is small size, it is easy to be used and it can pull variety range of useful data from vehicle's ECU.

ii. The key parameters of location prediction algorithm are analyzed and identified. There are a lot of parameters that can be taken into consideration when come to location prediction. For the location prediction algorithm uses in this study, last known coordinate, distance travelled and heading direction/bearing are the key parameters. The last known coordinates can be acquired from GPS that is integrated in smartphone while the heading directions/bearings can be obtained from sensors of smartphone. The distance travelled can be computed from the equation $d = \frac{v}{t}$, where d is the distance travelled, v is the velocity and t is the time. The velocity can be

retrieved from OBD-II.

iii. The location prediction algorithm is formulated and validated. The location prediction algorithm is $c_p = \begin{bmatrix} \emptyset_2 \\ \lambda_2 \end{bmatrix} = \begin{bmatrix} \emptyset_1 \\ \lambda_1 \end{bmatrix} + 9 \times 10^{-6} v \begin{bmatrix} \cos\theta \\ \sin\theta \end{bmatrix} + \begin{bmatrix} e_\emptyset \\ e_\lambda \end{bmatrix}$. The key parameters are inserted into the location prediction algorithm to obtain predicted coordinates. The results are validated by comparing with GPS coordinates. The results show the continuity and accuracy of location prediction algorithm.

iv. A smartphone-based GPS-integrated location prediction model is proposed and developed. The model is designed to provide GPS coordinates when GPS signal is available while location prediction algorithm will perform coordinate computation when GPS signal outages happen. The model is validated as well. It is functioning well. The accuracy is calculated and presented in Chapter 4. From the results obtained, the standard deviation of RMSE or accuracy is ranging from 5.2 m to 15.8 m within 5-10 minutes.

$$c_p = \begin{bmatrix} \emptyset_2 \\ \lambda_2 \end{bmatrix} = \begin{bmatrix} \emptyset_1 \\ \lambda_1 \end{bmatrix} + 9 \times 10^{-6} v \begin{bmatrix} \cos\theta \\ \sin\theta \end{bmatrix} \pm (5.2 \text{ to } 15.8 \text{ m})$$

vi. The portability, applicability, continuity, accuracy and price of smartphone-based GPS-integrated location prediction model are defined. The smartphone and OBD-II adaptor are smaller and portable. The location prediction model is applicable in smartphone and it is able to provide continuous coordinates under LOS and NLOS condition. The accuracy is ranging from 5.2 m to 15.8 m. The price of smartphone and OBD-II is affordable.

In conclusion, the objectives of this research work have been achieved. The smartphone-based GPS-integrated location prediction model for OBD-II-equipped vehicle localization is developed and verified to be portable, functional, applicable, reliable,

precise and accurate. This model will be useful to be implemented by civilian users/companies/government bodies (police or Jabatan Perangkutan Jalan) to monitor the location of vehicles in real-time. Tracking location of vehicle in real-time can prevent a personal to get lost in unknown area, can help a company to observe their employees/drivers/land vehicles, as well as can help government bodies to observe the traffic conditions.

5.2 Significant Findings and Research Contributions

This research work shows the ability of smartphone to provide high continuity vehicle localization with the integration of GPS, OBD-II and location prediction algorithm. The system can provide coordinates of vehicle without loss of data during the experiment work. Currently, most of the available positioning relies on satellites but satellite-based positioning fails to perform during NLOS condition. Thus, a smartphone-based GPS-integrated location prediction model is presented so that it can be easily implemented on OBD-II-equipped land vehicle. The civilian users/companies/government bodies (police or Jabatan Perangkutan Jalan) can pinpoint the location of OBD-II-equipped vehicles with smartphone under LOS and NLOS condition.

5.3 Future Research

The accuracy of the location prediction algorithm can be further improved by adding in low pass filter or other filtering such as Kalman Filter (KF). This is because KF is the best solution of integration and is widely implemented in the field of prediction. The extensions of KF can minimize the error and improve the accuracy of prediction.

In addition, the current smartphone's antenna is linear-polarized and particularly designed for GSM signal transfer. There are investigations on circular-polarized antenna or dual-band Planar Inverted-F Antenna (PIFA) design in smartphone. The designs aim multiband signal transfer and better satellite signal receive. Therefore, the improvement to be suggested is the deployment of smartphone with modified antenna (circular-polarized or PIFA) instead of smartphone with linear-polarized antenna,

Furthermore, the auto upload of data on server to store in database is another kind of improvement that can be done. This function is highly recommended as every smartphone has own data plan. The auto upload of data per second allows user to trace their driving route from the database whenever they want. This is helpful for a civilian user to keep the driving route as record, for a company to track the movement of company vehicles or for a government body to monitor the traffic on road.

Last but not least, the technology of Geographic Information System (GIS) should be utilized. With the help of GIS mapping, civilian users/companies/government bodies can view the location of vehicles in real time on map (Google Map or Google Earth), either on client side (smartphone) or server side (monitoring center).

REFERENCES

[1] S. C. Davis, S. W. Diegel, and R. G. Boundy, (2012). *Transportation Energy Data Book*, 31st ed. Oak Ridge National Laboratory.

[2] M. Samiei, M. Mehrjoo, and B. Pirzade, (2010). Advances of Positioning Methods in Cellular Networks. International Conference Communications Engineering, pp. 174-178.

[3] K. Serr, T. Windholz, and K. Weber, (2006). Comparing GPS Receivers : A Field Study. URISA Journal, 18(2): 19-23.

[4] C. N. Ping, W. A. W. Z. Abidin, and W. H. W. Ibrahim, (2015). A Review on Recent Available Positioning Technologies and Its Advancement. Malaysian Journal of Science, 34(1): 113-128.

[5] C. J. Hegarty and E. Chartre, (2008). Evolution of the Global Navigation Satellite System (GNSS). Proceedings of the IEEE, 96(12): 1902-1917.

[6] A. Schumacher, (2006). Integration of A GPS Aided Strapdown Inertial Navigation System for Land Vehicles, Royal Institute of Technology.

[7] C. Pinana-Diaz and R. Toledo-Moreo, (2011). GPS Multipath Detection and Exclusion with Elevation-Enhanced Maps. 14th International IEEE Conference on Intelligent Transportation Systems, pp. 19-24.

[8] A. Giremus and J. Y. Tourneret, (2005). Joint Detection/Estimation of Multipath Effects for the Global Positioning System. IEEE ICASSP, pp. 17-20.

[9] M. Irfan, M. Baig, F. Khan, and R. Hashmi, (2009). Management of Location Based Advertisement Services using Spatial Triggers in Cellular Networks. International Journal of Computer Science and Information Security (IJCSIS), 6(1): 181-185.

[10] M. Zhang, (2010). Data Fusion for Ground Target Tracking in GSM Networks. University of Siegen.

[11] F. Li and Y. Wang, (2007). Routing in Vehicular Ad Hoc Networks : A Survey. IEEE Vehicular Technology Magazine, pp. 12-22.

[12] M. Melega, S. Lazarus, A. Savvaris, and A. Tsourdos, (2013). GPS/INS Integration in a S&A Algorithm based on Aircraft Performances Estimation, pp. 513-518.

[13] D. J. Jwo, F. C. Chung, and K. L. Yu, (2013). GPS/INS Integration Accuracy Enhancement using the Interacting Multiple Model Nonlinear Filters. Journal of Applied Research and Technology, 11(4): 496-509.

[14] V. Sokolović, G. Dikić, G. Marković, R. Stančić, and N. Lukić, (2015). INS/GPS Navigation System based on MEMS Technologies. Journal of Mechanical Engineering, 61(7)–(8): 448-458.

[15] A. Noureldin, T. Karamat, and M. Eberts, (2005). Multipath-Adaptive GPS/INS Receiver. IEEE Transactions on Aerospace and Electronic Systems, 41(2): 645-657.

[16] K. W. Chiang, (2004). INS/GPS Integration using Neural Networks for Land Vehicular Navigation Applications. University of Calgary.

[17] A. Noureldin, R. Sharaf, A. Osman, and N. El-Sheimy, (2004). INS/GPS Data Fusion Technique utilizing Radial Basis Functions Neural Networks. PLANS 2004. Position Location and Navigation Symposium (IEEE Cat. No.04CH37556), pp. 280-284.

[18] J. Wang, Y. Gao, Z. Li, X. Meng, and C. Hancock, (2016). A Tightly-Coupled GPS/INS/UWB Cooperative Positioning Sensors System Supported By V2I Communication. Sensors, 16(7): 944-960.

[19] M. Malleswaran, V. Vaidehi, and M. Jebarsi, (2012). Neural Networks Review for Performance Enhancement in GPS/INS Integration. 2012 International Conference on Recent Trends in Information Technology, pp. 34-39.

[20] A. Nemra and N. Aouf, Robust INS/GPS Sensor Fusion for UAV Localization using SDRE Nonlinear Filtering. Sensors, 10(4): 789-798.

[21] M. Malleswaran, V. Vaidehi, and M. Mohankumar, (2011). A Hybrid Approach for GPS/INS Integration using Kalman Filter and IDNN, 2011 Third International Conference on Advanced Computing, pp. 378-383.

[22] J. Blakey, (2005). GPS/INS uses Low-Cost MEMS IMU. IEEE Aerospace and Electronic Systems Magazine, pp. 3-10.

[23] T. P. Van, T. N. Van, D. A. Nguyen, T. C. Duc, and T. T. Duc, (2015). 15-State Extended Kalman Filter Design for INS/GPS Navigation System. Journal of Automation and Control Engineering, 3(2): 109-114.

[24] J. Jack, J. Wang, D. Sinclair, and L. Watts, (2007). Neural Network Aided Kalman Filtering for Integrated GPS/INS Geo-Referencing Platform. 5th International Symposium on Mobile Mapping Technology.

[25] J. Fang and X. Gong, (2010). Predictive Iterated Kalman Filter for INS/GPS Integration and Its Application to SAR Motion Compensation. IEEE Transactions on Instrumentation and Measurement, 59(4): 909-915.

[26] O. M. Maklouf, Y. El Halwagy, M. Beumi, and S. D. Hassan, (2009). Cascade Kalman Filter Application in GPS/INS Integrated Navigation for Car Like Robot. 26th National Radio Science Conference.

[27] X.R.Li, (2002). Direct Kalman Filtering Approach for GPS/INS Integration. IEEE Transactions on Aerospace and Electronic Systems, 38(2): 687-693.

[28] Q. Li and F. Sun, (2013). Strong Tracking Cubature Kalman Filter Algorithm for GPS/INS Integrated Navigation System. Proceedings of 2013 IEEE International Conference on Mechatronics and Automation, pp. 1113-1117.

[29] E. Shi, (2012). An Improved Real-time Adaptive Kalman Filter for Low-Cost Integrated GPS/INS Navigation, pp. 1093-1098.

[30] G. Nan, W. Mengyuan, and Z. Long, (2016). An Integrated INS/GNSS Urban Navigation System based on Fuzzy Adaptive Kalman Filter. Proceedings of the 35th Chinese Control Conference, pp. 5732-5736.

[31] R. Giroux, R. Gourdeau, and R.Landry, (2005). Extended Kalman Filter Implementation for Low-cost INS/GPS Integration in a Fast Prototyping Environment. 16th Symposium on Navigation of the Canadian Navigation Society, pp. 26-27.

[32] T. Zhang and X. Xu, (2012). A New Method of Seamless Land Navigation for GPS/INS Integrated System. Measurement, 45(4): 691-701.

[33] C. Y. N, A. Shanmukha, A.B.M, and Basavaraj, (2017). Development of GPS/INS Integration Module using Kalman Filter. International Conference on Algorithms, Methodology, Models and Applications in Emerging Technologies, pp. 1-5.

[34] N. Q. Vinh, (2017). INS/GPS Integration System using Street Return Algorithm and Compass Sensor. Procedia Computer Science, 103: 475-482.

[35] N. El-Sheimy, (2009). Emerging MEMS IMU and Its Impact on Mapping Applications. Photogrammetric Week, pp. 203-216.

[36] V. Technologies, (n.d.). Inertial Measurement Units and Inertial Navigation. Available from: http://www.vectornav.com/support/library/imu-and-ins [1 August 2017].

[37] A. Noureldin, A. El-Shafie, and M. Bayoumi, (2011). GPS/INS Integration utilizing Dynamic Neural Networks for Vehicular Navigation. Information Fusion, 12(1): 48-57.

[38] A. Hiliuta, R. Landry, and F. Gagnon, (2004). Fuzzy Corrections in a GPS/INS Hybrid Navigation System. IEEE Transactions on Aerospace and Electronic Systems, 40(2): 591-600.

[39] B. Xu, G. Lan, L. Qu, C. Li, and H. Wang, (2012). Application of Dynamic Neural Network in the GPS/INS Navigation. 2nd International Conference on Applied Robotics for the Power Industry, pp. 942-945.

[40] R. Sharaf, A. Noureldin, A. Osman, and N. El-Shiemy, (2015). Online INS/GPS Integration with a Radial Basis Function Neural Network. IEEE Aerospace and Electronic Systems Magazine, pp. 8-14.

[41] Y. Zhou, J. Wan, Z. Li, and Z. Song, (2017). GPS/INS Integrated Navigation with BP Neural Network and Kalman Filter. Proceedings of the 2017 IEEE International Conference on Robotics and Biometics, pp. 2515-2520.

[42] J. A. França Junior and J. A. Morgado, (2010). Real Time Implementation of a Low-cost INS/GPS System using XPC Target. Journal of Aerospace Engineering, Sciences and Applications, 2(3): 29-38.

[43] H. Guan, L. Li, and X. Jia, (2013). Multi-Sensor Fusion Vehicle Positioning based on Kalman Filter. Third International Conference on Information Science and Technology, pp. 296-299.

[44] S. Baek, C. Liu, P. Watta, and Y. L. Murphey, (2017). Accurate Vehicle Position Estimation using a Kalman Filter and Neural Network-based Approach. IEEE Symposium Series on Computational Intelligence (SSCI), pp.1-8.

[45] L. T. Hsu, Y. Gu, Y. Huang, and S. Kamijo, (2016). Urban Pedestrian Navigation using Smartphone-based Dead Reckoning and 3-D Map-Aided GNSS. IEEE Sensors Journal, 16(5): 1281-1293.

[46] Y. J. Yoon, K. H. H. Li, J. S. Lee, and W. T. Park, Real-time Precision Pedestrian Navigation Solution using Inertial Navigation System and Global Positioning System. Advances in Mechanical Engineering, 7(3): 1-9.

[47] W. Y. Ochieng and K. Sauer, (2002). Urban Road Transport Navigation: Performance of the Global Positioning System after Selective Availability. Transportation Research Part C: Emerging Technologies, 10(3): 171-187.

[48] Y. Asakura and E. Hato, (2004). Tracking Survey for Individual Travel Behaviour using Mobile Communication Instruments. Transportation Research Part C: Emerging Technologies, 12(3-4): 273-291.

[49] J. J. H. Wang, (2012). Antennas for Global Navigation Satellite System (GNSS). Proceedings of the IEEE, 100(7): 2349-2355.

[50] Trimble, (2007). *GPS: The First Global Navigation Satellite System*. Trimble Navigation Limited, California.

[51] M. Shaw, (2004). Modernization of the Global Positioning System. Acta Astronautica, 54(11-12): 943-947.

[52] P. Herron, C. Powers, and M. Solomon, (2001). Global Positioning Technology in the Intelligent Transportation Space. Intelligent Vehicle Technologies, pp. 229-255.

[53] N. Qi, Y. Xu, B. Y. Chi, X. B. Yu, X. Zhang, N. Xu, (2012). A Dual-Channel Compass/GPS/GLONASS/Galileo Reconfigurable GNSS Receiver in 65 nm CMOS with on-Chip I/Q Calibration. IEEE Transactions on Circuits and Systems I: Regular Papers, 59(8): 1720-1732.

[54] T. Öcalan and N. Tunalıo, (2010). Data Communication for Real-Time Positioning and Navigation in Global Navigation Satellite Systems (GNSS)/Continuously Operating Reference Stations (CORS) Networks. Scientific Research and Essays, 5(18): 2630-2639.

[55] B. Li, S. Zhang, A. G. Dempster, and C. Rizos, (2011). Impact of RNSSs on Positioning in the Asia-Oceania Region. Journal of Global Positioning Systems, 10(2): 114-124.

[56] N. Inaba, A. Matsumoto, H. Hase, S. Kogure, M. Sawabe, and K. Terada, (2009). Design Concept of Quasi Zenith Satellite System. Acta Astronautica, 65(7-8): 1068-1075.

[57] V. G. Rao, G. Lachapelle, and V. K. S. B, (2011). Analysis of IRNSS Over Indian Subcontinent. ION ITM 2011, Session B5, pp. 1-13.

[58] R. Babu, T. Rethika, and S. C. Rathnakara, (2012). Onboard Atomic Clock Frequency Offset for Indian Regional Navigation Satellite System. International Journal of Applied Physics and Mathematics, 2(4): 270-272.

[59] A. Cezón, M. Cueto, I. Hidalgo, and L. Andrada, (2010). SACCSA-SBAS in the CAR/SAM Regions: Feasibility Analysis, 23rd International Technical Meeting of the Satellite Division of the Institue of Navigation, pp. 2002-2012.

[60] J. Blanch, T. Walter, and P. Enge, (2012). Satellite Navigation for Aviation in 2025. Proceedings of the IEEE. 100 (Special Centennial Issue), pp. 1821-1830.

[61] S. D. Ilcev, (2011). Comparison Between Extension of the European EGNOS and New African ASAS Network for Africa and Middle East. 2011 IEEE International Conference on Microwaves, Communications, Antennas and Electronic Systems, pp. 1-2.

[62] R. Juang, D. Lin, and H. Lin, (2007). Hybrid SADOA/TDOA Mobile Positioning for Cellular Networks. IET Communications, 1(2): 282-287.

[63] M. Bshara, U. Orguner, F. Gustafsson, and L. Van Biesen, (2011). Robust Tracking in Cellular Networks Using HMM Filters and Cell-ID Measurements. IEEE Transactions on Vehiclular Technology, 60(3): 1016-1024.

[64] I. Adusei and K. Kyamakya, (2002). Mobile Positioning Technologies in Cellular Networks: An Evaluation of Their Performance Metrics. MILCOM 2002, pp. 1-6.

[65] H. P. Mendoza, (2011). Distributed Localization for Wireless Distributed Networks in Indoor Environments, Virginia Polytechnic Institute and State University.

[66] M. Ibrahim and M. Youssef, (2012). CellSense : An Accurate Energy-Efficient GSM Positioning System. IEEE Transactions on Vehicular Technology, 61(1): 286-296.

[67] G. Kbar and W. Mansoor, (2005). Mobile Station Location Based on Hybrid of Signal Strength and Time of Arrival. Proceedings of the International Conference on Mobile Business (ICMB' 05), pp. 1-7.

[68] S. Wang, B. R. Jackson, and R. Inkol, (2012). Hybrid RSS/AOA Emitter Location Estimation Based on Least Squares and Maximum Likelihood Criteria. Communications (QBSC), 2012 26th Biennial Symposium, pp. 24-29.

[69] S. Al-Jazzar, M. Ghogho, and D. McLernon, (2009). A Joint TOA/AOA Constrained Minimization Method for Locating Wireless Devices in Non-Line-of-Sight Environment. IEEE Transactions on Vehicular Technology, 58(1): 468-472.

[70] L. Cong and W. Zhuang, (2002). Hybrid TDOA/AOA Mobile User Location for Wideband CDMA Cellular Systems. IEEE Transactions on Wireless Communications, 1(3): 439-447.

[71] P. H. Tseng and K. T. Feng, (2010). Hybrid TOA/TDOA Based Unified Kalman Tracking Algorithm for Wireless Networks. 21st Annual IEEE International Symposium on Personal, Indoor and Mobile Radio Communications, pp. 1707-1712.

[72] P. Deng and P. Z. Fan, (2000). An AOA Assisted TOA Positioning System, WCC 2000-ICCT 2000. 2000 International Conference on Communication Technology Proceedings, pp. 1501-1504.

[73] M. Laaraiedh, L. Yu, S. Avrillon, and B. Uguen, (2011). Comparison of Hybrid Localization Schemes Using RSSI, TOA and TDOA. Wireless Conference 2011-Sustainable Wireless Technologies (European Wireless), 11th European, pp. 626-630.

[74] J. Chen and A. Abedi, (2010). A Hybrid Framework for Radio Localization in Broadband Wireless Systems. IEEE Global Telecommunications Conference, pp. 1-6.

[75] G. Retscher and A. Kealy, (2005). Ubiquitous Positioning Technologies for Intelligent Navigation Systems. Proceedings of the 2nd Workshop on Positioning, Navigation and Communication(WPNC' 05) & 1st Ultra-WideBand Expert Talk, pp. 99-108.

[76] P. Uthansakul and M. Uthansakul, (2009). WLAN Positioning Based on Joint TOA and RSS Characteristics. International Journal of Electrical and Computer Science, 4(15): 942-949.

[77] L. P. Wen, C. W. Nee, K. M. Chun, T. S. Yen, and R. Idrus, (2011). Development of Handheld Directory System Built on WiFi-based Positioning Techniques. International Journal of Computers and Communications, 5(3): 188-197.

[78] B. Li, I. J. Quader, and A. G. Dempster, (2008). On Outdoor Positioning with Wi-Fi. Journal of Global Positioning Systems, 7(1): 18-26.

[79] C. M. Wong, B. Columbia, and G. G. Messier, (2006). Evaluating Measurement-Based AOA Indoor Location Using WLAN Infrastructure. Proceedings of the 20th International Technical Meeting of the Satellite Division of the Institute of Navigation, pp. 1139-1145.

[80] E. Hossain, G. Chow, V. C. M. Leung, R. D. McLeod, J. Misic, V. W. S. Wong, and O. Yang, (2010). Vehicular Telematics Over Heterogeneous Wireless Networks: A Survey. Computer Communications, 33(7): 775-793.

[81] P. Papadimitratos, A. La Fortelle, K. Evenssen, R. Brignolo, and S. Cosenza, (2009). Vehicular Communication Systems: Enabling Technologies, Applications, and Future Outlook on Intelligent Transportation. IEEE Communications Magazine, pp. 84-95.

[82] M. L. Sichitiu and M. Kihl, (2008). Inter-Vehicle Communication Systems: A Survey. IEEE Communications Surveys, 10(2): 88-105.

[83] Y. J. Li, (2010). An Overview of the DSR/WAVE Technology. International Conference on Heterogeneous Networking for Quality, Reliability, Security and Robustness, pp. 544-558.

[84] W. Wen, (2010). An Intelligent Traffic Management Expert System with RFID Technology. Expert Systems with Applications, 37(4): 3024-3035.

[85] A. M. Mustapha, M. Hannan, A. Hussain, and H. Basri, (2010). UKM Campus Bus Monitoring System Using RFID and GIS. 2010 6th International Colloquium on Signal Processing & its Applications (CSPA), pp. 62-66.

[86] K. Kamarulazizi, W. Ismail, (2010). Electronic Toll Collection System Using Passive RFID Technology. Journal of Theoritical and Applied Information Technology, 22(2): 70-76.

[87] M. P. Pelletier, M. Trépanier, and C. Morency, (2011). Smart Card Data Use in Public Transit: A Literature Review. Transportation Research Part C: Emerging Technologies, 19(4): 557-568.

[88] E. K. Lee, S. Y. Oh, and M. Gerla, (2012). RFID Assisted Vehicle Positioning in VANETs. Pervasive and Mobile Computing, 8(2): 167-179.

[89] D. Obradovic, H. Lenz, and M. Schupfner, (2007). Fusion of Sensor Data in Siemens Car Navigation System. IEEE Transactions on Vehicular Technology, 56(1): 43-50.

[90] W. Kang and Y. Han, (2015). SmartPDR: Smartphone-based Pedestrian Dead Reckoning for Indoor Localization. IEEE Sensors Journal, 15(5): 2906-2916.

[91] Q. Tian, Z. Salcic, K. I. K. Wang, and Y. Pan, (2016). A Multi-Mode Dead Reckoning System for Pedestrian Tracking Using Smartphones. IEEE Sensors Journal, 16(7): 2079-2093.

[92] D. Yuanfeng, Y. Dongkai, Y. Huilin, and X. Chundi, (2016). Flexible Indoor Localization and Tracking System Based on Mobile Phone. Journal of Network and Computer Applications, 69: 107-116.

[93] L. Zheng, W. Zhou, W. Tang, X. Zheng, A. Peng, and H. Zheng, (2016). A 3D Indoor Positioning System Based on Low-cost MEMS Sensors. Simulation Modelling Practice and Theory, 65: 45-56.

[94] L. Ojeda and J. Borenstein, (2007). Personal Dead-reckoning System for GPS-denied Environments. International Workshop on Safety, Security and Rescue Robotics, pp. 1-6.

[95] L. L. Shen and W. W. S. Hui, (2016). Improved Pedestrian Dead-Reckoning-Based Indoor Positioning By RSSI-Based Heading Correction. IEEE Sensors Journal, 16(21): 7762-7773.

[96] R. Harle, (2013). A Survey of Indoor Inertial Positioning Systems for Pedestrians. IEEE Communications Surveys and Tutorials, 15(3): 1281-1293.

[97] N. E. El Faouzi, H. Leung, and A. Kurian, (2011). Data Fusion in Intelligent Transportation Systems: Progress and Challenges - A Survey. Information Fusion, 12(1): 4-10.

[98] O. Maklouf and A. Adwaib, (2014). Performance Evaluation of GPS/INS Main Integration Approach. International Journal of Mechanical, Aerospace, Industrial, Mechatronic and Manufacturing Engineering, 8(2): 476-484.

[99] R. Faragher, (2012). Understanding the Basis of the Kalman Filter via a Simple and Intuitive Derivation. IEEE Signal Processing Magazine, 29(5): 128-132.

[100] G. Welch and G. Bishop, (2006). An Introduction to the Kalman Filter. In Practice, 7(1): 1-16.

[101] D. Simon, (2001). Kalman Filtering. Embedded System Programming, pp. 72-79.

[102] P. Dittrich and P. Chudý, (2011). Application of Kalman Filter to Oversampled Data from Global Position System for Flight Path Reconstruction. Electroscope, 2011(2): 6-10.

[103] D. Simon, (2010). Kalman Filtering with State Constraints: A Survey of Linear and Nonlinear Algorithms. IET Control Theory & Applications, 4(8): 1303–1318.

[104] R. Toledo-Moreo and M. Zamora-Izquierdo, (2007). High-Integrity IMM-EKF-Based Road Vehicle Navigation with Low-Cost GPS/SBAS/INS. IEEE Transactions on Intelligent Transportation Systems, 8(3): 491-511.

[105] R. Toledo-Moreo, M. Zamora-Izquierdo, and A. Gomez-Skarmeta, (2006). IMM-EKF Based Road Vehicle Navigation with Low Cost GPS/INS. 2006 IEEE International Conference on Multisensor Fusion and Integration for Intelligent Systems, pp. 433-438.

[106] I. Skog, (2005). A Low-cost GPS Aided Inertial Navigation System for Vehicular Applications. KTH Signals Sensors and Systems, Stockholm, Sweden.

[107] Z. Jiang, C. Liu, G. Zhang, Y. Wang, C. Huang, and J. Liang, (2013). GPS/INS Integrated Navigation based on UKF and Simulated Annealing Optimized SVM. IEEE 78th Vehicular Technology Conference (VTC Fall), pp.1-5.

[108] H. Benzerrouk, A. Nebylov, and H. Salhi, (2016). Quadrotor UAV State Estimation based on High Degree Cubature Kalman Filter. IFAC-PapersOnLine, 49(17): pp. 349-354.

[109] A. Noureldin, A. El-Shafie, and M. Reda Taha, (2007). Optimizing Neuro-Fuzzy Modules for Data Fusion of Vehicular Navigation Systems Using Temporal Cross-Validation. Engineering Applications of Artificial Intelligence, 20(1): 49-61.

[110] R. Sharaf, A. Noureldin, and A. Osman, (2009). Performance Enhancement of MEMS-Based INS/GPS Integration for Low-Cost Navigation Applications. IEEE Transactions on Vehicular Technology, 58(3): 1077-1096.

[111] M. Malleswaran, S. Angel Deborah, S. Manjula, and V. Vaidehi, (2010). Integration of INS and GPS Using Radial Basis Function Neural Networks for Vehicular Navigation. 2010 11th Conference Control, Automation, Robotics and Vision, pp. 2427-2430.

[112] W. Wang, (2009). License Plate Recognition Algorithm Based on Radial Basis Function Neural Networks. 2009 International Symposium on Intelligent Ubiquitous Computing and Education, pp. 38-41.

[113] R. Sharaf and A. Noureldin, (2007). Sensor Integration for Satellite-Based Vehicular Navigation Using Neural Networks. IEEE Transactions on Neural Networks, 18(2): 589-94.

[114] W. Wang, (2009). Vehicle Type Recognition Based on Radial Basis Function Neural Networks. 2009 International Joint Conference on Artificial Intelligence, pp. 444-447.

[115] Z. Shen, J. Georgy, M. J. Korenberg, and A. Noureldin, (2011). Low Cost Two Dimension Navigation Using An Augmented Kalman Filter/Fast Orthogonal Search Module for the Integration of Reduced Inertial Sensor System and Global Positioning System. Transportation Research Part C: Emerging Technologies, 19(6): 1111-1132.

[116] H. Liu, S. Nassar, and N. El-Sheimy, (2010). Two-filter Smoothing for Accurate INS/GPS Land-vehicle Navigation in Urban Centers. IEEE Transactions on Vehicular Technology, 59(9): 4256-4267.

[117] C. C. Wu, X. W. Chen, H. Li, Z. Z. Wu, and Y. C. Tao, (2004). Design and Development of Farm Vehicle Monitoring and Intelligent Dispatching System. Proceedings of the Third International Conference on Machine Learning and Cybernetics, pp. 352-355.

[118] K. Maurya, M. Singh, and N. Jain, (2012). Real Time Vehicle Tracking System Using GSM and GPS Technology-An Anti-theft Tracking System. Engineering, International Journal of Electronics and Computer Science, 1(3): 1103-1107.

[119] H. Tan, (2010). Design and Implementation of Vehicle Monitoring System Based on GSM/GIS/GPS. 2010 Second International Conference on Information Technology and Computer Science, pp. 413-416.

[120] H. Hu and L. Fang, (2009). Design and Implementation of Vehicle Monitoring System Based on GPS/GSM/GIS. 2009 Third International Symposium on Intelligent Information Technology Application, pp. 278-281.

[121] L. XuTao, C. DongSen, Z. ZhiJie, and S. YunQiang, (2010). Design of Transport Vehicles Remote Monitoring System. 2010 2nd International Conference on Education Technology and Computer, pp. 310-313.

[122] Q. Liu, H. Lu, H. Zhang, and B. Zou, (2006). Design of Intelligent Vehicle Monitoring System Based on GPS/GSM. 2006 6th International Conference on ITS Telecommunications Proceedings, pp. 1267-1270.

[123] D. Jose, S. Prasad, and V. G. Sridhar, (2015). Intelligent Vehicle Monitoring Using Global Positioning System and Cloud Computing. Procedia Computer Science, 50(2015): 440-446.

[124] C. Lin, Y. Shiao, C. Li, and S. Yang, (2007). Real-time Remote Onboard Diagnostics Using Embedded GPRS Surveillance Technology. IEEE Transactions on Vehicular Technology, 56(3): 1108-1118.

[125] I. Aris, M. F. Zakaria, S. M. Abdullah, and R. M. Sidek, (2007). Development of OBD-II Driver Information System. International Journal of Engineering and Technology, 4(2): 253-259.

[126] R. Malekian, N. R. Moloisane, L. Nair, B. T. Maharaj, and U. A. K. Chude-Okonkwo, (2017). Design and Implementation of a Wireless OBD II Fleet Management System. IEEE Sensors Journal, 17(4): 1154-1164.

[127] J. L. Wilson, (2007). Low-cost PND Dead Reckoning using Automotive Diagnostic Links. ION GNSS 20th International Technical Meeting of the Sateliite Division, pp. 25–28.

[128] P. C. Joseph and S. P. Kumar, (2015). Design and Development of OBD-II Compliant Driver Information System. Indian Journal of Science and Technology, 8(21): 1-7.

[129] J. Lin, S. Chen, Y. Shih, and S. Chen, (2011). *A Study on Remote On-Line Diagnostic System for Vehicles by Integrating the Technology of OBD, GPS and 3G*. Springer, Berlin, Heidelberg.

[130] Y. Yang, B. Chen, L. Su, and D. Qin, (2013). Research and Development of Hybrid Electric Vehicles CAN-bus Data Monitor and Diagnostic System through OBD-II and Android-based Smartphones. Advances in Mechanical Engineering, pp.1-9.

[131] M. Jyothi and S. Ravi, (2012). Vehicle Health Monitoring System. International Journal of Engineering Research and Applications, 2(5): 1162-1167.

[132] J. V. Moniaga, S. R. Manalu, D. A. Hadipurnawan, and F. Sahidi, (2018). Diagnostics Vehicle's Condition using Obd-II and Raspberry Pi Technology: Study Literature. Journal of Physics: Conference Series, 978(1).

[133] A. Sriramnath and S. Kolangiammal, (2015). Embedded System Based on Board Diagnostic (OBD) Tool for Vehicle Management and Safety. International Journal of Engineering Development and Research, 3(2): 221-229.

[134] K. M. Mak, H. W. Lai, K. M. Luk, and C. H. Chan, (2014). Circularly Polarized Patch Antenna for Future 5G Mobile Phones. IEEE Access, 2: 1521-1529.

[135] Z. Wu, H. Wang, P. Chen, W. Shen, and G. Yang, (2016). A Compact GPS/WLAN Antenna Design for Mobile Device with Full Metal Housing. International Workshop on Antenna Technology (IWAT), pp. 23-24.

[136] R. Singh, M. K. Meshram, and M. Agarwal, (2013). Linearly Polarised Planar Inverted F-antenna for Global Positioning System and Worldwide Interoperability for Microwave Access Applications. IET Microwaves, Antennas & Propagation, 7(12): 991-998.

[137] L. Naragani, K. Kumara Swamy, and N. V. Koteswararao, (2016). Proximity Coupled Multiband Antenna. Proceedings of the 2016 IEEE International Conference on Wireless Communications, Signal Processing and Networking, pp. 940-943.

[138] M. Matsunaga and M. Suzuki, (2015). An Electrically Small Three-Band Multi-polarization Cross Spiral Antenna, 9th European Conference on Antennas and Propagation, pp. 8-9.

[139] A. Ahmad and F. A. Tahir, (2017). A Planar GPS/GLONASS/LTE/WWAN Antenna for Ultra-Slim Smartphones. 11th European Conference on Antennas And Propagation, pp. 2973–2975.

[140] Y. Xu, Y. W. Liang, and H. M. Zhou, (2017). Small-size Reconfigurable Antenna for WWAN/LTE/GNSS Smartphone Applications. IET Microwaves, Antennas & Propagation, 11(6): 923–928.

[141] C. A. Ogaja, (2010). Geomatics Engineering: A Practical Guide to Project Design, CRC Press.

[142] M. Aatique, (1997). Evaluation of TDOA Techniques for Position Location in CDMA Systems, Virginia Polytechnic Institute and State University.

[143] V. Zeimpekis, G. Giaglis, and G. Lekakos, (2003). A Taxonomy of Indoor and Outdoor Positioning Techniques for Mobile Location Services. ACM SIGecom Exchanges - Mobile Commerce, 3(4): 19-27.

[144] C. A. A. O. Rodrigues, (2015). Smartphone-based Inertial Navigation System for Bicycles, Associação Fraunhofer Portugal Research.

[145] J. F. Vasconcelos, C. Silvestre, and P. Oliveira, (2011). INS/GPS Aided By Frequency Contents of Vector Observations with Application To Autonomous Surface Crafts. IEEE Journal of Oceanic Engineering, 36(2): 347-363.

[146] M. J. Yu, (2012). INS/GPS Integration System Using Adaptive Filter for Estimating Measurement Noise Variance. IEEE Transactions on Aerospace and Electronic Systems, 48(2): 1786-1792.

[147] T. Vincenty, (1975). Direct and Inverse Solutions of Geodesics on the Ellipsoid with Application of Nested Equations. Survey Review, 33(176): 88-93.

[148] R. W. Sinnott, (1984). Virtues of the Haversine. Sky and Telescope, 68(2): 159-160.

APPENDICES

Appendix A

Matlab Coding of Prediction Algorithm

```
for c = 2:size(z,1)

%Input

z(1,5) = z(1,1); %last known longitude
z(1,6) = z(1,2); %last known latitude

speed = z(c,3); %speed in meter per second
bearing = z(c,4); %bearing in degree

lon1 = z(c-1,5); %initial longitude
lat1 = z(c-1,6); %initial latitude

lat2 = lat1 + speed*0.000539957/60*cos(degtorad(bearing));
lon2 = lon1 + speed*0.000539957/60*sin(degtorad(bearing));

%Output

z(c,5) = lon2;
z(c,6) = lat2;

end
```

Appendix B

Matlab Coding of Prediction Model

```
for c = 2:size(z,1)

%Input

z(1,6) = z(1,1); %last known longitude
z(1,7) = z(1,2); %last known latitude

speed = z(c,3); %speed in meter per second
bearing = z(c,4); %bearing in degree

if z(c,5)> 10

z(c,6) = z(c,1); %GPS longitude
z(c,7) = z(c,2); %GPS latitude

else

lon1 = z(c-1,6); %initial longitude
lat1 = z(c-1,7); %initial latitude
lat2 = lat1 + speed*0.000539957/60*cos(degtorad(bearing));
lon2 = lon1 + speed*0.000539957/60*sin(degtorad(bearing));

%Output

z(c,6) = lon2;
z(c,7) = lat2;

end

end
```

Appendix C

Matlab Coding of Vincenty's Formula

```
for c = 2:size(z,1)

%Input:

z(1,6) = z(1,1); %last known longitude
z(1,7) = z(1,2); %last known latitude

speed = z(c,3)*0.277777778; %speed in meter per second
bearing = z(c,4); %bearing in degree

lon1 = z(c-1,6); %initial longitude
lat1 = z(c-1,7); %initial latitude

if z(c,5) > 15

z(c,6) = z(c,1); %GPS longitude
z(c,7) = z(c,2); %GPS latitude

else

a = 6378137; % semimajor axis
b = 6356752.31424518; % semiminor axis
f = 1/298.257223563; % flattening coefficient
lat1 = lat1 * .174532925199433295e-1; % intial latitude in radians
lon1 = lon1 * .174532925199433295e-1; % intial longitude in radians
% correct for errors at exact poles by adjusting 0.6 millimeters:
kidx = abs(pi/2-abs(lat1)) < 1e-10;

if any(kidx);
    lat1(kidx) = sign(lat1(kidx))*(pi/2-(1e-10));
end
```

```
alpha1 = bearing * .17453292519943295e-1; % inital azimuth in radians
sinAlpha1 = sin(alpha1);
cosAlpha1 = cos(alpha1);
tanU1 = (1-f) * tan(lat1);
cosU1 = 1 / sqrt(1 + tanU1*tanU1);
sinU1 = tanU1*cosU1;
sigma1 = atan2(tanU1, cosAlpha1);
sinAlpha = cosU1 * sinAlpha1;
cosSqAlpha = 1 - sinAlpha*sinAlpha;
uSq = cosSqAlpha * (a*a - b*b) / (b*b);
A = 1 + uSq/16384*(4096+uSq*(-768+uSq*(320-175*uSq)));
B = uSq/1024 * (256+uSq*(-128+uSq*(74-47*uSq)));
sigma = speed / (b*A);
sigmaP = 2*pi;

while (abs(sigma-sigmaP) > 1e-12)
    cos2SigmaM = cos(2*sigma1 + sigma);
    sinSigma = sin(sigma);
    cosSigma = cos(sigma);
    deltaSigma = B*sinSigma*(cos2SigmaM+B/4*(cosSigma*(-1+...
        2*cos2SigmaM*cos2SigmaM)-...
        B/6*cos2SigmaM*(-3+4*sinSigma*sinSigma)*(-3+...
        4*cos2SigmaM*cos2SigmaM)));
    sigmaP = sigma;
    sigma = speed / (b*A) + deltaSigma;
end

tmp = sinU1*sinSigma - cosU1*cosSigma*cosAlpha1;
lat2 = atan2(sinU1*cosSigma + cosU1*sinSigma*cosAlpha1,...
    (1-f)*sqrt(sinAlpha*sinAlpha + tmp*tmp));
lambda = atan2(sinSigma*sinAlpha1, cosU1*cosSigma - ...
    sinU1*sinSigma*cosAlpha1);
C = f/16*cosSqAlpha*(4+f*(4-3*cosSqAlpha));
L = lambda - (1-C) * f * sinAlpha * (sigma + C*sinSigma*(cos2SigmaM+...
    C*cosSigma*(-1+2*cos2SigmaM*cos2SigmaM)));
lon2 = lon1 + L;

%Output

lat2 = lat2 * 57.295779513082322865;
lon2 = lon2 * 57.295779513082322865;
lon2 = mod(lon2,360); % follow [0,360] convention

if nargout > 2

z(c,6) = lon2; %final longitude
z(c,7) = lat2; %final latitude

end
end
end
```

Appendix D

Matlab Coding of Haversine Formula

```
for c = 2:size(z,1)

%Input

z(1,6) = z(1,1); %last known longitude
z(1,7) = z(1,2); %last known latitude

speed = z(c,3)*0.277777778; %speed in meter per second
bearing = z(c,4); %bearing in degree

lon1 = z(c-1,6); %initial longitude
lat1 = z(c-1,7); %initial latitude

if z(c,5) > 15

z(c,6) = z(c,1); %GPS longitude
z(c,7) = z(c,2); %GPS latitude

else

lat2 = radtodeg(asin(sin(degtorad(lat1))*cos(degtorad(speed)/6371000) + ...
    cos(degtorad(lat1))*sin(speed/6371000)*cos(degtorad(bearing))));
lon2 = lon1 + radtodeg(atan2( sin(degtorad(bearing))*sin(speed/6371000)*...
    cos(degtorad(lat1)), cos(speed/6371000)-sin(degtorad(lat1))*...
    sin(degtorad(lat2))));

%Output

z(c,6) = lon2; %final longitude
z(c,7) = lat2; %final latitude

end
```